# Synthetic porous materials: *A study of adsorption selectivity and structure-property relationships*

by

**Dawie de Villiers**

*Submitted in partial fulfilment of the requirements for the degree*

*Master of Science*

at

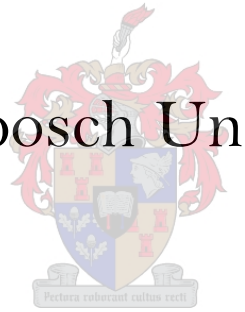

Stellenbosch University

Department of Chemistry and Polymer Science

Faculty of Science

Supervisor: Prof. L. J. Barbour

Co-Supervisor: Prof. C. Esterhuysen

December 2015

# Declaration

By submitting this thesis electronically, I declare that the entirety of the work contained therein is my own, original work, that I am the sole author thereof (save to the extent explicitly otherwise stated), that reproduction and publication thereof by Stellenbosch University will not infringe any third party rights and that I have not previously in its entirety or in part submitted it for obtaining any qualification.

_____

Signature

_____

Name in full

_____/_____/_____

Date

# Abstract

The aim of this thesis was to study structure-property relationships in porous materials using various adapted analytical techniques and in-house instruments. The thesis is divided into two sections, and the first section of work constitutes the majority of the thesis.

The first section of work deals with the theoretical versus experimental classification of sorption selectivity in porous compounds. A transiently porous metallocycle that can adsorb acetylene and carbon dioxide served as a model host for this experiment. A volumetric sorption instrument had to be constructed to carry out sorption with acetylene. Even though the metallocycle should theoretically be selective for acetylene over carbon dioxide based on single-gas sorption isotherms, this was not the case during the sorption of a mixture of the two gases. Furthermore, high-pressure single-crystal diffraction was carried out utilising an in-house environmental gas cell, and structural elucidation indicated that both acetylene and carbon dioxide coexist in a single cavity of the host. Additional complementary techniques are discussed that were used to confirm that both gases are present in a single host cavity. The techniques included infrared spectroscopy as well as high-pressure florescence and Raman spectroscopy, which had to be conducted with a specially designed pressure vessel and with adapted instrumentation. Finally, density functional theory calculations were employed to explain how host-guest and guest-guest interactions lead to the change in adsorption selectivity. It is concluded that researchers need to show experimentally that a compound is selective for the adsorption of a specific gas, because theoretical models are not always accurate.

The second part of this work focuses on a fundamental study of the structure-property relationships in a porous hydrogen-bonded organic framework. The section starts off by exploring the activation conditions and thermal stability of the framework. This is followed by an exploration of a possible phase transformation or thermal expansion in the framework, but neither of these occurred. Thereafter, an extended study of the framework's sorption behaviour with various gases is discussed. Then, a structural study of its solvated phase is used to explain the framework's stability. Finally, a novel analytical method is introduced, and two examples are used to demonstrate why the instrument is useful in the field of supramolecular chemistry. The chapter is concluded by stating the importance these fundamental studies, as well the development of new analytical techniques.

# Opsomming

Die doel van hierdie tesis was om die struktuur-afhanklike eienskappe van poreuse materiale te ondersoek. Die studie het gebruik gemaak van verskeie aangepasde analitiese metodes asook instrumente wat spesifiek vir die studie gebou was. Die werk word in twee dele verdeel, en die meerderheid van die tesis word in die eerste deel bevat.

In die eerste deel van die tesis word die validiteit van teoretiese- teen eksperimentele adsorpsie selektiwiteit opgeweeg. ’n Gasheer wat bestaan uit ringvormige koördinasie-verbindings en wat asetileen asook koolstof dioksied kan adsorbeer, dien as ’n model gasheer vir die studie. ’n Volumetriese sorpsie instrument was spesiaal vir die studie gebou sodat asetileen sorpsie gedoen kon word. Volgens asetileen en koolstof dioksied se enkel-gas adsorpsie isoterme moet asetileen teoreties met voorkeur geadsorbeer word gedurende ’n adsorpsie eksperiment waarin beide gasse teenwoordig is, maar eksperimenteel was dit bepaal dat dit nie so is nie, dus is daar ’n verandering in die gasheer se adsorpsie selektiwiteit. Hierna word strukturele data van die gasheer, onder ’n hoë druk van die gas mengsel, versamel deur gebruik te maak van enkel-kristal diffraksie en ’n spesiaal-gemaakde gas sel. Die strukturele data toon dat beide asetileen en koolstof dioksied teenwoordig is binne elke porie van die gasheer. Daar word dan van addisionele analitiese metodes gebruik te maak om die observasie te bevestig. Die analitiese metodes sluit in infrarooi spektroskopie asook hoë-druk fluoressensie en Raman spektroskopie wat geëis het dat ’n spesiale druk-bestande monster houer gebou moes word en dat analitiese instrumente gemodifiseer moet word. Ten slotte was daar van “*density functional theory*” gebruik gemaak om te verduidelik dat die interaksie tussen die gasheer en gas sowel as die interaksie tussen twee gasse lei tot die verandering in adsorpsie selektiwiteit. Uit hierdie bevinding word die gevolgtrekking gemaak dat navorsers met meer eksperimentele data vorendag sal moet kom voordat ’n gevolgtrekking gemaak kan word dat ’n raamwerk selektief een gas adsorbeer.

Die tweede afdeling van die werk fokus op ’n fundamentele studie van die struktuur-afhanklike eienskappe van ’n poreuse waterstof-verbinde organies raamwerk. Die afdeling begin deur ’n ondersoek van die aktivering kondisies sowel as die temperatuur-afhanklike stabiliteit van die raamwerk. Dit word gevolg deur te soek na moontlike fase veranderings of temperatuur-afhanklike uitsetting van die raamwerk, maar nie een van die twee eienskappe word waargeneem nie. Daarna word die deeglike ondersoek van die raamwerk se adsorpsie vermoë met verskeie gasse bespreek. Dit word gevolg deur ’n strukturele studie van die solvaat van die raamwerk, wat dan gebruik word om die stabiliteit van die raamwerk te verduidelik. Ten slotte word ’n analitiese metode bekend gestel, en twee voorbeelde word gebruik om te wys hoe nuttig die metode is om ’n kombinasie van

resultate te bekom. Die hoofstuk word saamgevat deur te verduidelik hoekom dit belangrik is om hierdie tipe fundamentele studies te doen asook waarom nuwe analitiese metodes ontwerp moet word.

# Acknowledgements

Firstly and foremostly I want to thank my two supervisors, Prof. Len Barbour and Prof. Catharine Esterhuysen. Both are excellent mentors who encouraged and inspired me throughout my years of undergraduate study, Honours and up until the printing of this manuscript. Prof. Barbour is a wealth of ideas and suggestions, and he played a crucial role in the design and construction of the instruments that enabled this work. I want to thank Prof. Esterhuysen for the helpful and reassuring discussions, and for her willingness to go to great lengths to assist, educate and reassure me. Then I want to acknowledge my past and present colleagues in the Supramolecular Chemistry Group, especially Dr. Vincent Smith and Dr. Tia Jacobs for their assistance in lab-work, crystallographic modelling and in writing. Then, I would like to thank my dear friends; I will always cherish your love and our fond memories. Finally my family, thank you for your never-ending support, and that you were my sanctuary in good and difficult times. Mother; without your strength, guidance, support and sacrifices I would not have been able to go through my years of studies.

# List of abbreviations

| | |
|---|---|
| *1D, 2D, 3D* | One-, two- and three dimensional |
| *a* | A van der Waals constant for a real gas |
| Å | Ångstrom = $1^{-10}$ m |
| amu | Atomic mass unit |
| ATR | Attenuated Total Reflectance |
| *b* | A van der Waals constant for a real gas |
| $b_1$ and $b_2$ | Heterogeneity parameters of guest *1* and guest *2* |
| bar | Bar of pressure (1 bar ≈ 1/1.01325 atmosphere = 100 kPa) |
| $C_1$ and $C_2$ | Concentrations of guest 1 and guest 2 |
| CEM | Continuous dynode Electron Multiplier |
| CIF | Crystallographic Information File |
| D Å | Debye Ångstrom |
| DFT | Density Functional Theory |
| DNP | Double Numerical Plus Polarisation |
| DSC | Differential Scanning Calorimetry |
| $e^-$ | Electron |
| eV | Electron Volt |
| *G* | Guest |
| GGA | Generalised Gradient Approximation |
| *H* | Host |
| *H·G* | Host-Guest complex |
| Ha | Hartree |
| HOF | Hydrogen-bonded Organic Framework |
| HS-MS | Hot Stage - Mass Spectrometry |
| IAST | Ideal Adsorbed Solution Theory |
| IGA | Intelligent Gravimetric Analyser |
| IR | Infrared spectroscopy |
| $K_1$ and $K_2$ | Average association constant of guest *1* or guest *2* |
| $K_{A:B}$ | Selectivity coefficient of guest *A* over guest *B* |
| mbar | Millibar |
| MO | Molecular Orbital |
| MOF | Metal-Organic Framework |
| mp | Melting point |

| | |
|---|---|
| MS | Mass spectrometer |
| $n$ | Number of moles |
| NDDO | Neglect of Diatomic Differential Overlap |
| $n_j$ | A measure of adsorption intensity |
| NMR | Nuclear Magnetic Resonance |
| $P$ | Pressure |
| $P_A$ | Pressure transducer A monitoring pressure in the gas reservoir |
| $P_B$ | Pressure transducer B monitoring pressure in sample chamber |
| PBE | Peperdew, Burke, Erzenhof functional |
| PM6 | Parametric Method 6 |
| PXRD | Powder X-ray Diffraction |
| $Q_1$ and $Q_2$ | Predicted quantity of guest *1* or guest *2* adsorbed |
| $q_i$ | Amount of solute adsorbed per unit of weight of solid |
| $R$ | Universal gas constant (8.3145 J $mol^{-1}$ $K^{-1}$) |
| RGA | Residual Gas Analyser |
| RHF | Restricted Hartree-Fock |
| *s, l or g* | Solid, Liquid or Gas |
| $S_{A/B}$ | Adsorption selectivity factor of guest *A* over guest *B* |
| sc-$CO_2$ | Supercritical carbon dioxide |
| SCD | Single-Crystal X-ray Diffraction |
| SCF | Self-Consistent Forcefield |
| SRS | Stanford Research Systems |
| $T$ | Temperature |
| $t$ | Time |
| TGA | Thermogravimetric analysis |
| V | Volume |
| $V_{1-3}$ | Valves numbered one, two or three |
| $V_A$ | Volume A of the gas reservoir |
| $v_A$ and $v_B$ | Mole fraction of adsorbed guest *A* and guest *B* |
| $Y_A$ and $y_B$ | Mole fraction of guest *A* and guest *B* in headspace |
| $V_B$ | Volume B of the sample chamber |
| $V_D$ | Volume of the “dead space” |
| $V_S$ | Sample Volume |
| $X_A$ and $X_B$ | Mole fraction of excluded guest *1* and guest *2* |

| | |
|---|---|
| $x_A$ and $x_B$ | Mole fraction of adsorbed guest *A* and guest B |
| $Z_A$ and $Z_B$ | Mole fraction of included guest *A* and guest *B* |
| α | angle between the crystallographic *b* and *c* axes |
| β | angle between the crystallographic *a* and *c* axes |
| γ | angle between the crystallographic *a* and *b* axes |
| δ | Chemical Shift (in ppm) |
| $\delta^-$ | Negative partial charge |
| $\delta^+$ | Positive partial charge |

# Atomic colour key

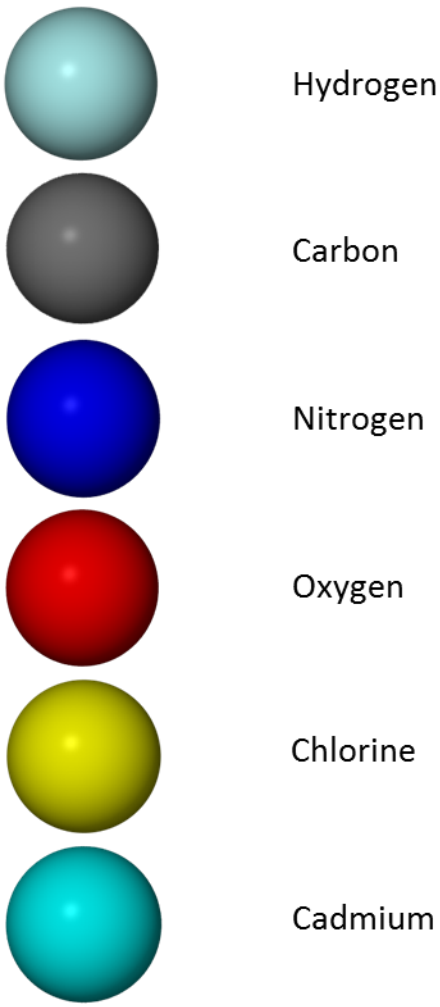

# Table of Contents

# List of Figures

# List of Tables

"Where nature finishes producing its own species, man begins, using natural things and with the help of its nature, to create an infinity of species"

**-Leonardo da Vinci**

# CHAPTER 1 | INTRODUCTION

## 1.1 Supramolecular chemistry

The field of supramolecular chemistry is relatively young, with most of its roots dating back to the late 1960s. However in the past few decades it has grown into one of the major fields in chemistry. Much of supramolecular chemistry arose from developments in macrocyclic chemistry, particularly the development of macrocyclic ligands for metal cations. Later on Donald Crams' work on cyclophanes, spherands, carcerands, and Jean-Marie Lehn's work on cryptands shaped many developments in the field.[1]

Supramolecular chemistry is a multi- and interdisciplinary field that draws from a broad scope of science, including all major fields of chemistry, physics and biology.[2] It can be defined as the study of systems constructed by the intelligent use of pre-organised templates. Furthermore, its broad purpose is to design and synthesise new molecular systems from which novel materials that possess unprecedented properties and applications can be shaped.[3]

When molecules in a solid are arranged in an ordered pattern in all three spatial directions, a crystal is formed. The crystal structure results from a balance between attractive and repulsive forces between molecules (subunits). These forces can be both directional and non-directional and operate over a range of distances. To a greater or lesser extent the design and interaction patterns between the crystal's components "programme" its properties. In supramolecular chemistry these molecular interactions are evaluated in order to understand how structure-property relations arise, and with this knowledge scientists strive to "engineer" novel materials.[3]

## 1.2 Crystal engineering

Desiraju defined crystal engineering as *"…the understanding of intermolecular interactions in the context of crystal packing and the utilization of such understanding in the design of new solids with desired physical and chemical properties."* [4] Later he went on to say that crystal engineering is comprised of three distinct strategies; *"… (i) the study of intermolecular interactions; (ii) the study of packing modes in the context of these interactions with the aim of designing a strategy for crystal construction and; (iii) the study of crystal properties."* [5]

During the first decade of crystal engineering most of the research in the field was devoted to the systematic and detailed examination of structural data such as packing patterns. Among others,

these studies enabled researchers to identify hydrogen bond preferences in various functional groups, and they are the foundation on which we build today. Single crystal X-ray diffraction (SCD) is a tool with which we can (with extreme accuracy) determine the three dimensional geometry of the atoms and molecules that compose a crystal and deduce their interaction patterns.[6] Today, SCD is far easier than when the Braggs shared the Nobel prize for the analysis of crystal structures by means of X-rays.[7] In addition, we have important tools such as the Cambridge Structural Database[8] (CSD), which contains a wealth of structural data. Furthermore, we can quickly and conveniently carry out SCD studies and, in conjunction with other analytical techniques, analyse structure-property relationships of crystalline compounds.

One of the interests within the field of crystal engineering is the study of inclusion compounds. These compounds are comprised of a host framework (or a lattice) that includes guest molecules, together known as host-guest assemblies. Host-guest assemblies have been shown to possess properties such as porosity, magnetism, anomalous thermal expansion, non-linear optics and mechanical properties.[9,10] These properties are of interest to us, especially if we can tailor materials to suit our needs.

## 1.3 The nature of supramolecular interactions

A single crystal can be thought of as an assembly of molecular objects, linked together in a regular fashion and extending in 3D space. The formation of a crystal is a thermodynamic process where self-assembly from a disordered system results in an organised structure as a consequence of local interactions between a set of building units (molecules). A vast array of supramolecular assemblies is possible with a given set of building units. Moreover, experimental conditions such as solvent choice, temperature, pressure and light can extend this range to different structures consisting of the same building units (polymorphs).[11,12] Supramolecular chemistry is the study of intermolecular or non-covalent interactions between molecules in molecular assemblies. In order to fully understand the supramolecular system the interplay of all interactions between the host and guest, as well as their surroundings, should be considered.[13]

Non-covalent interactions encompass a range of attractive and repulsive forces. The forces range in strength from 2 kJ $mol^{-1}$ for dispersion interactions to as much as 300 kJ $mol^{-1}$ for ion-ion interactions, although non-covalent interactions most often consist of hydrogen-bonding or π-cloud interactions. Nevertheless, other forces such as van der Waals interactions can be of crucial importance in supramolecular assemblies.[12, 14]

Interactions that direct crystal structure formation can broadly be classed into two categories. Firstly, there are medium-range forces that include C···H, C···C and H···H interactions. Secondly, there are long-range electrostatic forces between heteroatoms such as halogens, oxygen, sulphur and nitrogen, as well as between heteroatoms and carbon or hydrogen. Hydrogen bonds (including CH···π bonds) and halogen bonds are considered to be some of the most important interactions in supramolecular structure design.[10, 15]

Figure 1.1a represents a typical hydrogen bond. It is a particular kind of dipole-dipole interaction between: (i) a hydrogen atom attached to an electronegative (or electron-withdrawing) group (proton donor **D**) and (ii) a neighbouring molecule or functional group (proton acceptor **A**). Hydrogen bonding is directional and varies in strength from 4-120 kJ $mol^{-1}$.[16] Hydrogen-bonded Organic Frameworks (HOFs) are excellent examples of supramolecular systems that are primarily held together by hydrogen bonding, and they can be porous and thermally stable.[17,18] This shows that hydrogen bonds may individually be relatively weak but combine to form strong networks.

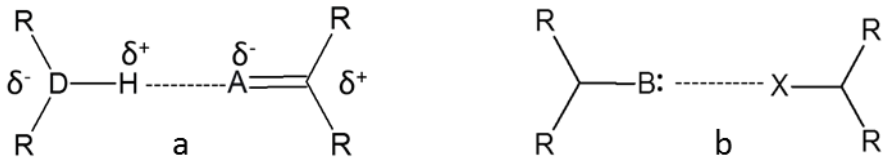


***Figure 1.1**: (a) A hydrogen bond is a dipole-dipole interaction with a proton donor (D) and proton acceptor(A). (b) A halogen bond occurs between a halogen atom(X) and a Lewis base(B).*

Halogen bonding is an attractive donor-acceptor interaction between an electrophilic area on a halogen atom and a Lewis base (Figure 1.1b). The highly directional nature of these interactions is based on the orbital-axis orientation of the Lewis base electrons. Halogen bonding strength ranges between 10 and 200 kJ $mol^{-1}$.[10,12]

Weaker electrostatic interactions such as π-π stacking are non-directional, with bond strengths ranging between 0 to 50 kJ $mol^{-1}$, allowing for more flexible or transformable molecular assemblies. These interactions are based on C···C and C···H interactions and are generally categorised as face-to-face (Figures 1.2a and 1.2b) or edge-to-face (Figures 1.2c and 1.2d) stacking. These interactions arise from the negatively charged π-electron cloud interacting with the positively charged σ-framework of an adjacent molecule.[1, 10]

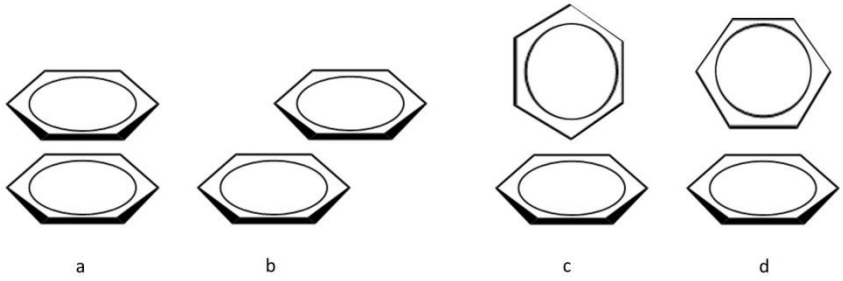


***Figure 1.2**: Possible π stacking arrangements. (a) Parallel face-to face, (b) offset face-to-face, (c) T-shaped edge-to-face and (d) Y-shaped edge-to face.[19]*

In hybrid materials that consist of inorganic and organic components the most dominant directional interaction is the coordination bond. The coordination bond is an ion-dipole interaction between an acceptor metal cation and a donor ligand. The interactions are mostly electrostatic in nature and their bond enthalpies range from 50 to 200 kJ $mol^{-1}$.[1] Metal-organic frameworks (MOFs) and metallocycles are examples of hybrid materials that consist of organic ligands coordinated to multiple metal cations. The specific geometry that arises from the metal's available d and f-orbitals provides the supramolecular chemist with a convenient tool to predict and control the architecture of hybrid materials.[12] An important benefit of the coordination bond in terms of structural flexibility is that it allows slight angle deformations, which in turn allow dynamic transformations in the solid state.[10]

## 1.4 Inclusion compounds

In 1948 H. M. Powell defined a host-guest assembly as an inclusion compound "*in which two or more components are associated without ordinary chemical union, but through a complete enclosure of one set of molecules in a suitable structure formed by another*".[1] In modern day chemistry host-guest assemblies can be categorised into two major classes according to the relative topological relationship between the host and its guest. Cavitands can be described as hosts with intramolecular cavities such that the host-guest aggregate is referred to as a cavitate. On the other hand, clathrands are hosts with extramolecular cavities, which upon host-guest aggregation are referred to as clathrates. The distinction between these two classes is illustrated in Figure 1.3.[1]

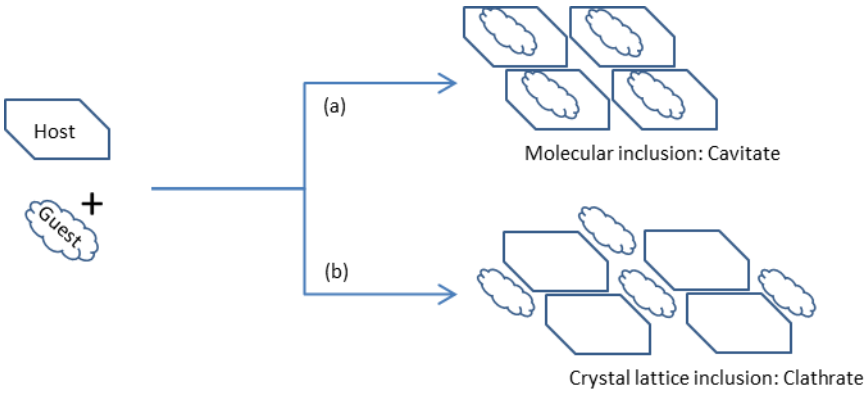


***Figure 1.3**: Illustration of the difference between a cavitate and a clathrate. (a) A cavitand is converted to a cavitate upon guest inclusion within the host. (b) A clathrand is converted to a clathrate when guests are included between the host molecules.*

Inclusion compounds are interesting to study because many of their macro properties can be interpreted in terms of their intermolecular interactions. In particular, the topology of the host-guest assembly allows supramolecular chemists to explain properties such as gas storage and separation, thermal stability, anisotropic expansion and non-linear optics. An application of inclusion compounds is in the crystal engineering of porosity. When one engineers porous compounds the aim is to produce robust frameworks or scaffolds from which the guests can be removed without rearrangement of the host lattice to a close-packed structure. An additional objective is to synthesise host frameworks that can accommodate a range of guest molecules that are selective for guests of a particular geometry or electrostatic topology.[11,16]

## 1.5 Porosity

There is a need for the development of robust porous materials due to their many applications such as drug delivery, chemical purification and pre-or post-combustion gas storage and separation. Molecules in crystals are driven by enthalpic gain to maximise attractive forces and minimise repulsive forces. This generally results in a crystal wherein molecules are as closely packed to one another as possible.[20] Therefore, molecular crystals with open channels or discreet lattice voids larger than about 25 $Å^3$ are rare. The intriguing phenomenon of porosity has resulted in the crystal engineering community devoting much attention to the development of materials that remain porous when guests are removed to yield what is known as the apohost. One engineering strategy is the crystallisation of irregularly shaped molecules such as calix[n]arenes or metallocycles that cannot close-pack in the solid state and thus possess inherent porosity. The advantage of engineering a material with porosity is that the cavities and channels of the host can be functionalised in order to incorporate host properties such as guest affinity.[9]

Porosity should adhere to two requirements. Firstly, the host's permeability should be demonstrated and secondly, porosity should apply to a specific host phase. Moreover, porosity can be subdivided in three categories:

(i) *Conventional porosity* refers to the standard notion of porosity, where guest molecules can be exchanged or removed without disrupting the size or shape of the host framework.[9]

(ii) *Transient porosity* describes hosts that allow guest transport without the presence of permanent channels.[9]

(iii) *Virtual porosity* is a fabricated porosity in which no permeability can be proven. For example, it can be illustrated by deleting small molecules (such as solvent molecules) from the structure file in order to show open channels or voids in the packing diagram, that do not exist otherwise.[9]

Of the three types of porosity, transient porosity is arguably the most unusual and interesting, because it occurs in materials that are porous without containing pores. Indeed, it seems absurd that guests can be exchanged or removed from a material that possesses no channels between voids. However, research by our group (and several others) has provided ample examples of such systems, one of which is described in this dissertation.[9,21-26] Although no permanent channels can be mapped to interconnect the voids, these crystals still allow volatile guests to enter, yielding single-crystal to single-crystal transformation of the structure. The phenomenon has been explained by dynamic motion of the host complexes, which allows momentary guest diffusion to take place.[9]

## 1.6 Gas sorption

The process of gases being taken up into a material is collectively known as sorption, and includes absorption and adsorption. The former is the process where a guest is taken up into the bulk volume of the absorbent whereas the latter involves a surface interaction between the host and guest. A molecule can either be physically (physisorption) or chemically adsorbed (chemisorption). During physisorption, the guest undergoes an exothermic van der Waals interaction with the host in the order of 20 kJ $mol^{-1}$.[27-29] This energy, albeit small, has a cumulative effect that drives the assembly towards a global minimum.[30] The small change in enthalpy keeps the guest molecule's geometry intact, even if it is distorted. Chemisorption, on the other hand, is a process where a guest forms a bond (usually covalent) with the host and such interactions can involve an order of magnitude greater enthalpic gain relative to physisorption.[28,29]

With regard to this dissertation, gas sorption in crystals is defined as the association of a guest molecule with the internal or external surface of a host through physisorption resulting from non-covalent intermolecular interactions between the host and guest.

A sorption isotherm represents the uptake of a guest by a host material at a constant temperature, and describes the relationship between the number of guest molecules absorbed and the equilibrium pressure. Three factors influence how a host takes up a guest:[10]

(i) The size/shape of the guest;

(ii) Thermodynamic considerations, such as host-guest interactions;

(iii) Kinetic effects, such as rate of diffusion.

The two methods of recording a sorption isotherm are volumetric and gravimetric sorption. In volumetric sorption, the amount of gas/solvent that is absorbed is measured by monitoring changes in pressure at a fixed volume. Gravimetric sorption records the amount of gas/solvent sorbed by measuring the change in the weight of the host at a constant pressure.

The International Union of Pure and Applied Chemistry (IUPAC) has categorised sorption isotherms into six categories (see Figure 1.4). The classification is based on an extensive literature survey by Brunauer in 1985.[31] It was realised that the pore size and type of sorption process leads to different sorption isotherms.[32]

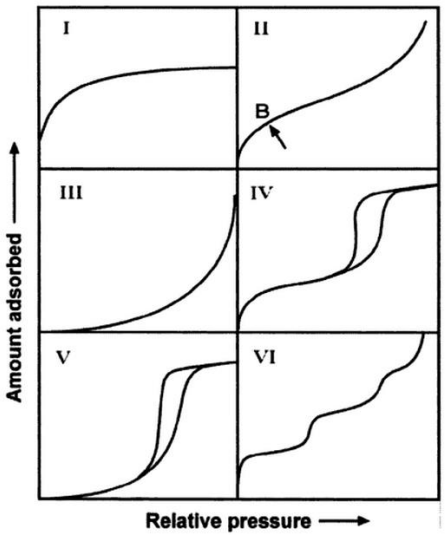


***Figure 1.4**: The IUPAC classification of sorption isotherms[31]*

A type I isotherm is obtained when sorption is limited to, at most, only a few layers of guest molecules on the surface of the host. The isotherm is reversible and most of the sorption occurs at lower pressures with an asymptotic approach to saturation. Microporous materials (with pore

diameters < 2 nm) often display type I sorption isotherms where the host saturation is limited to the amount of accessible pore space.[32,33]

Type II isotherms are commonly obtained with macroporous hosts (with pore diameters > 50 nm). The adsorption is an unrestricted mono-multilayer adsorption process, and the inflection point **B** indicates where monolayer coverage is complete and multilayer adsorption begins. [32,33]

Type III isotherms are convex and reversible. They are indicative of relatively weak host-guest interactions and stronger guest-guest interactions.[32]

Type IV isotherms are encountered for mesoporous materials (with pore diameters between 2 and 50 nm). As with type II isotherms, the inflection point indicates monolayer-multilayer adsorption. The limited uptake of guests results in a plateau in the isotherm. The most characteristic part of the isotherm is that the adsorption and desorption do not follow the same path, which can be associated with the condensation of guests in the host pores. [32,33]

Type V isotherms show hysteresis and pore condensation as for type IV isotherms. In addition, the convex curve indicates weak host-guest interactions, similar to those of type III isotherms.[32]

Finally type VI isotherms indicate stepwise multilayer adsorption on a uniform non-porous surface, particularly on non-polar adsorbates. As in other multilayer adsorption processes, a step occurs when a new layer of adsorption commences.[32]

## 1.7 Host-Guest selectivity

Host-guest assemblies involve the interplay of long-range electrostatic interactions as well as van der Waals dispersion interactions. In these systems the guest can be a volatile solid, a gas or a solvent.[10] Single crystal X-ray diffraction is one of the most powerful techniques to elucidate these interactions and subsequently determine how interactions in the host-guest assembly give rise to properties such as selectivity. In this dissertation the guests are exclusively gases and much emphasis is placed on the selectivity between a host and guest.

Extensive research over the past few years has been focused on the synthesis and characterisation of microporous materials (such as metallocycles) that have a high capacity for gas storage, or that can discriminate between gas species for gas separations.[34,35] Conventional wisdom dictates that porous materials with large surface areas are better for guest storage, whereas materials with restricted guest-accessible spaces are better able to discriminate between guests.[21] Understanding the host-guest interplay during the guest-uptake process is key to engineering

selective porous materials. Such knowledge could allow for the integration of specific functional groups into the host with the aim of increasing the affinity or selectivity for specific guests.[10]

It is vital to recognise and understand why selectivity is such an important aspect in host-guest chemistry. In a recent publication, Holst *et al.*[36] put the practical need for engineering of selectivity into perspective. They pointed out that gas storage and separation applications of porous materials have been investigated intensively, although many technical challenges have crippled their advancement in industry. Current porous materials simply do not absorb enough gas to meet the US Department of Energy targets under practical physical conditions. For example, MOF-200 and MOF-210 with large surface areas have been shown to store carbon dioxide up to 2.4 times their own weight; however a pressure of 50 bar is required for maximum occupancy. These conditions are not practical for the pre- and post-combustion capture of carbon dioxide. Moreover, the carbon dioxide is often mixed with nitrogen, water and acidic gases such as sulphur dioxide. Surface area is clearly not the key challenge here; instead it is important for the host material to have an affinity for the guest.[36]

If material scientists want to develop materials that can separate or store large amounts of gas on an industrial scale, selectivity will be one of the most important requirements. It is therefore important that selectivity is clearly defined and rigorous tests are in place to confirm actual selectivity as opposed to virtual selectivity. Currently, competition experiments are the best way to determine actual selectivity. However, these experiments require specialised equipment and a large amount of experimental data. Many research groups circumvent this problem by utilising theoretical models to calculate selectivity, and the variables used in the model are deduced from single-gas sorption isotherms. These models have given reliable results in many simple systems.[37] However, as will be clarified in this dissertation, there are more variables to be considered for an actual mixed-gas system. For example, different guests may form a hetero-dimer, which can act as a single unit during sorption which can influence how guests are adsorbed in the hosts. Chapter 3 expands on the theoretical and practical aspects of selectivity.

## 1.8 Computational chemistry overview

Computational chemistry, in essence, is a powerful tool for explaining and predicting physical observations at the molecular level, and is considered as the mathematical description of chemistry. Thus, it is crucial for understanding host-guest chemistry.[38,39]

With regard to this study, computational chemistry was used to:

(i) Describe the electrostatic potential that guests experience within a host lattice;

(ii) Describe the lowest energy geometries of the guests within the host, and the associated single-point energies.

Molecular modelling encompasses all theoretical methods that are used to describe the behaviour of molecules, and is generally classified into three groups: force-field methods, quantum mechanical methods and semi-empirical methods. Force-field methods are used to describe the potential energy of a system in terms of classical Newtonian mechanics. Quantum mechanical (or *ab initio)* methods rely on a wavefunction that is based on the Schrödinger equation. On the other hand, semi-empirical methods are a combination of classical mechanics and the Schrödinger equation. These techniques are widely used by computational chemists; however *ab initio* and semi-empirical methods are more commonly used as they calculate the electron density around a molecule in order to determine its energy and properties.[39,40]

In *ab initio* methods the description of a molecule's electron density relies on the determination of a wavefunction that describes the electrons in the molecule. The problem with a wavefunction is that it is not a physical observable; it is a mathematical construct that is used to predict a statistical probability of electron density in or around a molecule. However, even though the wavefunction does not physically exist it provides good predictions of the energy and other physical properties of a molecule. DFT addresses the theoretical nature of the wavefunction by using the observed electron density of a molecule.[41]

There are several advantages to this approach. The first is that the method is based on properties that exist in real molecules, not on a hypothetical mathematical description. The second is that DFT methods only depend on the *x*, *y* and *z* coordinates of individual atoms to describe electron density, whereas the description of the wavefunction becomes more complicated with an increase in the number of electrons. As a result DFT calculations require less computing time and are more accurate. As one might expect there are major approximations in DFT calculations that affect the computing time and accuracy for molecules that are evaluated by DFT methods.[41,42] Nevertheless, the increased accuracy and reduced computing time of DFT made it the method of choice for the molecular modelling described in this dissertation.

### 1.8.1 Energy minimisation and single point energies

If the set of internal coordinates of a molecular system has been determined, DFT methods can be used to find the coordinates of the atoms that will account for the lowest energy of the system. All bond angles, bond lengths, dihedral angles and the relative energy between different conformations of a given system can be evaluated in order to determine the minimum energy conformation.[43] From a computational point of view the minimum potential energy is the energy at which the first derivative with respect to all variables (such as bond distances and torsion angles) is zero. When a system has reached this minimum energy conformation it is said that it has *converged* (or its geometry is optimised).[39]

There are many algorithms that can be used for minimisation (geometry optimisation) calculations. Care must be taken therefore when choosing an algorithm as current algorithms are written for specific chemical systems. For example, some can incorporate calculations with metal ions whereas others cannot.

Essentially, all algorithms have an energy function *F(x)* that describes all the parameters of the chemical system. By changing variables within the function (and in most cases applying corrections), the function converges to an energy minimum where all repulsive and attractive forces within the system are optimised.

One of the simplest algorithms that can describe this concept is *gradient descent*. In this method an arbitrary value for all the variables in the multivariable function *F(x)* is chosen to describe a point ***a*** on *F(x)* (see Figure 1.5). The energy that corresponds to the variables is calculated, and then the derivative of the function (*F'(**a**)*) is calculated. The variables of point ***a*** are then adjusted to describe a subsequent point (***b***) on *F(x)* that is in the direction of *–F'(**a**).* The process is iterated until *F'(x)* is equal to zero, which is where the local minimum is located.

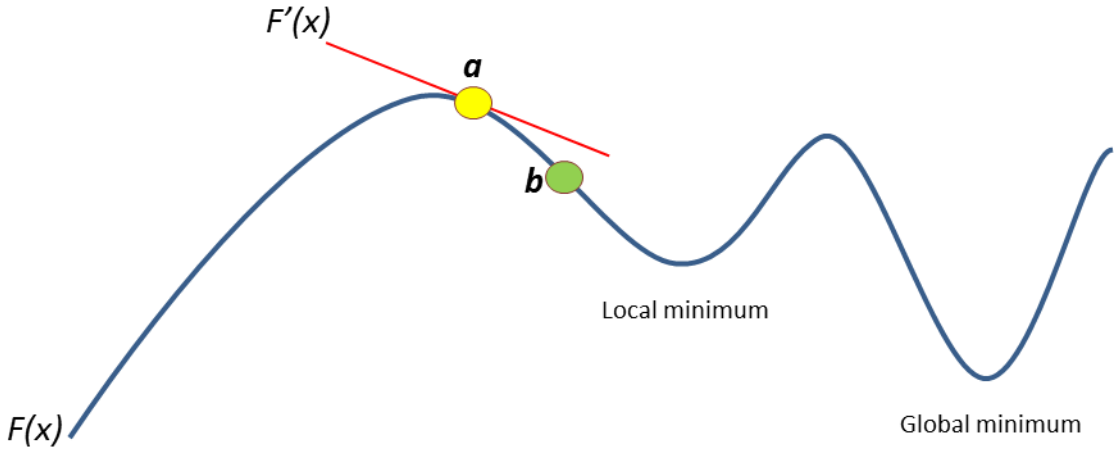


***Figure 1.5**: The gradient descent method is based on the observation that if a multivariable function, F(x), (blue line) is defined at point **a**, the fastest method to move from point **a** to a minimum would be to choose variables that describe points in direction of – f'(**a**) (red line). However, this often leads to convergence at a local minimum instead of a global minimum.*

The problem with the original method is that the variables defining point ***a*** were always chosen at random. In addition, ***a***'s variables will always be adjusted such that the energy described by *F(x)* will not increase. The implication is that, if an increased energy "barrier" separates a local minimum from the global minimum, the function would rather converge to the local minimum. Therefore, the arbitrary variables that define ***a*** in the initial function have a large impact on the accuracy of the results. In order to correct such problem, more complex codes have been developed to implement correction functions, thus resulting in more accurate data.

With regard to this dissertation a method known as *density mixing*[44] was used. In this method the energy and variables at the end of a number of minimisation steps are combined (mixed) and the combination of variables is used to drive the function to convergence. This method can therefore overcome the barrier that separates local minima from the global minimum. In addition, a method that speeds up convergence, known as *preconditioning*[45], was incorporated in the calculation. In essence it determines a rough estimate of the errors in the next optimisation step's variables, and determines more accurate variables to use in the calculation. In addition, a *Grimme's*[46] dispersion correction method was incorporated into the calculation to account for van der Waals interactions, which are not correctly described during DFT calculations. Grimme corrections are important because van der Waals interactions such as London dispersion can have a significant impact on the physical properties of a material.

Single point calculations at a higher level of theory are often performed on a converged structure in order to obtain a more accurate value for the optimum-geometry energy.[6]

## 1.9 Aims and objectives

The aim of the research described in this dissertation was to study the host-guest interplay in a transiently porous metallocycle. More specifically, the simultaneous interaction of acetylene and carbon dioxide with the metallocyclic host was explored in order to explain true selectivity. Acetylene and carbon dioxide have similar dimensions and similar boiling points but inverse electrostatic profiles. When only one of the two gases is adsorbed its orientation within the host is governed by its electrostatic profile and relative to one another the molecules are offset by approximately 45 degrees within the host. Moreover, the ideal adsorb solution theory predicts that more acetylene than carbon dioxide will be adsorbed from a mixture of acetylene and carbon dioxide, but it is described how guest-guest and guest-host interactions can influence this predicted selectivity. Various analytical techniques such as infrared spectroscopy as well as computational chemistry were used to elucidate the nature of the binary-gas-host interactions. Furthermore a Hydrogen-bonded Organic Framework (HOF) was synthesised and its properties, including thermal stability and host-guest interactions, were studied. The molecular interactions between the hosts and guests were elucidated using single-crystal X-ray diffraction as well as other adapted analytical techniques.

The main objectives were:

(i) The construction of new instruments, namely a volumetric sorption analyser and a multi-purpose gas cell, and the adaptation of commercial analytical instruments to undertake analysis such as high-pressure solid-state fluoroscopy and solid-state high pressure Raman spectroscopy.

(ii) To determine if and how both acetylene and carbon dioxide are absorbed in the metallocyclic host with the aid of analytical techniques such as SCD and infrared spectroscopy.

(iii) To elucidate and confirm the observed spectroscopic and sorption results with the aid of computational chemistry, more specifically to use crystallographic data to build models, to calculate single point energies and create electrostatic profiles with the aid of CASTEP, Dmol$^3$ and VAMP molecular mechanics methods.

(iv) To synthesise a HOF and to study its inclusion of guests, thermal properties and to use the framework as a model compound in the development of a novel analytical technique.

## 1.10 Outline of dissertation

The main objective of this study was to explore some structure-property relationships in porous molecular crystals. The first part of the study explores adsorption selectivity in porous materials, whereas the second part concerns itself with a study of the structure-property relationships of a hydrogen-bonded organic framework.

In Chapter 2 the experimental techniques and instrumentation used during this study are described.

Chapter 3 discusses the sorption selectivity of a porous material. A compound is generally said to be selective for the adsorption of one gas over another if the single-gas isotherms show that one gas is adsorbed to a greater extent than the other. In addition, theory is frequently used in the industry to predict adsorption selectivity based on single-gas sorption isotherms. To this end a previously reported metallocycle with discrete void space, which can include either two acetylene or two carbon dioxide molecules was studied. The previous study established that the metallocycle shows a preference for acetylene sorption over carbon dioxide. The aim of the present study was to investigate whether the metallocycle's adsorption would change when presented with a 1:1 molar mixture of the two gases. As part of this the role of guest-guest and guest-host interactions in influencing the adsorption selectivity of the host was investigated. Single-crystal X-ray diffraction studies and infrared analysis were used to show that when the metallocycle is exposed to a gas mixture it adsorbs one molecule each of carbon dioxide and acetylene in each void space. DFT studies were used to determine the interaction energies between the guests and between the host and guests in order to justify the simultaneous adsorption. In addition, the DFT studies were used to shed some light on the electrostatic potential that the guests in the single- and mixed-gas systems experience when they are included in the host.

In Chapter 4 the structure-property relationships of a porous hydrogen-bonded organic framework (HOF) are described, because little attention has been devoted to these frameworks owing to their low stability upon guest removal. Nevertheless, some HOFs possess useful properties such as catalytic activity and gas separation and storage abilities, which warrants a fundamental study of such a compound. Initially, adapted synthetic and activation methods of HOF-8 are discussed. Then, there is a brief discussion regarding the HOF's ability to undergo a phase transformation or thermal expansion, with reference to DSC, variable temperature PXRD and variable temperature SCD analysis. This is followed by a comprehensive sorption study using carbon dioxide, nitrogen, ethylene, ethane, methane, propane and butane gases, and the sorption

behaviour of the HOF is explained in terms of quadrupole moments of the gases and size/shape exclusion. The next part of the chapter describes the use of SCD structure elucidation to explain how the molecular subunits of HOF-8 assemble into crystals that have relatively high thermal stability, followed by a postulation of why there is seemingly selective inclusion of chloroform when the crystals are grown from a methanol/chloroform mixture. The chapter ends with an introduction to a novel hot stage-mass spectrometry analytical technique, and two examples are used to describe what useful information can be gained with a single experiment.

Chapter 5 presents a summary and a general conclusion of the work discussed in Chapters 3 and 4.

## 1.11 References


(1) Steed, J. W.; Atwood, J. L. *Supramolecular Chemistry*; John Wiley & Sons: West Sussex, 2000.

(2) Ungaro, R. *Supramolecular science: Where it is and where is it going*; Kluwer Academic Publishers: Dordrecht 1998.

(3) Jones , W.; Rao, C. N. R. *Supramollecular Organization and Materials Design*; Cambridge University Press: Cambridge, 2002; Vol. 1.

(4) Desiraju, G. R. *Crystal Engineering, the Design of Organic Solids* Elsevier: Amsterdam, 1989.

(5) Desiraju, G. R. *J. Chem. Sci.* **2010**, *122*, 667.

(6) Seddon, K. R.; Zaworotko, M. *Crystal Engineering: The Design and Application of Functional Solids*; Kluwer Academic Publishers: Canada, 1999; Vol. 539.

(7) Authier, A. *Early Days of X-ray Crystallography*; Oxford, 2013.

(8) Davies, J. E.; Allen, F. H.; Galloy, J. J.; Johnson, O.; Kennard, O.; Macrae, C. F.; Mitchell, E. M.; Mitchell, G. F.; Smith, J. M.; Watson, D. G. *J. Chem. Inf. Comput. Sci.* **1991**, *31* 187.

(9) Barbour, L. J. *Chem. Commun.* **2006**, 1163.

(10) Grobler, I. PhD, University of Stellenbosch, 2013.

(11) Tsoucaris, G.; Atwood, J. L.; Lipkowski, J. *Crystallography of Supramolecular Compounds*; Kluwer Academic Publishers: Erice, 1995; Vol. 480.

(12) Steed, J. W.; Gale, P. A. *Supramolecular Chemistry: From Molecules to Nanomaterials*; Wiley, 2012.

(13) Steed, J. W.; Atwood, J. L. *Supramolecular Chemistry*; Wiley: West Sussex, 2013.

(14) Lindoy, L. F.; Atkinson, I. M. *Self-assembly in Supramolecular Systems*; 1 ed.; Royal Society of Chemistry: Cambridge, 2000.

(15) Desiraju, G. R. *The Crystal as a Supramolecular Entity*; 1 ed.; Wiley: West Sussex, 2008; Vol. 1.

(16) Atwood, J. L.; Steed, J. W. *Encyclopedia of Supramolecular Chemistry*; Marcel Dekker: New York, 2004.

(17) He, Y.; Xiang, S.; Chen, B. *J. Am. Chem. Soc.* **2011**, *133*, 14570.

(18) Luo, X.-Z.; Jia, X.-J.; Deng, J.-H.; Zhong, J.-L.; Liu, H.-J.; Wang, K.-J.; Zhong, D.-C. *J. Am. Chem. Soc.* **2013**, *135*, 11684.

(19) Martinez, C. R.; Iverson, B. L. *Chem. Sci.* **2012**, *3*, 2191.

(20) Jones, W.; Rao, C. N. R. *Supramolecular Organization and Materials Design*; Cambridge University Press: Cambridge, 2008.

(21) Jacobs, T.; Lloyd, G. O.; Gertenbach, J.-A.; Müller-Nedebock, K. K.; Esterhuysen, C.; Barbour, L. J. *Angew. Chem. Int. Ed.* **2012**, *51*, 4913.

(22) Thallapally, P. K.; Kirby, K. A.; Atwood, J. L. *New J. Chem.* **2007**, *31*, 628.

(23) Thallapally, P. K.; McGrail, B. P.; Atwood, J. L. *Chem. Commun.* **2007**, 1521.

(24) Thallapally, P. K.; Lloyd, G. O.; Atwood, J. L.; Barbour, L. J. *Angew. Chem. Int. Ed.* **2005**, *44*, 3848.

(25) Cheih, C.; University of Waterloo: Waterloo, 2014; Vol. 2014.

(26) Atwood, J. L.; Barbour, L. J.; Thallapally, P. K.; Wirsig, T. B. *Chem. Commun.* **2005**, 51.

(27) Smith, I. W. M.; Cockell, C. S.; Leach, S. *Astrochemistry and Astrobiology*; Springer: London, 2012.

(28) McMurry, J. *Fundamentals of Organic Chemistry*; 7th ed.; Cengage Learning: Belmont, 2010.

(29) Verma, N. K.; Khanna, S. K.; Kapila, B. *Comprehensive Chemistry XII*; 7th ed.; Laxmi Publications: Daryaganj.

(30) Somasundaran, P. *Encyclopedia of Surface and Colloid Science*; 2nd ed.; Taylor & Francis: New York, 2006.

(31) Haul, R. A. W.; Moscou, L.; Pierotti, R. A.; Rouquerol, J.; Siemieniewska, T.; Everett, D. H.; Sing, K. S. W. *Pure Appl. Chem.* **1985**, *57*, 603.

(32) Lowell, S. *Characterization of Porous Solids and Powders: Surface Area, Pore Size and Density*; Springer, 2004.

(33) Rouquerol, J.; Avnir, D.; Fairbridge, C. W.; Everett, D. H.; Haynes, J. H.; Pernicone, N.; Ramsay, J. D. F.; Sing, K. S. W.; Unger, K. K. *J. Pure Appl. Chem* **2009**, *66*, 1793.

(34) Farha, O. K.; Eryazici, I.; Jeong, N. C.; Hauser, B. G.; Wilmer, C. E.; Sarjeant, A. A.; Snurr, R. Q.; Nguyen, S. T.; Yazaydın, A. Ö.; Hupp, J. T. *J. Am. Chem. Soc.* **2012**, *134*, 15016.

(35) Dias, H. V. R.; Diyabalanage, H. V. K.; Gamage, C. S. P. *Chem. Commun.* **2005**, 1619.

(36) Holst, J. R.; Cooper, A. I. *Adv. Mater.* **2010**, *22*, 5212.

(37) Novoa, J. J.; Braga, D.; Addadi, L. *Engineering of Crystalline Materials Properties: State of the Art in Modeling, Design and Applications*; 1 ed.; Springer: Dordrecht, 2008; Vol. 1.

(38) Young, D. C. *Computational Chemistry: A Practical Guide for Applying Techniques to Real World Problems*; Wiley: Canada, 2004.

(39) Marais, C. G. MSc, Stellenbosch University, 2008.

(40) Jensen, F. *Introduction to Computational Chemistry*; Wiley, 2013.

(41) Holm, C.; Arnold, A.; Fyta, M.; Institute for Computational Physics: Stuttgart, Germany, 2014; Vol. 2014.

(42) Lewars, E. *Computational Chemistry: Introduction to the Theory and Applications of Molecular and Quantum Mechanics*; 2nd ed.; Springer: London, 2010.

(43) Vlachakis, D. *An Introduction to Molecular Modelling, from Theory to Application*; Dimitrios P. Vlachakis, 2007.

(44) Kresse, G.; Furthmüller, J. *Phys. Rev. B* **1996**, *54*, 11169.

(45) Payne, M. C.; Teter, M. P.; Allan, D. C.; Arias, T. A.; Joannopoulos, J. D. *Rev. Mod. Phys.* **1992**, *64*, 1045.

(46) Grimme, S. *J. Comput. Chem.* **2004**, *25*, 1463.

# CHAPTER 2 | EXPERIMENTAL TECHNIQUES

The work presented in this dissertation involved the use of several common instrumental techniques and routine methodologies that are well documented; therefore they will only be discussed briefly. In addition, the software packages used that may not be familiar to the reader are discussed. Other apparatus and procedures that were specifically developed for this work are discussed in more detail.

## 2.1 Single-Crystal X-Ray Diffraction (SCD)

Diffraction data were collected either on a Bruker SMART Apex II CCD or a Bruker-Nonius Kappa Apex II CCD single-crystal diffractometer using graphite monochromated Mo-$K_\alpha$ radiation (λ= 0.71073 Å).[1] Both instruments are equipped with an Oxford Cryostream cooling system. Data reduction was carried out by means of standard procedures using the Bruker software package SAINT[2] and all empirical corrections to the data were performed using SADABS.[3,4] Crystal structures were solved by direct methods using SHELXS-97[5] and refined with SHELXL-97[5] within the X-Seed[6] environment. Hydrogen atoms were placed in calculated positions using riding models and assigned isotropic displacement parameters of 1.2 times that of their parent atoms for $CH_2$ and aromatic carbon atoms, and 1.5 times in $CH_3$ groups.

The supplementary material for all crystal structures elucidated as part of this study can be found on the attached CD, including the Crystallographic Information Files (CIF) along with the final SHELX '.res' and '.hkl' files

## 2.2 X-Ray Powder Diffraction (PXRD)

Powder X-ray Diffraction (PXRD) is often used to analyse the phase purity and crystallinity of a material. Therefore, one can use PXRD to confirm the correct host phase before undertaking experiments such as sorption. In addition, one can use variable temperature PXRD to determine if a crystalline material undergoes phase changes, thermal expansion, or decomposition as it is heated or cooled. In PXRD a gradual shift in peaks can be caused by thermal expansion or solvent loss, whereas a radical change in a powder pattern indicates that the host undergoes a phase change.

X-ray powder diffraction patterns were measured on a PANalytical X'Pert PRO instrument with Bragg-Brentano geometry using Cu-Kα radiation (λ = 1.5418 Å) and an X'Celerator detector with 2Θ scans in the range of 5-40°.

Sample preparation involved grinding single crystals with a mortar and pestle. Two sample stage configurations of the instrument were used: (i) A reflection-transmission spinner was rotated at 15 rpm during data collection in order to minimise preferred orientation contributions to intensity data; (ii) the sample was sealed within a capillary with an inside diameter of 0.5 mm and placed in the capillary spinner configuration. The temperatures for variable temperature data collections were regulated with a short-nozzle Oxford Cryostream 700+.

## 2.3 ThermoGravimetric Analysis (TGA)

TGA has a wide range of applications. For example, one can measure the increase in mass as temperature-related oxidation occurs in a material, or one can measure the amount of purge gas adsorbed at a constant temperature. However, TGA is most commonly used as an analytical technique to determine the temperature at which temperature-related solvent loss and sample decomposition occurs, as well as the relative amount of volatile content in the sample.

TGA traces were generated by measuring the percentage mass loss as the samples were heated at a constant rate in an adiabatic environment. TGA was carried out using a TA Instruments Q500 thermogravimetric analyser. The balance and sample were purged with dry $N_2$ at 50 ml $min^{-1}$, and the samples were heated at 10 °C $min^{-1}$. Thermograms were analysed with the TA Instruments Universal Analysis program.

## 2.4 Differential Scanning Calorimetry (DSC)

DSC is an analytical technique that measures the heat flow into or out of a sample, relative to a reference (often an empty sample pan), as a function of temperature and time.

Differential scanning calorimetry was performed using a TA instruments Q100 DSC. Typical samples of 3 to 10 mg were crimpled between an aluminium pan and a lid with two pin holes. Reference pans were prepared in the same manner. Nitrogen with a flow rate of 50 ml $min^{-1}$ was used as a purge gas for the furnace and liquid nitrogen was used as coolant for temperatures below ambient temperature. Both the maximum and minimum temperatures of the DSC traces were chosen depending on the sample. The resulting thermograms were analysed with the TA Instruments Universal Analysis program.

## 2.5 Gravimetric Gas Sorption

An Intelligent Gravimetric Analyser (IGA-002) by Hiden Analytical (Ltd) was used to measure all gravimetric sorption isotherms. The instrument measures precise changes in sample mass as a

function of pressure between 0 and 20 bar. Temperature was regulated by means of a Grant refrigerated recirculating bath with an accuracy of ± 0.05 °C. An accurate estimate of the sample density was required for buoyancy correction, and was determined from the single-crystal structures.

Data collection is controlled by Real-Time Processing computer software.[7-13] The software continually monitors for pressure/weight equilibrium. In this study a Linear-Driving-Force relaxation model was used, with each equilibrium point recorded when 99% of the model predicted mass gain was reached, or after two hours of equilibration.

## 2.6 Volumetric Gas sorption

The IGA could not be used to study the sorption of acetylene, as the balance mechanism in the instrument contains a winding of copper wire (exposure of acetylene to pure copper poses an explosion hazard). Therefore a volumetric sorption analyser that has been reported in the literature[14] was constructed. A detailed discussion of the construction and operation of the instrument follows.

### 2.6.1 Construction of a Volumetric Sorption Analyser

The method of recording volumetric isotherms is based on measuring changes in gas pressure over time in a constant volume and at a constant temperature. Figures 2.1 (a) and (b) show a schematic layout and a photograph of the volumetric sorption analyser respectively. The device was constructed from modular stainless steel Swagelok® and in-house brass components (the brass poses less of a threat to spontaneous combustion of acetylene than does pure copper). The device consists of two chambers A and B with volumes $\boldsymbol{V}_A$ and $\boldsymbol{V}_B$, respectively. In addition, each chamber incorporates its own high precision Wika® Eco-1 pressure transducer to monitor the gas pressure. The pressures in the chambers are isolated from the environment and from one another with valves $\boldsymbol{V}_1$ to $\boldsymbol{V}_3$. Valves $\boldsymbol{V}_1$ and $\boldsymbol{V}_2$ can be connected to a vacuum pump and the gas reservoir respectively. The device shown in Figure 2.1 (b) is housed in a refrigerator that contains a light bulb and fan (Figure 2.2). The refrigerator serves as an adiabatic environment. The temperature is regulated by the interplay between the refrigerator's continuous cooling and the heat produced by switching the light bulb on or off. The fan is used to ensure that the temperature is uniform throughout the refrigerator.

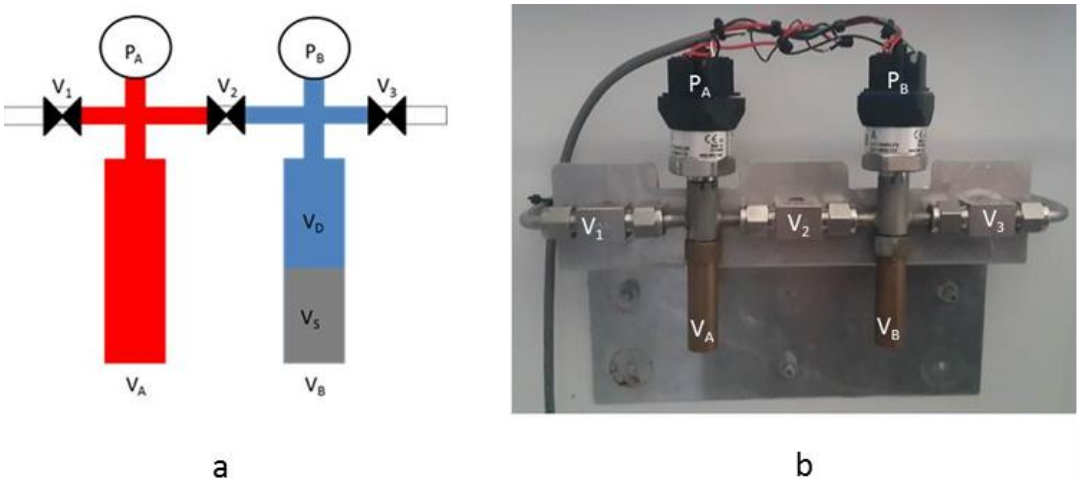


***Figure 2.1**: (i) A schematic layout and (ii) a photograph of the volumetric sorption analyser. $V_1$, $V_2$ and $V_3$ are ball valves; $P_A$ and $P_B$ are pressure transducers; $V_A$ and $V_B$ represent the volumes in chambers A and B, respectively. $V_D$ is "dead space" volume and $V_S$ is the sample volume. Collectively $V_B = V_D + V_S$.*

***Figure 2.2**: The adiabatic environment around the sorption device consists of a refrigerator, light bulb and fan.*

In this volumetric sorption method the volume of gas adsorbed during an experiment is calculated using the van der Waals equation of state (Equation 2.1), which relates gas pressure to the number of moles:

$$\left(P + \frac{n^2 a}{V^2}\right)(V - nb) = nRT \tag{2.1}$$

where $n$ is the number of moles, $P$ is the pressure, $V$ is the volume, $T$ is the temperature in Kelvin and $R$ is the universal gas constant. $a$ and $b$ are gas-specific constants; $a$ represents the magnitude of intermolecular attraction between gas molecules and $b$ represents the excluded volume of a gas molecule.

In this study a 1:1 molar mixture of acetylene and carbon dioxide was used. There are no *a* and *b* constants for gas mixtures such as these. Therefore, in order to calculate the volume of gas-mixture adsorbed we assumed that the *a* and *b* constants for the gas mixture are the average of the constants for acetylene and carbon dioxide: for acetylene *a* = 4.448 $L^2$ bar $mol^{-1}$ and *b* = 0.05136 L $mol^{-1}$, and for carbon dioxide *a* = 3.590 $L^2$ bar $mol^{-1}$ and *b* = 0.04270 L $mol^{-1}$ .[15] The gas-mixture's constants were approximated to be 4.019 $L^2$ bar $mol^{-1}$ and 0.04703 L $mol^{-1}$, respectively.

In order to test the validity of this assumption the data for the sorption of the gas mixture were used to plot three isotherms (Figure 2.3). For the red isotherm, acetylene's *a* and *b* constants were used to calculate the amount of adsorbed gas assuming that only acetylene was adsorbed. Similarly, for the blue isotherm, carbon dioxide's constants were used and for the green isotherm the assumed average *a* and *b* constants were used. The comparison shows that even if only acetylene or only carbon dioxide was adsorbed during a mixed-gas sorption experiment, there would be no substantial deviations from the sorption isotherm by using the average *a* and *b* constants. Therefore, if only acetylene or only carbon dioxide is adsorbed during mixed-gas sorption, the sorption isotherm would still be similar to either acetylene's or carbon dioxide's single-gas sorption isotherms, because the *a* and *b* constants that were assumed to be an average does not have a substantial effect on the profile of the sorption isotherm.

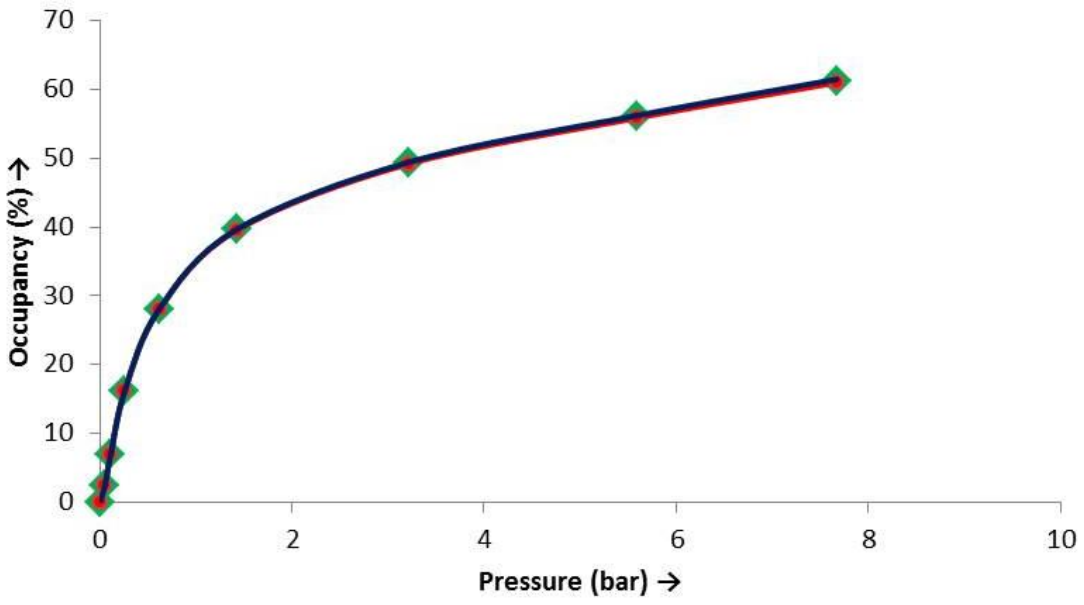


***Figure 2.3**: A comparison of sorption isotherms calculated from mixed-gas sorption data using the van der Waals equation of state a and b constants for acetylene (red), carbon dioxide (blue) and an average (green) shows that even if only acetylene or carbon dioxide was adsorbed during mixed-gas sorption the use of average a and b constants to calculate the isotherm would not have an substantial change in the isotherm's profile.*

Owing to the accuracy of the pressure transducers, the largest contribution to statistical uncertainty is the error in the calculated values of $\boldsymbol{V}_A$ and $\boldsymbol{V}_B$. Due to the nature of volumetric sorption and the values needed in the equation of state, there are crucial conditions that the sorption device should adhere to, including:[16,17]

(1) The determination of $\boldsymbol{V}_A$ and $\boldsymbol{V}_B$ should be accurate and precise;
(2) Accurate sample and dead volumes ($\boldsymbol{Vs}$ and $\boldsymbol{V}_D$ in Figure 2.1 (a)) should be known;
(3) The device should be kept at a known and constant temperature;
(4) Accurate pressure measurements should be recorded;
(5) Long-term stability of the instrument with regard to electronic components, physical components and temperature should be maintained.

To prepare the instrument for sorption experiments, the pressure sensors and volumes of chamber *A* and chamber *B* have to be calibrated. The Wika® Eco-1 transducer has a linear voltage output of 0 to 10 V over its specified pressure range. In order to calibrate the pressure transducer the transducer is exposed to a series of known pressures and the output voltage of the transducer recorded. A linear plot relates pressure (*P*) to the output voltage (*V*) of the transducer. The equation of the linear plot is given in Equation 2.2; where *C* is the y-axis intercept and is the *z* the slope of the curve.

$$P = zV + C \tag{2.2}$$

After the pressure transducers were calibrated the camber volumes were determined using nitrogen gas, since it exhibits near ideal-gas behaviour and consequently the ideal gas law (Equation 2.3) could be used to derive the values of $\boldsymbol{V}_A$ and $\boldsymbol{V}_B$.

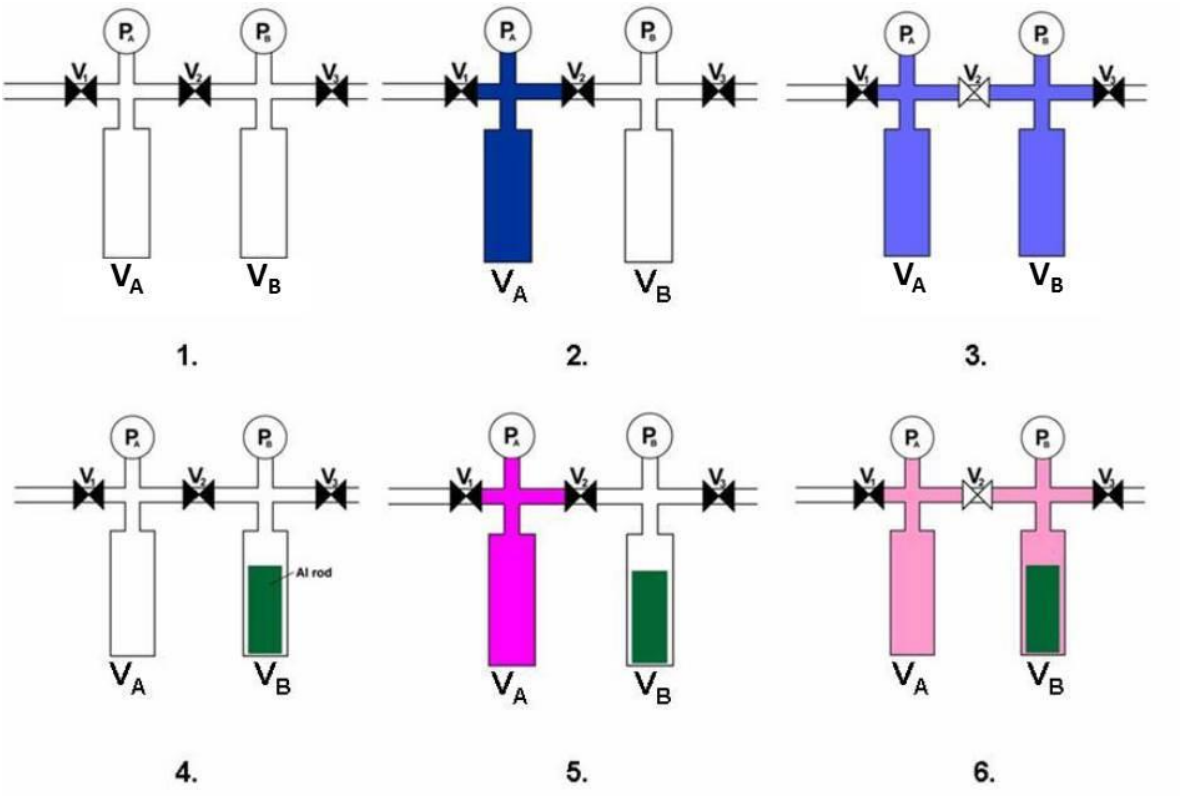


*Figure 2.4: The schematic illustration of the process used to calculate $V_A$ and $V_B$.*[17]

The six steps required for the calculation of volumes $\boldsymbol{V}_A$ and $\boldsymbol{V}_B$ are illustrated in Figure 2.4 and are as follows:

(1) Chambers *A* and *B* are evacuated.

(2) A gas at known pressure is introduced into chamber *A*. The number of moles introduced is calculated with the ideal gas law in Equation 2.3

$$P_1 V_A = nRT \tag{2.3}$$

(3) Valve $\boldsymbol{V}_2$ is opened, and the gas in $\boldsymbol{V}_A$ is equilibrated between volumes $\boldsymbol{V}_A$ and $\boldsymbol{V}_B$. The total number of moles of gas remains constant, therefore Equation 2.3 is expanded to:

$$P_2(V_A + V_{\boldsymbol{B}}) = nRT \tag{2.4}$$

(4) An aluminium rod of known volume ($\boldsymbol{V}_{Al}$) is inserted into chamber *B*, and both chambers *A* and *B* are evacuated.

(5) As in step one, a known pressure of gas is introduced into chamber *A* and the number of moles is calculated using Equation 2.5.

$$P'_1 V_A = n'RT \tag{2.5}$$

(6) Valve $\boldsymbol{V}_2$ is opened, and the gas in $\boldsymbol{V}_A$ is equilibrated between volumes $\boldsymbol{V}_A$ and $\boldsymbol{V}_B$-$\boldsymbol{V}_{Al}$. The total moles of gas remains constant, therefore Equation 2.6 becomes:

$$P'_2(V_A + V_B - V_{Al}) = n'RT \tag{2.6}$$

The constant volumes $\boldsymbol{V}_A$ and $\boldsymbol{V}_B$ are then calculated in the following manner:

$$P_1 V_A = nRT = P_2(V_A + V_{\boldsymbol{B}}) \tag{2.7}$$

Therefore:

$$\frac{P_1}{P_2} = \frac{(V_A + V_{\boldsymbol{B}})}{V_A} \tag{2.8}$$

Consequently:

$$\frac{P_1}{P_2} = 1 + \frac{V_{\boldsymbol{B}}}{V_A} \tag{2.9}$$

Similarly:

$$\frac{P\prime_1}{P\prime_2} = 1 + \frac{V_{\boldsymbol{B}}}{V_A} - \frac{V_{Al}}{V_A} \tag{2.10}$$

With the known values of $P_1$, $P_2$, $P'_1$ $P'_2$ and $V_{Al}$ the values of $V_A$ and $V_B$ can be determined by:

$$V_A = \frac{V_{Al}(P_2 P\prime_2)}{(P\prime_2 P_1) - (P_2 P\prime_1)} \tag{2.11}$$

$$V_B = \frac{V_{Al} P\prime_2 (P_1 - 1)}{P\prime_2 P_1 - P_2 P\prime_1} \tag{2.12}$$

### 2.6.2 A typical experiment: Theory and practice.

During the sorption experiment, data such as temperature and pressure are monitored and recorded in real-time with the aid of a computer. In a typical experiment a known mass (and volume) of an apohost sample is placed in the sample chamber *B*. The temperature of the system is allowed to equilibrate, during which time chambers *A* and *B* are evacuated. When the instrument and sample are stable at the experimental temperature the test gas is introduced into chamber *A*, while chamber *B* is kept under vacuum. When the pressure in $\boldsymbol{V}_A$ has equilibrated the pressure reading of $\boldsymbol{P}_A$ is recorded as $\boldsymbol{P}_{A\ initial}$. Valve $\boldsymbol{V}_2$ is then briefly opened and then closed. Once the pressure in $\mathbf{V_B}$ has equilibrated the pressure reading of $\boldsymbol{P}_A$ is recorded as $\boldsymbol{P}_{A\ end}$ and the pressure reading in $\boldsymbol{P}_B$ is recorded as $\boldsymbol{P}_{B\ eq}$.

The van de Waals equation of state is used to calculate the molar amount of gas that was introduced into the sample chamber ***B.***

$$n_{introduced} = n(P_{A\ initial}) - n(P_{A\ end}) \tag{2.13}$$

Consequently the molar amount of adsorbed gas can be calculated as:

$$n_{adsorbed} = n_{introduced} - n(P_{B\ eq}) \quad (2.14)$$

The number of adsorbed molecules can then be used to plot appropriate isotherms.

## 2.7 Environmental gas cell

An in-house environmental gas cell was used to collect crystallographic data under a controlled atmosphere of various gases. The gas cell can typically withstand 0 to 60 bar of pressure.

The gas cell consists of a 0.3 mm diameter Lindemann glass capillary fixed to a stainless steel nut using epoxy resin. The steel nut screws into a port on a nickel-coated brass cell and is sealed with an embedded rubber O-ring. On the other end of the brass cell there is stainless steel valve stem that also serves as a gas inlet port. The gas cell is screwed into a modified goniometer head (Figure 2.5), which is then mounted onto the diffractometer.

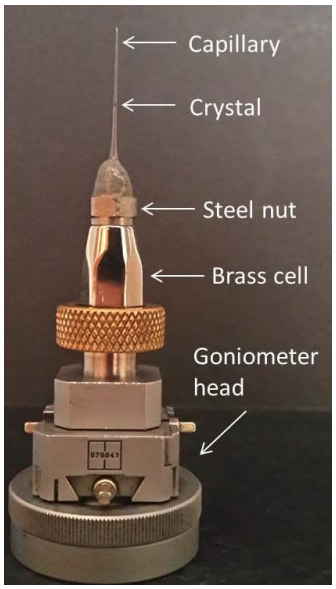


***Figure 2.5**: An environmental gas cell that allows SCD under a controlled atmosphere.*

Typically a Lindemann capillary is pre-sealed at the narrow end with a small flame, and is then fixed to the end of the stainless steel nut with epoxy resin to render the glass-to-metal seal leak-proof. Thereafter, a crystal suitable for SCD is selected and glued with epoxy resin to the end of a glass microfibre. The microfibre is inserted into the Lindemann capillary and then glued to the side of the capillary. Finally, the steel nut is screwed to the brass cell. During gas loading the gas cell is connected to a manifold via a detachable gas inlet arm.

## 2.8 Gas mixing device

During this study a 1:1 molar mixture of acetylene and carbon dioxide was used, and the gas mixture had to be uniform and of a known composition before sorption experiments could be performed. To obtain uniform gas mixtures a gas mixing device was constructed.

A photograph of the gas mixing device is given in Figure 2.6. The device has two reservoirs that are separated by three valves $V_1$, $V_2$ and $V_3$. $V_1$ and $V_2$ are 3-way valves that serve as a junction between the two reservoirs or inlet/outlet ports. A circulation pump separates $V_1$ and $V_2$ and therefore the two reservoirs. The pressure in each reservoir is monitored using an analogue pressure gauge.


***Figure 2.6**: Gas mixing device. The two reservoirs are connected by $V_3$. $V_1$ and $V_2$ are 3-way valves that serve as junctions between the two reservoirs and are separated by a circulation pump. Alternatively $V_1$ and $V_2$ can connect the reservoirs to inlet/outlet ports.*

The volumes and temperatures of the two reservoirs and the adjoining components are sufficiently identical. Therefore, according to the ideal gas law, the number of moles of gas introduced into both reservoirs would be equal if the pressure of gas introduced into the two reservoirs is equal. Typically the 1:1 molar gas mixture was prepared by pressurising both reservoirs to 15 bar of acetylene and carbon dioxide, respectively, with $V_3$ closed. $V_1$, $V_2$ and $V_3$ are then positioned to connect the reservoirs at both ends. The circulation pump then circulates the gases for 12 hours to form a uniform mixture.

## 2.9 Pressure vessel

A multi-purpose pressure vessel was constructed for Raman spectroscopy and fluoroscopy (Figure 2.7). The pressure vessel is equipped with 6 mm thick CaF windows that are transparent between 170-7800 nm and can withstand pressures above 60 bar.

The sample inside the cell had to be a firm pellet. The pellet was prepared by grinding single crystals of **1** to a fine powder, which was then compressed with 10 tons of pressure while under vacuum. A PXRD pattern of the pellet was compared to that of the pre-compressed powder (Figure 2.8) to ensure no phase changes had occurred when the pellet was prepared.

***Figure 2.7**: Multi-purpose pressure vessel for high-pressure fluorescence and high-pressure Raman spectroscopy experiments.*

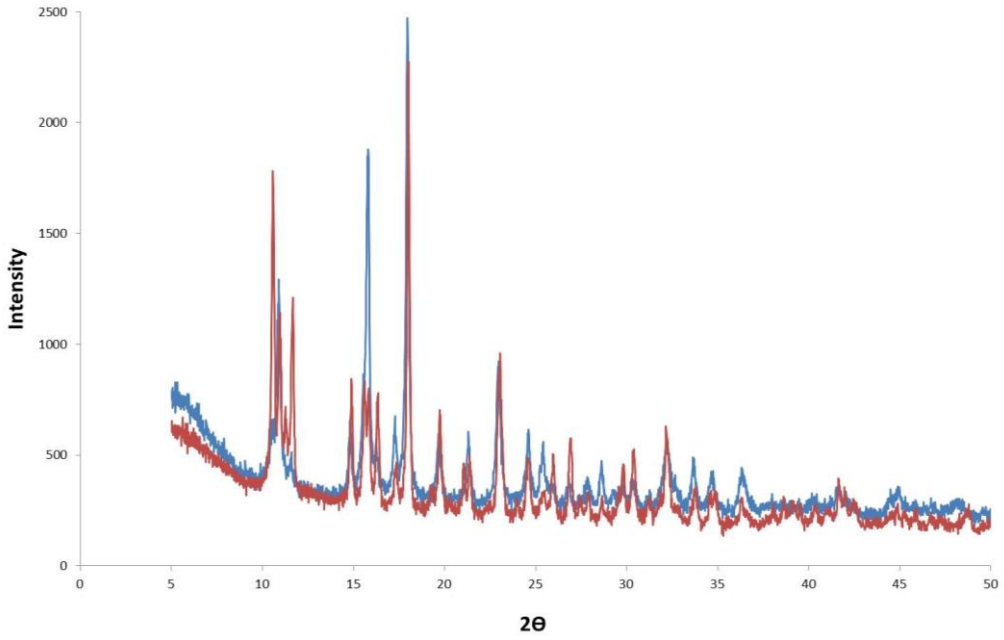


***Figure 2.8**: PXRD traces of **1** as a pellet (blue) and as a pre-compressed powder (red).*

## 2.10 Infrared spectroscopy

The pressure vessel could not be used in standard infrared (IR) transmission experiments because the IR bands of the gases in the head space relative to those for the adsorbed gases were much stronger. Therefore the bands of the adsorbed gases were obscured by those of the headspace gases. One way of obtaining stronger adsorbed-gas signals is to increase sample thickness, and therefore the relative concentration of adsorbed gas. However, a slight increase in sample thickness caused a substantial reduction in the laser's transmission, leading to useless data. In order to circumvent the problem, the sample was placed in a high-pressure sample holder and exposed to $C_2H_2$, $CO_2$ or the gas-mixture for 48 hours after activation. Thereafter, the sample chamber was cooled to -78 °C. The sample was then removed from the chamber and analysed with Attenuated Total Reflectance-IR (ATR-IR). The ATR-IR allows analysis without headspace gas, thus only recording the bands of the adsorbed gases.

The analyses were performed on a Thermo Nicolet Nexus 670 Fourier transform IR spectrometer. The resolution was set to 2 $cm^{-1}$ representing data point spacings of 0.964 $cm^{-1}$. The spectrometer is equipped with a Ge-on-KBr beam splitter and DTGS/CsI detector, and was continuously purged with high purity nitrogen gas from AFROX during recording. Operation and data manipulation were carried out with basic OMNIC package.

## 2.11 Fluorescence spectroscopy

Fluoroscopic analysis was carried out with a Hitachi F-3000 spectrometer equipped with a xenon lamp. Samples were analysed at 0 °C using a scan speed of 60 nm $min^{-1}$ and a response time of 2 seconds. The excitation and emission bandpasses were set to 2.5 and 3 nm, respectively. Excitation wavelengths are sample dependant, and are given in the relevant sections of this document.

## 2.12 Hot stage–Mass spectrometry (HS-MS)

During the course of this work a novel coupling between two instruments allowed the development of a useful analytical technique (see Figure 2.9). The instrument consists of a temperature controlled pressure hot stage (HS) coupled to a mass spectrometer (MS) and is useful for observing the guest molecules released from a host and the change in the host's morphology during temperature induced guest loss while, simultaneously identifying the guest(s) that are released.

The temperature controlled pressure stage (THMS600PS) was supplied by Linkam Scientific Instruments and operated with the standard Linksys 32 software. The MS was supplied by Setaram and included a Stanford Research System (SRS) Residual Gas Analyser (RGA) head with a mass range of 1 to 200 amu. The RGA head is equipped with an electron impact ioniser and a quadrupole mass filter. Furthermore, the RGA has a Faraday-cup detector and a continuous dynode electron multiplier (CEM), which increases the detection limit to 5 x $10^{-14}$ torr.

In a typical experiment a sample is placed in the pressure hot stage, which is then sealed. The pressure hot stage is connected to the MS with modular Swagelok components. Subsequently the hot stage is evacuated to 1 x $10^{-5}$ bar. Thereafter, the Linksys 32 software is used to ramp the temperature at 10 °C $min^{-1}$ to a desired maximum temperature while images are captured at specific intervals, typically every 60 seconds. The mass spectrometer is set to pressure vs time mode to detect the principal mass signal of a species as a function of time, and the electron multiplier is used to increase sensitivity. The heating phase of the pressure stage and the MS scan are then started simultaneously, and stopped once the heating phase is complete.


***Figure 2.9**: Pressure hot stage coupled to a mass spectrometer taking images of crystals as they release volatile guests during a heating phase while the MS detects the released guests.*

## 2.13 X-Seed

X-Seed[6] was used to model crystal structures. It is a graphical user interface for SHELX-97, POV-RAY and MSROLL.

## 2.14 Electron density studies (SQUEEZE)

Platon[18]/SQUEEZE[19] uses crystallographic data obtained from SCD analysis to calculate the geometric void volume and number of residual electrons within each void. The occupancy can then

be determined from the number of electrons by comparison to the known number of electrons in the guest molecules.

The SQUEEZE procedure takes into account the electron density of an unmodelled guest in the solvent-accessible region of the host material. In addition, difference electron density maps can be generated and used to locate the positions of guests in the solvent-accessible void space. Difference maps are two-dimensional planes taken along the third dimension of the unit cell, and give the residual electron density after the modelled electron density is subtracted from the observed electron density.

## 2.15 Graphical representation and calculations of volumes and guest-accessible surfaces

The programs POV-RAY[20] and Materials Studio[21] were used to produce high quality molecular graphics. The atoms and volumes function of Materials Studio[21], as well as MSROLL[22,23] were used to calculate high quality three-dimensional volumes of accessible void spaces in crystal structures. Both programs work on the principle that the solvent-accessible surface of the void space is calculated by "rolling" a probe of a given radius through the structure.

## 2.16 Materials Studio

The Materials Studio[21] program suite serves as an interface for various computational methods such as Density Functional Theory (DFT) and molecular mechanics and dynamics. With regard to this dissertation, the CASTEP, Dmol$^3$, and VAMP modules were used.

### 2.16.1 CASTEP

CASTEP is materials modelling software based on a first-principles quantum mechanical description of atoms and nuclei. The code uses DFT to calculate a wide range of a material's properties, including energetics and vibrational properties. CASTEP is well suited for crystallographic models as it can calculate the properties of periodic structures.

The code was used to perform periodic-structure optimisation and to calculate single-point energies of the structures of host-guest complexes, as well as those of guests and empty hosts. The parameters used for geometry optimisation and single-point energy calculations are given in Table 2.1.

**Table 2.1**: CASTEP geometry optimisation and single-point energy calculation parameters.

| Geometry optimisation parameters | | | Single-point energy parameters | | |
|---|---|---|---|---|---|
| **Geometry Optimisation** | | | **Energy** | | |
| | Quality | Ultra-fine | | Quality | Ultra-fine |
| | Optimised cell | FALSE | | | |
| **Functional** | | GGA-PBE | **Functional** | | GGA-PBE |
| | Dispersion correction | Grimme | | Dispersion correction | Grimme |
| **Electronic** | | | **Electronic** | | |
| | Energy cut-off | 380.0 eV | | Energy cut-off | 380.0 eV |
| | SCF tolerance | Ultra-fine | | SCF tolerance | Ultra-fine |
| | Pseudo potentials | Ultrasoft | | Pseudo potentials | Ultrasoft |

### 2.16.2 Dmol$^3$

Dmol$^3$ is a DFT quantum mechanical module commonly used to simulate chemical processes or to predict the properties of materials. The module is often used to investigate the origin of the chemical, electronic and structural properties of a system without the need for experimental input. Dmol$^3$ uses simple non-periodic molecular systems for calculations. Consequently, the single-point energy values calculated by Dmol$^3$ were not used for the periodic crystal structures.

The electron density of a molecule is calculated in single-point energy calculations, and Dmol$^3$ gives a more accurate description of a molecule's electron density in smaller, non-periodic structures. Therefore, Dmol$^3$ was used to calculate the electron density of guest molecules in order to generate an isosurface of point charges at 0.0067 $e^-/Å^3$, similar to the van der Waals volume of the guest molecules. The isosurface, in turn, serves as a template upon which the electron density of the host is mapped in order to visualise its electrostatic potential on the guest molecules. In addition to single point energies, Dmol$^3$ was used to calculate the infrared and Raman vibrational modes of guest molecules. The parameters for Dmol$^3$ single-point and vibrational mode calculations are given in Table 2.2.

**Table 2.2**: Dmol$^3$ Single-point energy calculation parameters.

| Single point energy parameters: Dmol$^3$ | | |
|---|---|---|
| **Energy** | | |
| | Quality | Fine |
| **Functional** | | GGA-PBE |
| | Dispersion correction | Grimme |
| **Electronic** | | |
| | Integration accuracy | Fine |
| | SCF tolerance | Fine |
| | Core treatment | All electron |
| | Polarisation Basis set | DNP |
| | Orbital cut-off quality | Fine |

### 2.16.3 VAMP

The VAMP module is a semi-empirical molecular modelling package for organic and inorganic systems. It serves as an intermediate between force-field and first principals methods in order to rapidly calculate physical and chemical properties of a system. More specifically, it calculates reliable structural and electronic properties of molecules in a system based on semi-empirical Molecular Orbital (MO) theory, and is useful to perform scans over wide areas of a potential energy surface on thousands of atoms.

With regard to this thesis, VAMP was used to calculate the electron density in the void space of a host from CASTEP single-point optimised structures. The electron density is then mapped onto the guests' Dmol$^3$ isosurfaces. Therefore the mapped isosurfaces represent the host's electrostatic potential exerted on a guest. The parameters for energy calculations used to obtain the electrostatic density of a host are given in Table 2.3.

**Table 2.3**: VAMP electrostatic energy calculation parameters.

| VAMP electrostatic potential energy | | |
|---|---|---|
| **Energy** | | |
| | Hamiltonian | NDDO-PM6 |
| | Multiplicity | Auto-RHF |
| **Electronic** | | |
| | Convergence scheme | Standard |
| | SCF tolerance | Fine |

## 2.17 References


(1) Version 5.629 ed.; Bruker AXS Inc.: Madison, WI, 2003.

(2) Version 6.54 ed.; Bruker AXS Inc.: Madison, WI, 2003.

(3) Version 2.05 ed.; Bruker AXS Inc.: Madison, WI, 2002.

(4) Blessing, R. *Acta Crystallogr., Sect. A: Found. Crystallogr.* **1995**, *51*, 33.

(5) Sheldrick, G. *Acta Crystallogr., Sect. A: Found. Crystallogr.* **2008**, *64*, 112.

(6) Barbour, L. J. *Journal of Supramolecular Chemistry* **2001**, *1*, 189.

(7) Fletcher, A. J.; Thomas, K. M. *Langmuir* **1999**, *15*, 6908.

(8) Fletcher, A. J.; Thomas, K. M. *Langmuir* **2000**, *16*, 6253.

(9) Foley, N. J.; Thomas, K. M.; Forshaw, P. L.; Stanton, D.; Norman, P. R. *Langmuir* **1997**, *13*, 2083.

(10) Harding, A. W.; Foley, N. J.; Norman, P. R.; Francis, D. C.; Thomas, K. M. *Langmuir* **1998**, *14*, 3858.

(11) O'Koye, I. P.; Benham, M.; Thomas, K. M. *Langmuir* **1997**, *13*, 4054.

(12) Reid, C. R.; Thomas, K. M. *Langmuir* **1999**, *15*, 3206.

(13) Reid, C. R.; O'Koy, I. P.; Thomas, K. M. *Langmuir* **1998**, *14*, 2415.

(14) Atwood, J. L.; Barbour, L. J.; Thallapally, P. K.; Wirsig, T. B. *Chem. Commun.* **2005**, 51.

(15) Ball, D. *Physical Chemistry*; Cengage Learning: Stamford, 2014; Vol. 2.

(16) Rouquerol, F.; Rouquerol, J.; Sing, K. S. W. *Adsorption by Powders and Porous Solids: Principles, Methodology and Applications*; 2nd ed.; Academic Press: Oxford, 1999.

(17) Marais, C. G. MSc, Stellenbosch University, 2008.

(18) Spek, A. *J. Appl. Crystallogr.* **2003**, *36*, 7.

(19) van der Sluis, P.; Spek, A. L. *Acta Crystallogr., Sect. A: Found. Crystallogr.* **1990**, *46*, 194.

(20) Version 3.6 ed.; Persistence of Vision Raytracer Pty.Ltd.: Williamstown, Australia, 2004.

(21) 6.0.0 ed.; Accelrys Software Inc.: San Diego, 2011.

(22) Connolly, M. L. *Science* **1983**, *221*, 709.

(23) Connolly, M. L. *J. Mol. Graphics,* **1993**, *11*, 139.

# CHAPTER 3 | ADSORPTION SELECTIVITY

## 3.1 Introduction

The release of harmful substances into the atmosphere has become a worldwide concern. A number of industrial chemicals produced in excess of one million tons per year are highly detrimental to the environment and to those who are exposed to them. We are therefore entering an era where there is a growing need for materials that are capable of capturing, storing and purifying hazardous chemicals without requiring large amounts of energy, since energy-intensive processes also contribute substantially to the global energy and pollution crisis. Physisorption with activated carbons, zeolites and modified porous silica is a common process whereby this is achieved.[1-3] However, in the past two decades synthetic materials such as porous metal-organic frameworks (MOFs),[4,5] covalent organic frameworks,[5,6] metallocycles,[7,8] organic cages[9,10] and hydrogen-bonded organic frameworks (HOFs)[11,12] have shown great promise for capture, storage and separation of chemicals without the need for large energy inputs, and they can be engineered to specifically address a need such as gas separation. For example, xylene isomers have similar boiling and melting points (*o-xylene* bp: 144.4°C, mp: -25.2 °C; *m-xylene* bp: 139.1 °C, mp: -47.9°C and *p-xylene* bp: 138.4 °C, mp: 13.3 °C) and their separation is currently achieved by a combination of distillation and crystallisation or adsorption processes.[13] In such energy-intensive industrially important processes a porous material that can selectively separate one isomer from a mixture of three becomes exceptionally appealing. One example of separating xylene isomers using a porous host has been reported by Lusi and Barbour.[14] They reported a Werner complex which selectively absorbs *o*-xylene vapour in the presence of all three isomers; thereafter the complex showed the same selectivity for *m*-xylene over *p*-xylene; thus the material can potentially separate all three isomers without large energy inputs. Even though examples such as these exist, there are currently limits to the implementation of synthetic porous materials (e.g. HOFs, MOFs) and marked improvements in performance on natural porous materials (e.g. zeolites) are still rare. One of the greatest obstacles has been the lack of control over pore specificity. Selectivity in all chemical separation fields encompasses a wide range of work; therefore this dissertation will only focus on selectivity in gas adsorption.

Currently, it is well known that porous materials can either sequester relatively substantial amounts of gas using large surface areas,[5,15,16] or separate gases by utilising small pore apertures.[4,5] However, it has become apparent that, in both cases, selectivity is of utmost importance for performance. Selectivity can be derived from size-shape considerations and/or the thermodynamic

factors related to host-guest interactions. Typically, when a compound's selectivity is studied, experimental or computational sorption isotherms for the uptake of each of two (or more) pure gases are compared in order to establish selectivity coefficients.[9,17,18] These selectivity trends are then assumed to hold true for gas mixtures and little consideration is given to the possibility that selectivity might be affected when the gases in a gas mixture interact with one another. Therefore, additional data are needed from pressure-swing sorption,[19-22] breakthrough experiments[1,2,23,24] or chromatographic separations.[5,25] Even then, elucidating the modes of host-guest and guest-guest interactions requires in-situ structural studies of gas-loaded materials.

A host's selectivity can be explained using the concept of molecular recognition, which allows a host to discriminate between a mixture of guests and to selectively adsorb one specific guest. A host's selectivity depends on the topology of the guest as well as the nature and extent of non-bonding interactions between the host and guest.[26] The adsorption interaction between a single guest, *G,* and host, *H,* can be written as an equilibrium reaction (Equation 3.1) where *n* represents the stoichiometric number of guests absorbed. [27]

$$H_{(s)} + nG_{(s,l\ or\ g)} \leftrightharpoons H \cdot G_{n(s)} \tag{3.1}$$

When there is a mixture of guests Equation 3.1 may be extended to Equation 3.2, where *A* and *B* represent the two separate guest species.

$$H_{(s)} + nA_{(s,\ \ l\ or\ g)} + \ mB_{(s,\ \ l\ or\ g)} \leftrightharpoons H \cdot A_{n(s)} + mB_{(s,\ \ l\ or\ g)} \tag{3.2}$$

Equation 3.2 represents perfect selectivity, where only guest *A* is adsorbed and *B* can be removed from the head space. This process need only be carried out once, and the guest *A* can be released, regenerating the apohost *H*.

This process seldom occurs in practice. Instead, it is necessary for scientists and engineers to establish the ideal selectivity, which is mostly achieved with competition experiments. In these experiments the host is exposed to varying molar ratios of guest in order to determine if there is actual selectivity, or if the selectivity is concentration dependent. By analysing the crystalline inclusion compounds the mole fraction (*Z*) of guests included can be calculated. The ratio between the mole fraction of guests included and guests in the liquid/gas mixture can then be used to calculate a selectivity coefficient, $K_{A:B}$ (Equation 3.3). In the Equation $X_A$ is the mole fraction of guest *A* in the liquid or gas mixture and $Z_A$ is that of the guest included in the host.[26]

$$K_{A:B} = {}^{Z_A}/_{Z_B} \times {}^{X_B}/_{X_A} \tag{3.3}$$

To determine the type of selectivity a host exhibits, the mole fraction of guests in the bulk phase is plotted against that of the included guests, and typically one of three profiles arises (Figure 3.1). The diagonal line **(a)** represents no selectivity, **(b)** represents selectivity over the whole concentration range and **(c)** displays concentration-dependent selectivity.[26]

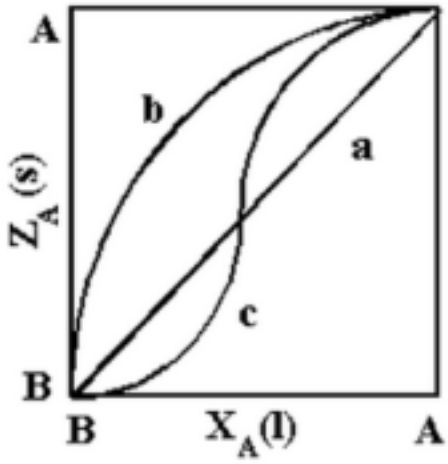


***Figure 3.1**: The type of selectivity a host exhibits is determined by plotting the mole fraction of guests in the bulk phase against that of the included guests; (a) represents no selectivity, (b) represents selectivity towards a whole concentration range and (c) displays concentration-dependent selectivity.[26]*

Competition experiments are generally not conducted because the experimental measurement of multicomponent gas-mixture sorption isotherms is time consuming. It requires specialised equipment and complex thermodynamic models with a large number of variables in order to predict binary and multicomponent equilibria. Competition experiments are currently circumvented by deriving most of the thermodynamic model's variables from single-component sorption isotherms. Even though there has been success in this method for the prediction of simple binary-component sorption, there is still no established method with universal application.[26,28]

One model that is currently used to circumvent competition experiments is the Extended Langmuir-Freundlich model, which has been shown to provide a reasonably good empirical correlation of binary equilibrium data.[29] The model predicts that the amount of one gas adsorbed ($Q_1$ or $Q_2$) in a binary gas system can be described as shown in Equations 3.4 and 3.5:[30]

$$Q_1 = \frac{Q_{max,1} \times (K_1 \times C_1)^{b_1}}{1 + (K_1 \times C_1)^{b_1} + (K_2 \times C_2)^{b_2}} \quad (3.4)$$

$$Q_2 = \frac{Q_{max,1} \times (K_1 \times C_1)^{b_2}}{1 + (K_1 \times C_1)^{b_1} + (K_2 \times C_2)^{b_2}} \quad (3.5)$$

Here $K_1$ and $K_2$ (L mmol$^{-1}$) are the average association constants, $b_1$ and $b_2$ are heterogeneity parameters, and $C_1$ and $C_2$ are the concentrations of the gases in the binary system. All of the variables in these equations are obtained from single gas adsorption studies.

Most researchers use Myers and Prausnitz's[29] Ideal Adsorbed Solution Theory (IAST), which is based on the Langmuir-Freundlich model.[31] The IAST method is based upon three assumptions: (i) that there is the same amount of surface area available to all adsorbates, (ii) that the adsorbent is inert (no chemisorption takes place), and (iii) that the multicomponent mixture behaves as an ideal solution (the mean strength of interactions is equal between all molecules in the solution).[32]

The model's greatly simplified Equation 3.6 describes how the IAST theory calculates the adsorbed concentration $C$ of the $i^{th}$ component in a multicomponent mixture.[33]

$$C_i = \frac{q_i}{\sum_{J=1}^{N} q_j}\left(\frac{\sum_{j=1}^{N} n_j q_j}{n_i K_i}\right)^{n_i} \quad \text{for } i = 1 \; to \; N \tag{3.6}$$

Here $q_i$ is the amount of solute adsorbed per unit weight of solid (typically mg g$^{-1}$) at equilibrium. $n_i$ is a measure of adsorption of the $i^{th}$ gas component onto the surface, and when $n < 1$ the adsorption is favoured. $K$ is the adsorption capacity of the host.[33] In addition, one method of calculating selectivity according to IAST is given in Equation 3.7:[32,34,35]

$$S_{A/B} = \frac{x_A/x_B}{y_A/y_B} \tag{3.7}$$

Here the selectivity factor, $S$, of component $A$ over component $B$ is calculated. $x_A$ and $x_B$ are, respectively, the mole fractions of adsorbed guests $A$ and $B$, whereas $y_A$ and $y_B$ are the mole fractions of guests $A$ and $B$ in their respective headspaces. As in the Extended Langmuir-Freundlich model, all of the components required in Equation 3.6 and 3.7 are derived from single-system adsorption isotherms. As a result of the assumptions made in the theory, no correction factors are used to account for strong guest-guest interactions or adsorption competition between guests.

To demonstrate that more experimentation is required to prove selectivity, a porous metallocycle (**1**) was used as a model compound for selective adsorption studies. As previously reported,[36] **1** crystallises in the monoclinic space group $C2/m$ and is composed of metallocycles that stack as 1D columns, producing discrete voids of approximately 125 Å$^3$. However, despite the absence of permanent channels, the voids are still accessible to small guest molecules. Crystallographic models of the host with two carbon dioxide or two acetylene guest molecules are shown in Figure 3.2. The guests are oriented to achieve maximum electrostatic attraction to the host and minimum van der Waals repulsion with the surroundings. In Figure 3.2(a) the carbon dioxide

molecules filling the cavities are shown oriented almost perpendicular to the Cl···Cl vector. In Figure 3.2(b) the acetylene molecules exhibit pseudo head-on C-H···Cl hydrogen bonds that, owing to steric guest-guest repulsion, are canted by approximately 38° relative to the Cl···Cl vector.

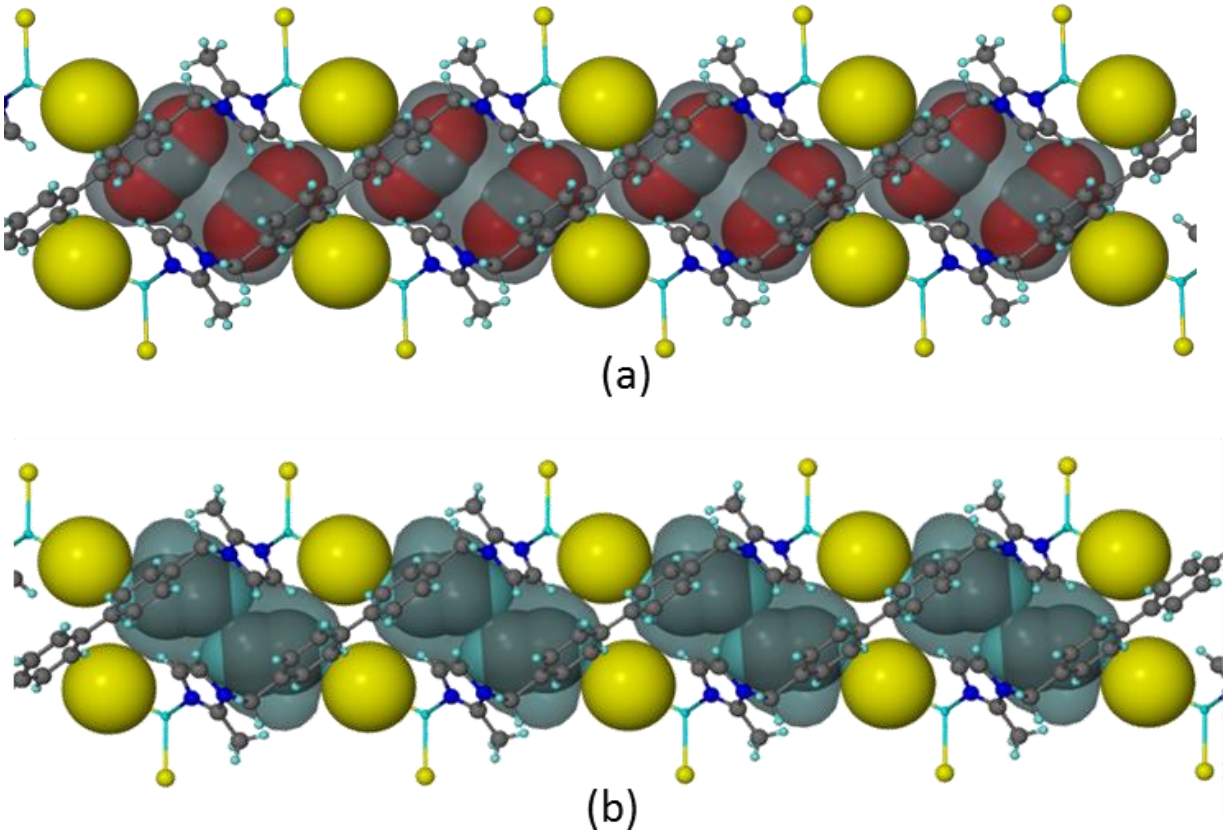


***Figure 3.2**: SCD models of the metallocycle host occupied by (i) two molecules of carbon dioxide and (ii) two molecules of acetylene per host cavity. The yellow spheres show the van der Waals volume of the chlorine atoms that form the barriers closing off the void space. The transparent blue Connolly surface represents the guest-accessible void space.*

Acetylene and carbon dioxide have similar dimensions and physical properties, with opposite electrostatic profiles as shown in Figure 3.3. *a* and *b* are the van der Waal Equation of state constants, which are unique for each gas, where *a* represents the magnitude of intermolecular attraction, and *b* the excluded volume in a body of gas. The similar properties of the two gases explain why, in both single-gas sorption cases, two molecules of each gas can fit into the void-space of **1**. Moreover, the opposing electrostatic profiles explain the different orientations of the guests within the host.

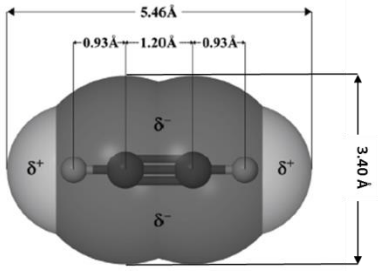


**Acetylene**
Boiling point = - 84.7 °C
Molecular volume = 33.4 Å³
Van der Waals constants:
*a* = 4.516 bar $L^2/mol^2$
*b* = 0.0522 *L/mol*

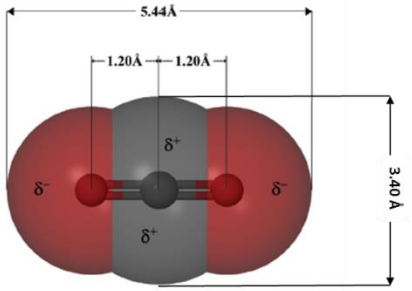


**Carbon dioxide**
Boiling point = - 78.5 °C
Molecular volume = 33.9 Å³
Van der Waals constants:
*a* = 3.658 bar $L^2/mol^2$
*b* = 0.0429 *L/mol*

***Figure 3.3**: A comparison of the properties and dimensions of acetylene and carbon dioxide.*

The acetylene and carbon dioxide single-gas sorption isotherms of **1** are shown in Figure 3.4. Both are type I isotherms, however acetylene has an inflection point, which was shown to be where the second molecule of acetylene enters the host void space.[36] At first glance one could assume that the host would be far more selective for acetylene adsorption from 1 bar onwards, based on the higher occupancy.

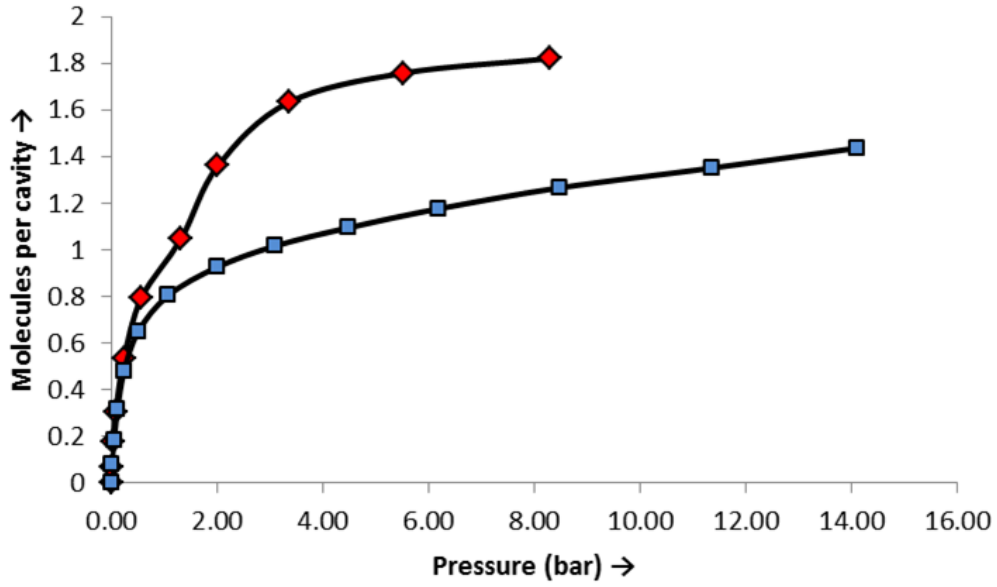


***Figure 3.4**: Sorption profiles of 1 for acetylene (red) and carbon dioxide (blue).*

Utilising the single-gas sorption data the selectivity factors, as defined in Equation 3.7, of the host can be calculated. The selectivity factors can then be used to determine what the influence of

increasing pressure and saturation of host would be. The calculated selectivity factors of acetylene over carbon dioxide between 0 and 8.5 bar are shown in Figure 3.5.

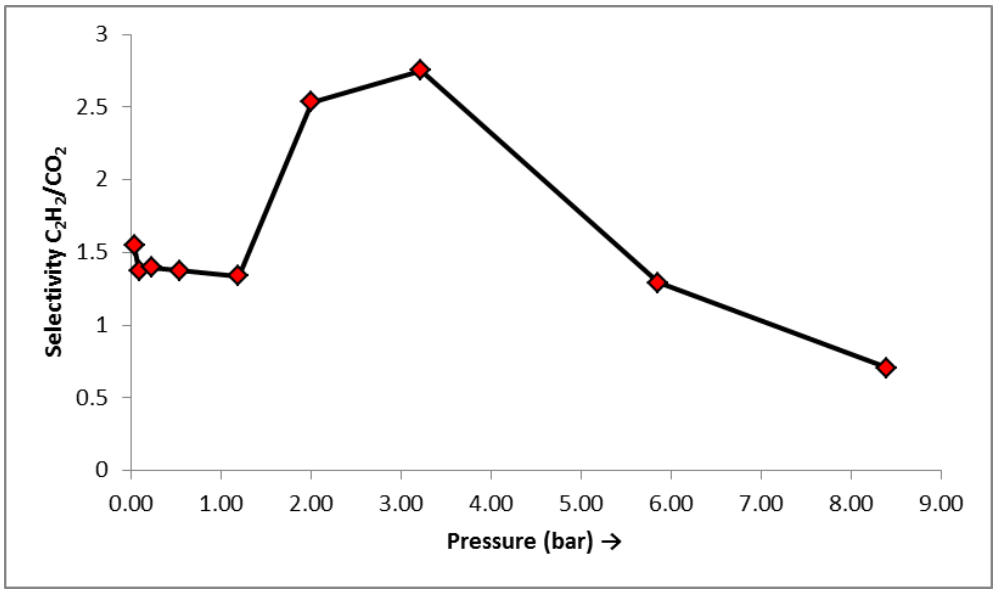


***Figure 3.5**: IAST selectivity factors of **1** calculated for acetylene adsorption over carbon dioxide in an equimolar acetylene - carbon dioxide mixture. The selectivity factors are derived from single-gas adsorption isotherm data, and are calculated with Equation 3.7.*

The first notable aspect of the selectivity curve is the inflection point. This can be explained by the acetylene sorption isotherm's inflection point (Figure 3.4 red), where the host deforms enough to allow a second molecule of acetylene into the void space, thereby increasing the sorption capacity of the host. In addition, the selectivity for acetylene decreases as pressure increases, which is expected as the host's affinity for guest molecules will decrease as occupancy rises. If the selectivity factor is greater than 1, the host will theoretically prefer the uptake of acetylene; when the selectivity factor is 1 there is no selectivity, while a selectivity factor smaller than 1 indicates a preference for carbon dioxide sorption, or saturation of the host at higher pressures. It is clear that up to 90% of full occupancy (6 bar) the host prefers acetylene uptake, according to IAST. In fact, at about 3 bar the host is almost three times more selective for acetylene, which according to the single-gas sorption isotherm at 3 bar, corresponds to the host being 80 % occupied by acetylene. Therefore, a logical assumption would be that, during mixed-gas sorption, the host would prefer to adsorb acetylene, and acetylene would fill the host before carbon dioxide could.

Given that carbon dioxide and acetylene are physically similar, and that both gases can be adsorbed, a perceived preference for acetylene raises a question: would the adsorption selectivity prevail if the host is presented with a 1:1 molar ratio of acetylene and carbon dioxide, and would the host-guest interactions be influenced? We postulated that there are four possible scenarios for guest inclusion in the host.

(1) Only one of the gases, acetylene or carbon dioxide, is adsorbed;

(2) Both gases are adsorbed, and in the host there are cavities containing only acetylene and others containing only carbon dioxide;

(3) Alternatively, both gases are adsorbed, and in each cavity there is one molecule of acetylene and one molecule of carbon dioxide;

(4) The sorption is completely random; there are cavities with two molecules of the same gas and others with both gases.

## 3.2 Chapter outline

This chapter concerns itself with the proof of concept that more research needs to be devoted to understanding how factors such as guest-guest interactions influence sorption and selectivity in the adsorption of multicomponent gas mixtures. In broad terms, a metallocycle that is capable of accommodating two molecules of either acetylene or carbon dioxide is used as a model host (**1**). The host possesses discreet void space, which allows for the meticulous study of host-guest interactions. According to most literature the metallocycle seems to be selective for acetylene uptake. However, when it is exposed to a 1:1 molar mixture of acetylene and carbon dioxide the metallocycle's selectivity changes and it prefers to adsorb a 1:1 mixture of the gases.

## 3.3 Results and discussion

### 3.3.1 Synthesis of 4,4′-bis(2-methylimidazol-1-ylmethyl)biphenyl (L)[36]

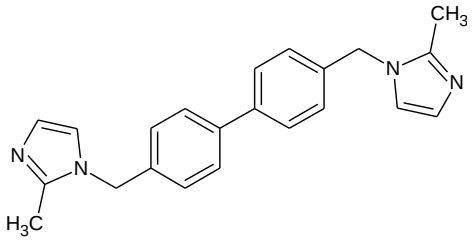


4,4'-Bis(chloromethyl)-1,1'-biphenyl (1.457 mmol, 0.366 g, 1 eq), 2-methylimidazole (5.78 mmol, 0.474 g, 4 eq ) and triethylamine (5.84 mmol, 0.812 ml, 4 eq) were suspended in acetonitrile (60 ml). The reaction was then stirred under reflux for 12 hours. The reaction mixture turned from colourless to light yellow. The solvent was then removed under vacuum to produce yellow oil. The crude product was dissolved in dichloromethane and washed with water, dried ($MgSO_4$), filtered and the solvent removed under vacuum, resulting in an off-white powder. Further purification was achieved by dissolution of the product in chloroform, drop-wise addition of the chloroform solution to pentane at 0 °C and subsequent filtration. Yield of 48.5%, M.p. 169-171 °C. **$\delta_H$ ($CDCl_3$, 400 MHz):** 2.37 (3H, s), 5.10 (2H, s), 6.88 (1H, d, $^3J$ = 1.14), 6.99 (1H, d, $^3J$ = 1.14), 7.13 (2H, d, $^3J$ = 8.23), 7.54 (2H, d, $^3J$ = 8.19). **$\delta_C$ ($CDCl_3$, 100 MHz)** 13.12, 49.37, 119.85, 127.11, 127.45, 127.51, 135.65, 140.05, 144.87.

### 3.3.2 Synthesis of $[Cd_2Cl_4L_2]\cdot 2CH_3OH$ (1·2MeOH)

Single crystals suitable for SCD studies were grown by interlayer diffusion of **L** (0.02 mmol, 6.84 mg) in 2 ml chloroform and $CdCl_2\cdot 2.5H_20$ (0.02 mmol, 4.66 mg) in 2 ml methanol to afford **1**·2MeOH.

The apohost **1** can be generated under mild heating at 80 °C under vacuum of 2-3 mmHg**.**

### 3.3.3 Sorption

Owing to acetylene's reactivity towards copper the commercial gravimetric sorption analyser (IGA) could not be used since it contains various parts made of copper. Therefore, the in-house volumetric analyser was used to record the sorption isotherms. The sorption isotherms were recorded at 20 °C, with 45 mg of the apohost **1**. A 1:1 molar mixture of acetylene and carbon dioxide was prepared using the mixing device described in section 2.8.

Figure 3.6 compares the mixed-gas sorption isotherm (green) to that of the acetylene (red) and carbon dioxide (blue). Counterintuitively, the mixed-gas isotherm resembles neither that for acetylene nor for carbon dioxide. If only acetylene was adsorbed, the mixed-gas isotherm should have been higher and resemble acetylene's isotherm, while the opposite would be true if only carbon dioxide was adsorbed. Clearly, there are factors that have influenced the host's selectivity for acetylene.

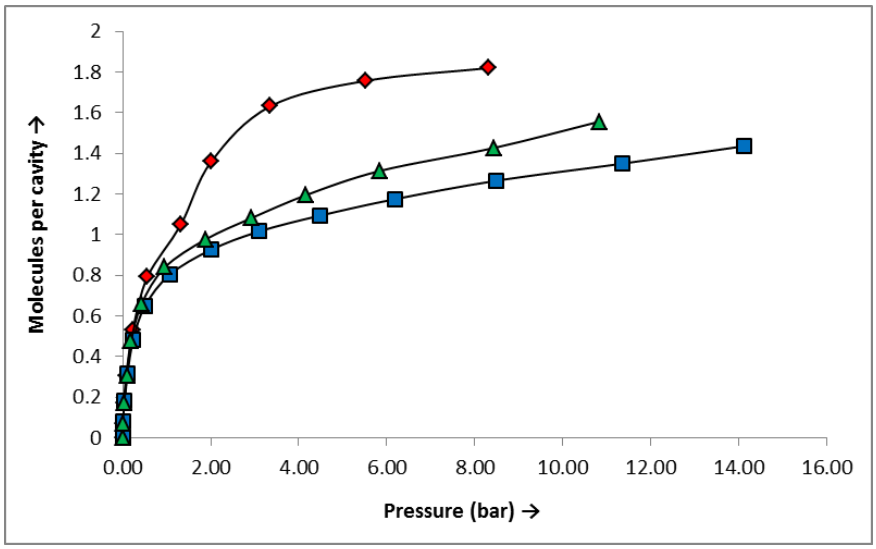


***Figure 3.6**: A mixed-gas isotherm (green) is compared to sorption isotherms for acetylene (red) and carbon dioxide (blue).*

In the mixed-gas sorption there could be a guest-guest interaction that affects the sorption behaviour on the molecular level. One has to consider that the guests can act as two single components, which are unaffected by one another, such that the sorption behaviour of each

component remains unchanged. On the other hand it might be possible that the guests interact with one another and form a single entity with completely different sorption properties, and that the degree of interaction determines the extent of the change in selectivity.

This latter possibility seems reasonable given that an acetylene-carbon dioxide complex has been detected in the gas phase using infrared spectroscopy.[37-39] The molecules in the observed complex were oriented parallel to one another with $C_{2v}$ symmetry (Figure 3.7 a). In addition, *ab initio* studies have confirmed the parallel structure and an additional stable linear structure has also been inferred (Figure 3.7 b).[40]

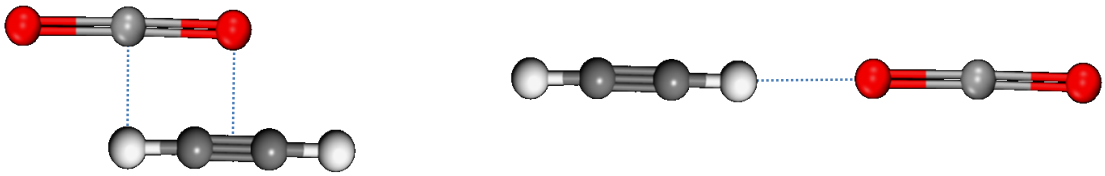

(a) (b)

***Figure 3.7**: Gas-phase interactions between acetylene and carbon dioxide can form (a) parallel or (b) head-on complexes.*

If one assumes that there is no selectivity, then the mixed-gas sorption would be an average of the two single gas sorption processes. To calculate an average sorption isotherm for mixed-gas sorption one has to consider single-gas occupancies of both gases at their partial pressures in the gas mixture, as well as the stress on the host at the total pressure. For example, when the mixed-gas headspace is at 5 bar the host is exposed to 2.5 bar acetylene and 2.5 bar carbon dioxide, but the host is still experiencing the stress of 5 bar. Therefore, to calculate the average occupancy at 5 bar one can sum half the occupancies of the two single-gas isotherms at 5 bar as given by Equation 3.8, where, $O_M$ is the calculated average occupancy of the gas mixture at *x* bar. $O_A$ and $O_C$ are, respectively, the occupancy of acetylene and carbon dioxide at ½ *x* in their single-gas isotherms.

$$O_M(x) = \frac{O_{A(0.5x)} + O_{C(0.5x)}}{2} \qquad (3.8)$$

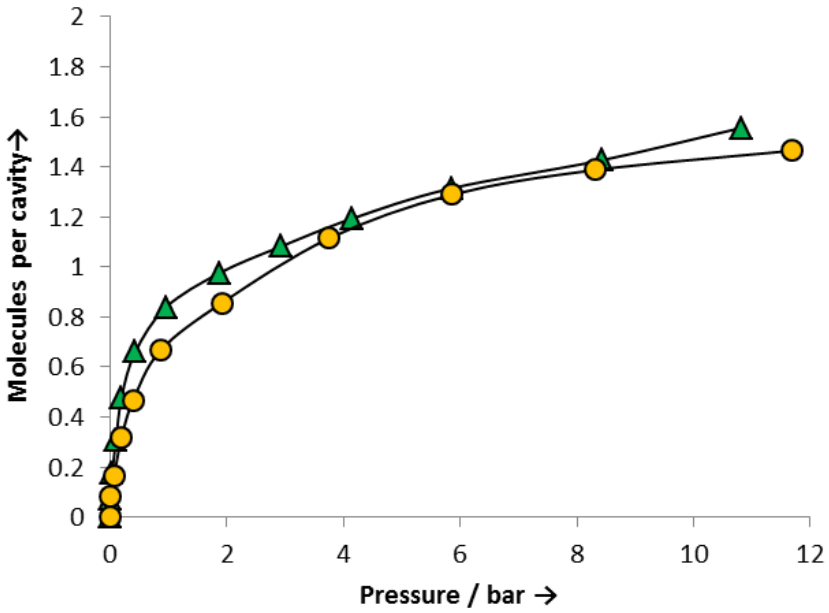


*Figure 3.8: A predicted average isotherm (orange) is compared to the experimental mixed-gas isotherm (green).*

In Figure 3.8, a calculated average isotherm (orange) is compared to the experimental mixed-gas isotherm (green). There is a remarkable similarity between the two isotherms, but in the range of 0.5 to 4 bar and above 8 bar one can see that the host takes up more guest molecules than predicted. The assumption then that the host has equal selectivity for the two gases in a mixed gas system seems reasonable. The equal selectivity can be due to acetylene-carbon dioxide guest-guest interactions, in that the guests are adsorbed as a dimeric entity rather than individual gases.

It is clear that the IAST method of calculating selectivity does not hold in this system, and that a combination of gases is adsorbed, possibly in a 1:1 ratio. However the ratio is unknown at this point. In order to investigate the ratio of adsorbed gases SCD studies were employed. SCD is a powerful tool that can be used to elucidate host-guest and guest-guest interactions in the solid state. In the following section the SCD investigations of **1** under various gas pressures are discussed.

## 3.4 Single-Crystal X-Ray Diffraction studies of 1

### 3.4.1 Incremental gas loading structural studies

Single-crystal diffraction is not routinely carried out at high pressures; therefore the environmental gas cell described in section 2.7 was used to preform high-pressure structural studies of the mixed-gas system. Single-crystal X-ray diffraction data of **1** were collected at 20, 0 and -40 °C and at 0.5, 1, 2, 3, 6 and 15 bar of mixed-gas pressure. The series of structures fabricates tracking of pressure-dependent structural changes, and certain lattice parameters were recorded as a function of equilibrium pressure. These lattice parameters are summarised in Tables 3.1, 3.2 and 3.3. The

atomic numbering used in the tables is given in Figure 3.9, and the subscript *x* in $\mathbf{1}_x$ represents the mixed-gas pressure at room temperature that **1** was exposed to.

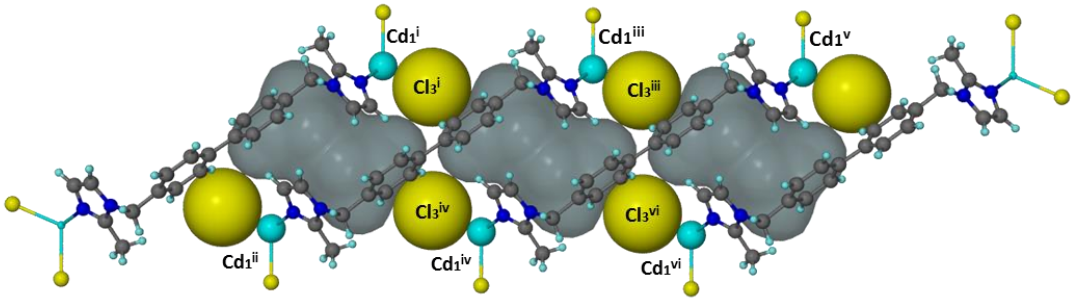


***Figure 3.9**: Atomic numbering of relevant atoms of **1**, in Tables 3.1 to 3.3 showing changes in size and shape of the void bounded by the $Cl_3^{i}\cdots Cl_3^{vi}$ and $Cd_1^{iii} \cdots Cd_1^{iv}$ vectors.*

To demonstrate the amount of structural information obtainable from such a series of systematic measurements, the change in structural parameters for the mixed-gas system at –40 °C will be discussed. As previously reported,[41] **1** undergoes progressive adjustment in order to accommodate guest molecules. For example, as is shown in Figure 3.10 the increase from 111.6 to 121.2 Å$^3$ in void volume correlates with the increasing void electron count (or guest occupancy). The change in void volume can be visualised as a parallelogram increasing in the length of the $Cl_3^{i}\cdots Cl_3^{vi}$ vector and decreasing in the length of the $Cl_3^{iv}\cdots Cl_3^{iii}$ vector, accompanied by a gradual decrease in the crystallographic β-angle (Figure 3.11). The gradual pressure-related changes in the length of the $Cl_3^{i}\cdots Cl_3^{vi}$ and the $Cl_3^{iv}\cdots Cl_3^{iii}$ vectors are given in Figure 3.12. Furthermore, the $Cl_3^{i}\cdots Cl_3^{iv}$ vector, which is the gateway between void spaces, decreases with the increase in pressure, however as the guest molecules are 3.40 Å wide (Figure 3.3.) they are still able to fit between the chlorines in order to transfer between voids at 15 bar. It should be noted that under vacuum and at – 40 °C, **1** has a void space volume of 108.3 Å$^3$ and, the $Cl_3^{i}\cdots Cl_3^{vi}$ vector is 10.734 Å long. Considering these dimensions and that that the volume of two acetylene, two carbon dioxide, or a combination of each would be 66.8, 67.8 or 67.3 Å$^3$, respectively (see Figure 3.3) one can imagine that the host need not expand a great deal to include the guests. Therefore, with an increase in pressure, and occupancy, one will expect an increase in void volume and in the unit cell volume, however these will not be substantial as can be seen in Tables 3.1 -3.3.

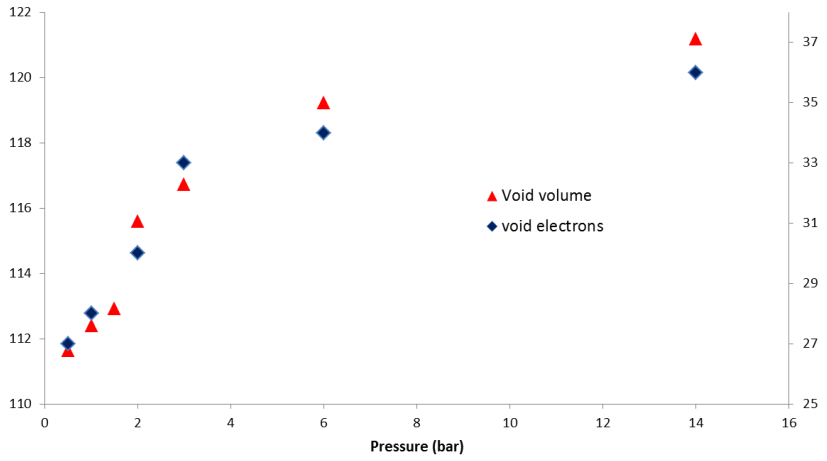


***Figure 3.10**: The increase in void space and electron count are directly related, which is indicative of a progressive adjustment of host void space in order to accommodate guests.*

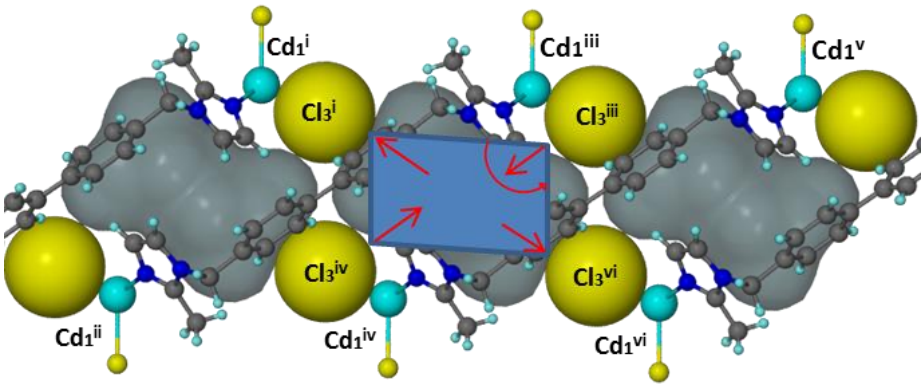


***Figure 3.11**: The change in void volume of **1** can be visualised as a parallelogram increasing in length and decreasing in width accompanied with a gradual decrease in the crystallographic β-angle.*

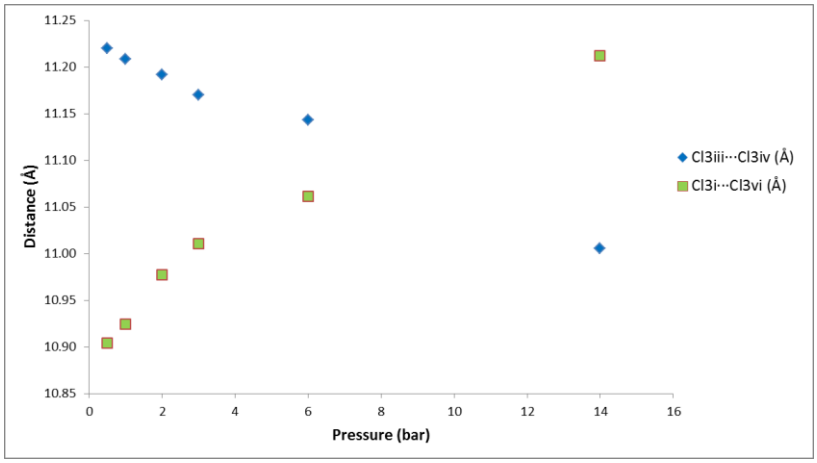


***Figure 3.12**: The void space of **1** increases along the $Cl_3^{i}\cdots Cl_3^{vi}$ vector, whereas the $Cl_3^{iv}\cdots Cl_3^{iii}$ vector decreases in length in order to accommodate the increasing guest occupancy.*

**Table 3.1**: Structural parameters, electron counts and occupancies of $\mathbf{1}_{0.5}$ to $\mathbf{1}_{15}$ at different mixed-gas pressures at 20 °C. Volumes are calculated with MSROLL ($r_{probe}$=1.7 Å). Full occupancy is assumed to be one molecule of $CO_2$ and one molecule of $C_2H_2$.

| **Mixed-gas pressure** | 0.5 bar | 1 bar | 2 bar | 3 bar | 6 bar | 15 bar |
|---|---|---|---|---|---|---|
| **Cell length *a* (Å)** | 17.978(1) | 17.942(1) | 17.921(1) | 17.913(1) | 17.82(1) | 17.83(1) |
| **Cell length *b* (Å)** | 15.605(1) | 15.610(1) | 15.616(1) | 15.635(1) | 15.638(1) | 15.658(1) |
| **Cell length *c* (Å)** | 9.447(7) | 9.456(7) | 9.472(7) | 9.476(6) | 9.510(7) | 9.517(8) |
| **Cell angle α = γ (°)** | 90 | 90 | 90 | 90 | 90 | 90 |
| **Cell angle β (°)** | 114.33(1) | 114.26(1) | 114.18(1) | 114.11(1) | 114.00(1) | 113.93(1) |
| | | | | | | |
| **void electrons** | 18 | 19 | 19 | 24 | 25 | 29 |
| **Void volume (Å$^3$)** | 112.2 | 114.5 | 114.8 | 115.5 | 115.7 | 118.7 |
| **Occupancy** | 50% | 53% | 53% | 56% | 69% | 81% |
| | | | | | | |
| **$Cd_1$–$N_4$ (Å)** | 2.218(3) | 2.221(3) | 2.219(3) | 2.217(3) | 2.221(3) | 2.221(2) |
| **$Cd_1$–$Cl_3$ (Å)** | 2.422(1) | 2.424(1) | 2.425(2) | 2.422(1) | 2.424(2) | 2.423(1) |
| **$Cd_1$–$Cl_2$ (Å)** | 2.442(1) | 2.441(1) | 2.443(1) | 2.441(1) | 2.443(1) | 2.440(1) |
| | | | | | | |
| **$Cd_1^{i}$···$Cd_1^{iv}$ (Å)** | 8.757(9) | 8.762(1) | 8.772(1) | 8.788(9) | 8.791(1) | 8.818(9) |
| **$Cd_1^{iii}$···$Cd_1^{iv}$ (Å)** | 9.230(1) | 9.198(1) | 9.172(1) | 9.156(9) | 9.087(1) | 9.090(1) |
| **$Cd_1^{i}$···$Cd_1^{vi}$ (Å)** | 15.706(1) | 15.742(1) | 15.787(1) | 15.819(1) | 15.903(1) | 15.940(1) |
| **$Cd_1^{ii}$···$Cd_1^{iii}$ (Å)** | 16.499(1) | 16.471(1) | 16.454(1) | 16.433(1) | 16.394(1) | 16.391(1) |
| | | | | | | |
| **$Cl_3^{i}$···$Cl_3^{iv}$ (Å)** | 5.710(5) | 5.713(6) | 5.707(6) | 5.720(6) | 5.658(6) | 5.707(5) |
| **$Cl_3^{i}$···$Cl_3^{vi}$ (Å)** | 10.895(3) | 10.928(3) | 10.971(4) | 11.007(3) | 11.050(6) | 11.069(5) |
| **$Cl_3^{iii}$···$Cl_3^{iv}$ (Å)** | 11.181(5) | 11.167(5) | 11.145(6) | 11.153(5) | 11.083(4) | 11.126(3) |

Symmetry codes: (i) *x, y, z;* (ii) *x, y, 1+z;* (iii) *x, y, 2-z;* (iv) *-x, y, 1-z;* (v) *x, y, 4-z*; (vi) *-x, y, 3-z.*

**Table 3.2**: Structural parameters, electron counts and occupancies of $\mathbf{1}_{0.5}$ to $\mathbf{1}_{15}$ at different mixed-gas pressures at 0 °C. Volumes are calculated with MSROLL ($r_{probe}$=1.7 Å). Full occupancy is assumed to be one molecule of $CO_2$ and one molecule of $C_2H_2$.

| **Mixed-gas Pressure** | 0.5 bar | 1 bar | 2 bar | 3 bar | 6 bar | 15 bar |
|---|---|---|---|---|---|---|
| **Cell length *a* (Å)** | 17.910(3) | 17.902(5) | 17.872(5) | 17.859(3) | 17.785(4) | 17.742(1) |
| **Cell length *b* (Å)** | 15.669(2) | 15.706(4) | 15.683(5) | 15.660(3) | 15.667(4) | 15.646(9) |
| **Cell length *c* (Å)** | 9.446(1) | 9.454(2) | 9.460(3) | 9.472(1) | 9.511(2) | 9.517(5) |
| **Cell angle α = γ (°)** | 90 | 90 | 90 | 90 | 90 | 90 |
| **Cell angle β (°)** | 114.20(3) | 114.06(5) | 114.06(5) | 114.00(3) | 113.82(4) | 113.88(9) |
| | | | | | | |
| **void electrons** | 21 | 26 | 29 | 29 | 30 | 33 |
| **Void volume (Å$^3$)** | 111.4 | 114.7 | 115.6 | 114.6 | 117.5 | 119.1 |
| **Occupancy** | 58% | 72% | 81% | 81% | 83% | 92% |
| | | | | | | |
| **$Cd_1$–$N_4$ (Å)** | 2.225(3) | 2.223(3) | 2.222(3) | 2.227(2) | 2.219 (3) | 2.219(2) |
| **$Cd_1$–$Cl_3$ (Å)** | 2.431(2) | 2.432(2) | 2.429(2) | 2.430(1) | 2.428(2) | 2.418(2) |
| **$Cd_1$–$Cl_2$ (Å)** | 2.442(1) | 2.445(1) | 2.441(2) | 2.440(1) | 2.445(2) | 2.437(2) |
| | | | | | | |
| **$Cd_1^{i}$···$Cd_1^{iv}$ (Å)** | 8.762(1) | 8.791(2) | 8.787(2) | 8.771(1) | 8.811(2) | 8.798(4) |
| **$Cd_1^{iii}$···$Cd_1^{iv}$ (Å)** | 9.161(1) | 9.143(2) | 9.123(2) | 9.117(1) | 9.044(2) | 9.022(5) |
| **$Cd_1^{i}$···$Cd_1^{vi}$ (Å)** | 15.751(2) | 15.803(4) | 15.817(5) | 15.854(3) | 15.950(4) | 15.955(9) |
| **$Cd_1^{ii}$···$Cd_1^{iii}$ (Å)** | 16.417(2) | 16.391(3) | 16.378(4) | 16.378(2) | 16.337(3) | 16.326(7) |
| | | | | | | |
| **$Cl_3^{i}$···$Cl_3^{iv}$ (Å)** | 5.771(6) | 5.787(6) | 5.769(7) | 5.780(5) | 5.695(7) | 5.681(6) |
| **$Cl_3^{i}$···$Cl_3^{vi}$ (Å)** | 10.936(4) | 10.987(5) | 11.005(3) | 11.042(3) | 11.044(7) | 11.015(7) |
| **$Cl_3^{iii}$···$Cl_3^{iv}$ (Å)** | 11.202(6) | 11.182(6) | 11.156(7) | 11.168(4) | 11.128(5) | 11.151(7) |

Symmetry codes: (i) *x, y, z*; (ii) *x, y, 1+z*; (iii) *x, y, 2-z*; (iv) *-x, y, 1-z*; (v) *x, y, 4-z*; (vi) *-x, y, 3-z*.

**Table 3.3**: Structural parameters, electron counts and occupancies of $\mathbf{1}_{0.5}$ to $\mathbf{1}_{15}$ at different mixed-gas pressures at -40 °C. Volumes are calculated with MSROLL ($r_{probe}$=1.7 Å). Full occupancy is assumed to be one molecule of $CO_2$ and one molecule of $C_2H_2$.

| **Mixed gas Pressure** | 0.5 bar | 1 bar | 2 bar | 3 bar | 6 bar | 15 bar |
|---|---|---|---|---|---|---|
| **Cell length *a* (Å)** | 17.860(1) | 17.844(1) | 17.839(3) | 17.820(1) | 17.737(2) | 17.700(2) |
| **Cell length *b* (Å)** | 15.666(1) | 15.652(1) | 15.654(1) | 15.642(1) | 15.645(2) | 15.629(2) |
| **Cell length *c* (Å)** | 9.439(8) | 9.446(7) | 9.467(7) | 9.476 (7) | 9.556(1) | 9.582(1) |
| **Cell angle α = γ (°)** | 90 | 90 | 90 | 90 | 90 | 90 |
| **Cell angle β (°)** | 114.30(1) | 114.25(1) | 114.18(1) | 114.11(1) | 114.04(2) | 113.95(2) |
| | | | | | | |
| **void electrons** | 27 | 28 | 30 | 33 | 34 | 36 |
| **Void volume (Å$^3$)** | 111.6 | 112.4 | 115.6 | 116.7 | 119.2 | 121.2 |
| **Occupancy** | 75% | 78% | 83% | 92% | 94% | 100% |
| | | | | | | |
| **$Cd_1$–$N_4$ (Å)** | 2.199(3) | 2.219(3) | 2.219(3) | 2.216(2) | 2.223(4) | 2.223(2) |
| **$Cd_1$–$Cl_3$ (Å)** | 2.431(1) | 2.430(1) | 2.432(2) | 2.429(1) | 2.432(2) | 2.428(1) |
| **$Cd_1$–$Cl_2$ (Å)** | 2.444(1) | 2.444(1) | 2.444(1) | 2.443(1) | 2.448(2) | 2.446(1) |
| | | | | | | |
| **$Cd_1^{i}\cdots Cd_1^{iv}$ (Å)** | 8.722(1) | 8.726(9) | 8.748(1) | 8.756(8) | 8.770(1) | 8.786 (1) |
| **$Cd_1^{iii}\cdots Cd_1^{iv}$ (Å)** | 9.134(1) | 9.122(1) | 9.110(1) | 9.091(9) | 9.017(1) | 8.986(1) |
| **$Cd_1^{i}\cdots Cd_1^{vi}$ (Å)** | 15.713(1) | 15.733(1) | 15.790(1) | 15.820(1) | 15.973(2) | 16.040(2) |
| **$Cd_1^{ii}\cdots Cd_1^{iii}$ (Å)** | 16.401(1) | 16.392(1) | 16.393(1) | 16.377(1) | 16.381(1) | 16.369(2) |
| | | | | | | |
| **$Cl_3^{i}\cdots Cl_3^{iv}$ (Å)** | 5.770(6) | 5.767(6) | 5.765(6) | 5.761(4) | 5.652(7) | 5.621(4) |
| **$Cl_3^{i}\cdots Cl_3^{vi}$ (Å)** | 10.903(3) | 10.924(3) | 10.977(4) | 11.010(3) | 11.061(7) | 11.212(3) |
| **$Cl_3^{iii}\cdots Cl_3^{iv}$ (Å)** | 11.219(5) | 11.208(5) | 11.191(6) | 11.170(4) | 11.143(4) | 11.005(4) |

Symmetry codes: (i) *x, y, z*; (ii) *x, y, 1+z*; (iii) *x, y, 2-z*; (iv) *-x, y, 1-z*; (v) *x, y, 4-z*; (vi) *-x, y, 3-z*.

### 3.4.2 Crystallographic modelling of **1**

The position of the atoms in a crystallographic model is deduced from SCD electron density data. After electron density has been assigned to the atoms of a host, a difference electron density map can be generated that will show the residual electron density that make up the guest molecules, thus making it possible to infer the positions of the guests within the host void space.

In Figure 3.13 the difference Fourier map of the guest accessible void space in $\mathbf{1}_{15}$ is given. The difference Fourier map is that of the unmodelled electron density halfway down the *b*-axis, the *a*-axis lies horizontal and the *c*-axis is off-vertical. It can be seen that the residual electron density is distributed over two symmetry-related areas within the cavity, each area containing four peaks of relatively high electron density.

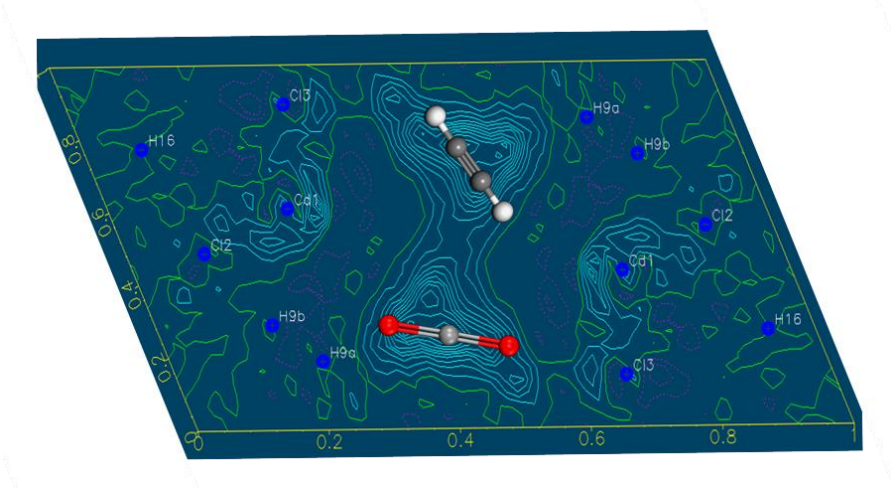


***Figure 3.13**: Difference Fourier map of **1** at 15 bar and –40 °C down the b-axis, and in plane with the centre of the guest accessible void space. The map shows electron density in two symmetry-related areas with four peaks of relatively high electron density. The peaks are predicted to be a molecule of acetylene and of carbon dioxide per host cavity, which are shown in with ball-and-stick models.*

The positions of these peaks might be a carbon dioxide (with three peaks) and an acetylene molecule (with two peaks) in every void space. However, during crystallographic modelling no sensible model could be generated that refined to the observed electron density. Therefore the electron density was used to anticipate the positions of the guest molecules in a model used in computational studies (discussed in section 3.6). Figure 3.14 shows the lowest energy computational model overlaid on the difference Fourier map of **1**. It is clear that the minimum energy position of the guests have good correlation with the observed electron density. In addition, the summation of electron densities[42] in the void space of $\mathbf{1}_{15}$ at –40 °C amounts to 36 electrons. 36 electrons correspond exactly to the sum of electrons for one molecule each of acetylene and carbon dioxide per host cavity. Two carbon dioxide molecules would correspond to 44 electrons, while two

acetylene molecules would correspond to 28 electrons. The SCD data makes it reasonable to assume that there is a molecule of each of acetylene and carbon dioxide in every host void space.

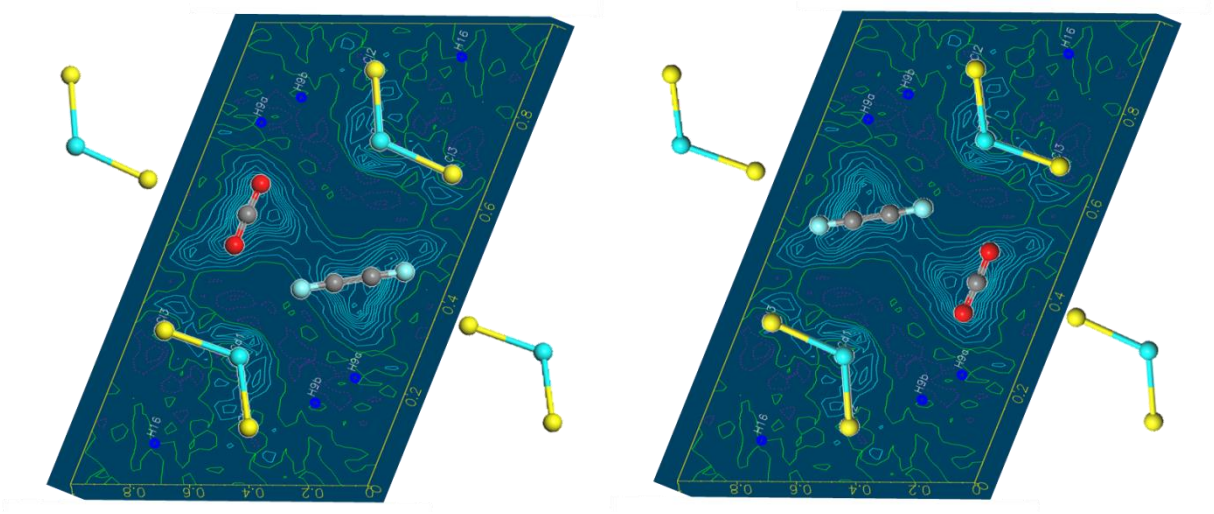

***Figure 3.14**: Difference Fourier map of **1** at 15 bar and –40 °C. The electron density correlates to the positions of carbon dioxide and acetylene in the host void-space.*

Even though the difference Fourier map yields convincing evidence that there might be a 1:1 mixture of gases in all the voids of the host, the SCD data cannot be used quantitatively. Therefore additional analytical methods were required to determine the composition of guests in the host. Infrared (IR), high-pressure Raman and fluorescence spectroscopy were used to elucidate how guests are included in **1** as described in the next section.

## 3.5 Spectroscopy

To determine if there is a 1:1 mixture of acetylene and carbon dioxide in every cavity of the host, the differences in the environment around the guests in single-gas and mixed-gas systems was investigated. If the voids in the mixed gas system each had two of the same guests, as in the single-gas systems, the vibrational modes should remain constant.

### 3.5.1 Raman and infrared spectroscopy

Both carbon dioxide and acetylene have $D_{\infty h}$ point group symmetry. Acetylene has an irreducible representation of $\Gamma = 2\sum_g^+ + \Pi_g + \sum_u^+ + \Pi_u$, which represents seven vibrational degrees of freedom, two of which produce bands that are doubly degenerate, $v_4$ and $v_5$. In Table 3.4 one can see that the symmetry classes of the irreducible representation give rise to three Raman-active vibrations and two infrared-active vibrations. The fundamental frequencies for the vibrational modes of acetylene are given in Table 3.5.

Carbon dioxide has an irreducible representation of $\Gamma = \sum_g^+ + +\sum_u^+ + \Pi_u$. Therefore it should have four vibrational degrees of freedom with one doubly degenerate vibrational mode, $\nu_2$. The symmetry classes in the irreducible representation of carbon dioxide represent one Raman-active vibration and two infrared-active vibrations. The three fundamental vibrational modes for carbon dioxide are given in Table 3.6.

**Table 3.4**: Standard character table for the $D_{\infty h}$ point group.[43]

| $\mathbf{D}_{\infty\mathbf{h}}$ | $2C_\infty^\phi$ | $\infty\sigma_V$ | $i$ | $2S_\infty^\phi$ | $\infty C_V$ | Infrared | Raman |
|---|---|---|---|---|---|---|---|
| $\sum_g^+$ | 1 | 1 | 1 | 1 | 1 | | $x^2+y^2, z^2$ |
| $\sum_g^-$ | 1 | -1 | 1 | 1 | -1 | $R_z$ | |
| $\Pi_g$ | 2 cos ϕ | 0 | 2 | -2 cos ϕ | 0 | $(R_x, R_y)$ | $(xz, yz)$ |
| $\Delta_g$ | 2 cos ϕ | 0 | 2 | 2 cos ϕ | 0 | | $x^2 - y^2, 2xy$ |
| $\sum_u^+$ | 1 | 1 | -1 | -1 | -1 | | |
| $\sum_u^-$ | 1 | -1 | -1 | -1 | 1 | | |
| $\Pi_u$ | 2 cos ϕ | 0 | -2 | 2 cos ϕ | 0 | $(x, y)$ | |
| $\Delta_u$ | 2 cos 2ϕ | 0 | -2 | -2 cos 2ϕ | 0 | | |

**Table 3.5**: Fundamental vibrational modes of acetylene.[44]

| Vibration mode | Symmetry class | Raman band ($cm^{-1}$) | Infrared band ($cm^{-1}$) |
|---|---|---|---|
| $\nu_1$ (Symmetric C-H stretch) | $\sum_g^+$ | 3373.7 | inactive |
| $\nu_2$ (C≡C stretch) | $\sum_g^+$ | 1973.8 | inactive |
| $\nu_3$ (Asymmetric C-H stretch) | $\sum_u^+$ | inactive | 3281.9 |
| $\nu_4$ (C-H Bend) | $\Pi_g$ | 611.8 | inactive |
| $\nu_5$ (C-H Bend) | $\Pi_u$ | inactive | 630.3 |

**Table 3.6**: Fundamental vibrational modes of carbon dioxide.[44]

| Vibration mode | Symmetry class | Raman ($cm^{-1}$) | Infrared ($cm^{-1}$) |
|---|---|---|---|
| $\nu_1$ (Symmetric C=O stretch) | $\sum_g^+$ | 1388.15 | inactive |
| $\nu_2$ (O=C=O bend) | $\Pi_u$ | inactive | 667.38 |
| $\nu_3$ (Asymmetric C=O stretch) | $\sum_u^+$ | inactive | 2349.16 |

### 3.5.2 Infrared spectroscopy

Infrared spectroscopy is sensitive to minor changes in vibrations between atoms. The aim of carrying out IR spectroscopy on **1** was to determine whether there are any changes in the gas vibrational modes between the single- and mixed-gas systems. By comparing the orientation of the guests in the mixed-gas computational model (Figure 3.14) to that of the single-gas models Figure 3.2 (i) and (ii) one would expect the $\nu_3$ asymmetric C-H stretch band of acetylene and the $\nu_3$ asymmetric C=O stretch band of carbon dioxide to change, owing to the interaction between the gases in the mixed-gas system.

The IR spectra of **1** exposed to acetylene (red), carbon dioxide (blue) and a mixture of gases (orange) are shown in Figure 3.15. From the spectra there are two observations that can be made: (i) In the mixed-gas system both acetylene and carbon dioxide are adsorbed, because the $\nu_3$ bands of

both the gases are present in the mixed-gas spectrum and (ii) there is a band shift in the mixed-gas sorption relative to the single-gas sorption (Table 3.7).

The asymmetric C-H stretch band of pure acetylene is centred at 3281.92 $cm^{-1}$.[44] Upon sorption into **1,** the $v_3$ band of acetylene is shifted to 3222.52 $cm^{-1}$, and then an additional red-shift of 4.83 $cm^{-1}$ to 3218.66 $cm^{-1}$ occurs in the mixed-gas system. The $v_3$ band of pure carbon dioxide is centred at 2349.16 $cm^{-1}$,[44] which is shifted to 2329.66 $cm^{-1}$ when $CO_2$ is adsorbed in **1.** When $CO_2$ is adsorbed in the mixed-gas system, its $v_3$ band is blue-shifted by 1.93 $cm^{-1}$ to 2331.56 $cm^{-1}$. Although the changes in vibrational frequencies are small, they indicate a change in the vibrational energy when the gases are included in single-gas systems, and additional changes occur in the mixed-gas system.

As the $v_3$ bands of both acetylene and carbon dioxide are shifted when the gas mixture is adsorbed, it can be concluded that in the mixed-gas system the gases are in a different chemical environment relative to those of the single-gas systems. Therefore, it appears that the gases are not included as single-gas dimers during mixed gas sorption, but rather as mixed-gas dimers.

The optimised structures described in Section 3.6 were used to calculate the vibrational frequencies of the gases within the hosts. The calculations were performed with the Generalized Gradient Approximation (GGA) - Perdew-Burke-Ernzerhof (PBE)[45] functional and Grimme[46] dispersion correction (PBE-D). Furthermore an atomic orbital double numerical basis set with polarisation (DNP) was used. In general, without any scaling applied, the correlation between calculated and observed frequencies was off by 30-70 $cm^{-1}$. However, the difference in the $v_3$ frequencies between the single-gas and mixed-gas systems correlated well with the observed results (see Table 3.7).

**Table 3.7**: Calculated and observed wavelengths for acetylene and carbon dioxide included in **1** as single gases (SG) or a mixture of gases (MG).

| | Vibration Mode | Calc. v SG ($cm^{-1}$) | Calc. v MG ($cm^{-1}$) | Δ calc.v $_{SG\ \&\ MG}$ ($cm^{-1}$) | Obs. v SG ($cm^{-1}$) | Obs. v MG ($cm^{-1}$) | Δ obs v. $_{SG\ \&\ MG}$ ($cm^{-1}$) |
|---|---|---|---|---|---|---|---|
| **Acetylene** | $v_1$ Raman | 3378.3 | 3475.7 | 97.4 | Not obs | - | - |
| | $v_2$ Raman | 2016.2 | 2015.5 | 0.7 | 1962.3 | 1965.4 | 2.3 |
| | $v_3$ Infrared | 3376.5 | 3383.7 | 7.2 | 3222.52 | 3218.7 | 3.8 |
| | $v_4$ Raman | 752.0 | 741.4 | 10.6 | Not obs | - | - |
| | $v_5$ Infrared | 712.0 | 701.8 | 10.2 | Not obs | Not obs | - |
| **$CO_2$** | $v_1$ Raman | 1301.1 | 1302.2 | 1.1 | Not obs | Not obs | - |
| | $v_2$ Infrared | 722.4 | 701.3 | 21.1 | 655.7 | 655.7 | 0.0 |
| | $v_3$ Infrared | 2286.3 | 2283.8 | 2.5 | 2329.7 | 2331.6 | 1.9 |

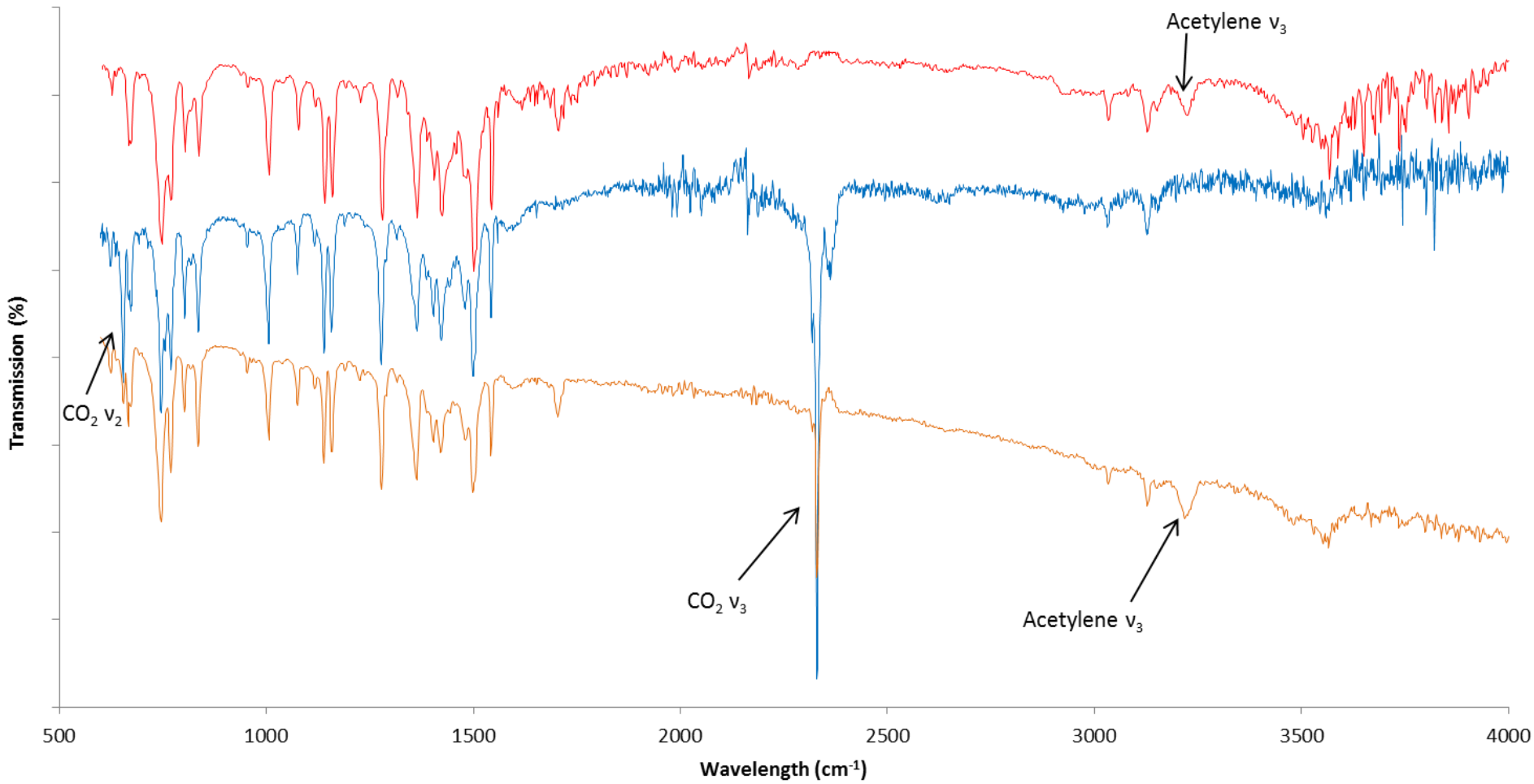


***Figure 3.15**: Infrared spectra of **1** occupied by acetylene (red), carbon dioxide (blue) and a gas mixture (orange). The $\nu_3$ bands of both acetylene and carbon dioxide are present in the spectrum for the gas mixture, confirming that both gases are adsorbed simultaneously in **1**.*

### 3.5.3 Raman spectroscopy

One of the major challenges with regard to Raman spectroscopy in this study was to record spectra under high pressure. The pressure vessel described in Section 2.9 was used in a Raman spectrometer built by Dr. Pieter Neethling and housed in the Physics Department of Stellenbosch University.

Figure 3.16 shows the Raman spectra for the apohost (green), the host occupied with acetylene (red), the host occupied with carbon dioxide (blue) and the host occupied with a gas mixture (orange).Ideally one would monitor the Raman bands for acetylene and carbon dioxide gases in **1**. However, carbon dioxide only has one Raman active band, which is weak and could not be detected. Acetylene has three active Raman bands (Table 3.5), but we could only detect $\nu_2$ at 1962.26 $cm^{-1}$ in the pure acetylene system. A small peak around the position of acetylene's $\nu_2$ band appears to be present in the mixed-gas system, however the signal is too weak to draw conclusions. By only monitoring acetylene's $\nu_2$ there are no substantial conclusions that may be drawn. Therefore, we monitored the Raman bands of the host instead.

The Raman spectrum of the apohost (Figure 3.16 green) shows four strong signals arising from the ligand. The logical vibration to monitor would be that corresponding to the strongest interaction between the guests and host. As this is the interaction between the guest and the chlorine atom on the host, the Cd-Cl stretching band would be ideal to monitor. However, the Cd-Cl bond has a very weak Raman band centred at 212 ± 5 $cm^{-1}$ that could not be detected by the instrument.[47] The frequencies of the observed bands are given in Table 3.8.

The peak in the apohost spectrum with the strongest signal is centered at 1620.61 $cm^{-1}$, and most probably corresponds to the quadrant ring stretch of the benzene or imidazole ring.[48] The peak undergoes a red-shift when acetylene or carbon dioxide occupies the host. When the gas mixture is adsorbed the peak undergoes an additional, more pronounced red-shift to 1614.15 $cm^{-1}$. The second strongest peak centered at 1294.25 $cm^{-1}$ in the apohost spectrum could be the $CH_2$ in-phase twist band.[48] Similarly to the first peak, there is a red-shift in the peak when acetylene or carbon dioxide are adsorbed, and a more pronounced shift when the gas mixture is adsorbed. The third band centered at 1198.53 $cm^{-1}$ could be either the radial in-phase stretch of imidazole or benzene, whereas the fourth peak centred at 837.97 $cm^{-1}$ is either due to adjacent hydrogen wag-vibrations in benzene or imidazole's quadrant ring in-phase bend.[48] The same red-shift trends were observed for both of these peaks.

**Table 3.8**: Observed Raman bands of **1** ($cm^{-1}$)

| | Apohost | $C_2H_2$ system | $CO_2$ system | Mixed-gas system |
|---|---|---|---|---|
| **Band 1 ($cm^{-1}$)** | 1620.612 | 1619.561 | 1618.665 | 1614.148 |
| **Band 2 ($cm^{-1}$)** | 1294.250 | 1293.275 | 1293.16 | 1289.632 |
| **Band 3 ($cm^{-1}$)** | 1198.534 | 1198.998 | 1197.432 | 1194.107 |
| **Band 4 ($cm^{-1}$)** | 837.9741 | 835.3203 | 835.8632 | 831.4566 |

It is uncertain which vibrations in the host give rise to the observed bands; therefore one might draw false conclusions from the data. Nevertheless, it is evident that the interactions between the guests and host do not have a substantial effect on the host's electronic configuration, and it is apparent that the extent of host-guest interactions differs between the three systems. Moreover, the more substantial shifts of the mixed-gas system emphasises how the host's environment changes when a gas mixture is adsorbed, showing that the shift is not simply an average of single-gas systems. This implies strongly that there is a mixture of gases in the host's void-space.

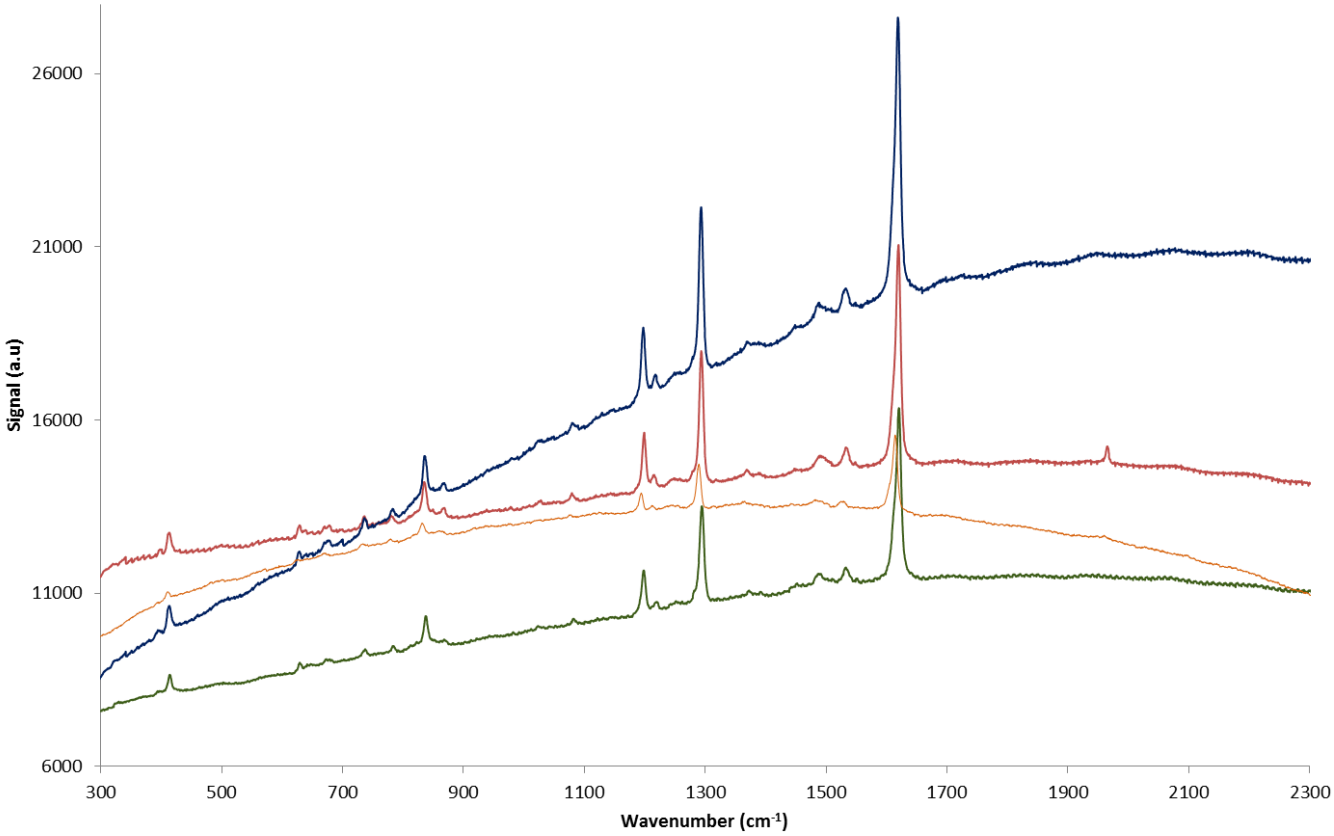


***Figure 3.16**: Raman spectra for the apohost (green), the host occupied with acetylene (red), the host occupied with carbon dioxide (blue) and the host occupied with a gas mixture (orange).*

### 3.5.4 Fluorescence spectroscopy

*NOTE: At this stage in the project the safety hazard of pressurising a vessel with 8 bar of acetylene did not justify the results gained, as there were no peak shifts in the excitation or emission spectra of **1** exposed to 15 bar mixed gas, 20 bar carbon dioxide or under vacuum ( see Figures 3.18 and 3.19). In addition, the nature of the adapted instrument required the pressure vessel to be removed when gases were changed. As a result the location of the excitation beam on the sample was not constant in all of the experiments. As a consequence no conclusions can be drawn from the intensity variation between spectra.*

Organic linkers with π-conjugated backbones, such as **L** used in **1**, usually exhibit the strongest fluorescence emission from the lowest excited singlet state to the singlet ground state. Hence the emissions correspond to π* → π or π* → n transitions. Luminescence from organic frameworks joined by $d^{10}$ transition-metal ions such as Cd(II), which has filled core-like d-orbitals, is commonly centred on the ligand rather than the metal because of the absence of d-d transitions in the metal ions.[49] The host**, 1,** has a Cd(II) metal ion joining the organic linkers, therefore linker-based fluorescence and Ligand to Metal Charge Transfer (LMCT) is expected for the host.

The ligand's emission spectrum between 220 to 800 nm upon excitation at 220 nm is shown in Figure 3.17. When the ligand coordinates to Cd(II) the emission spectrum changes to those shown in Figure 3.19. The change in the emission spectrum is expected since the LMCT influences the ligand's electronic configuration.

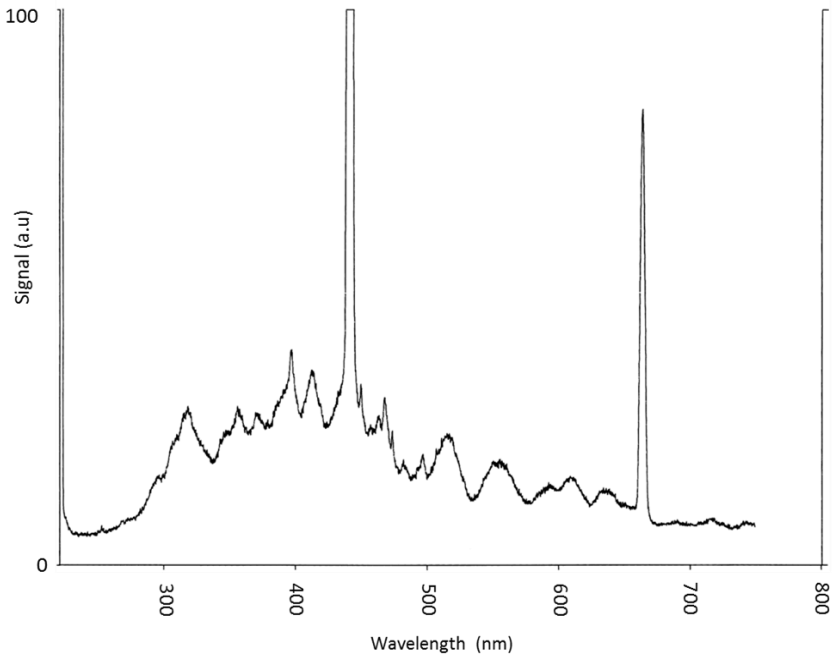


***Figure 3.17**: Emission spectrum of the ligand, **L**, upon excitation at 220 nm.*

In order to test the postulation made, based on the Raman spectroscopy results, that the interactions between the guests and host do not have a substantial effect on the host's electronic configuration, excitation and emission spectra of **1** were recorded under vacuum (green in Figures 3.18 and 3.19), 20 bar $CO_2$ (blue) and 15 bar mixed-gas (orange).

The excitation spectrum in Figure 3.18 was obtained using a simultaneous excitation and emission spectral scan. The highest energy excitation maximum occurs at 250 nm. Therefore emission spectra for the host systems were recorded at an excitation wavelength of 250 nm. All spectra were recorded at 0° C.

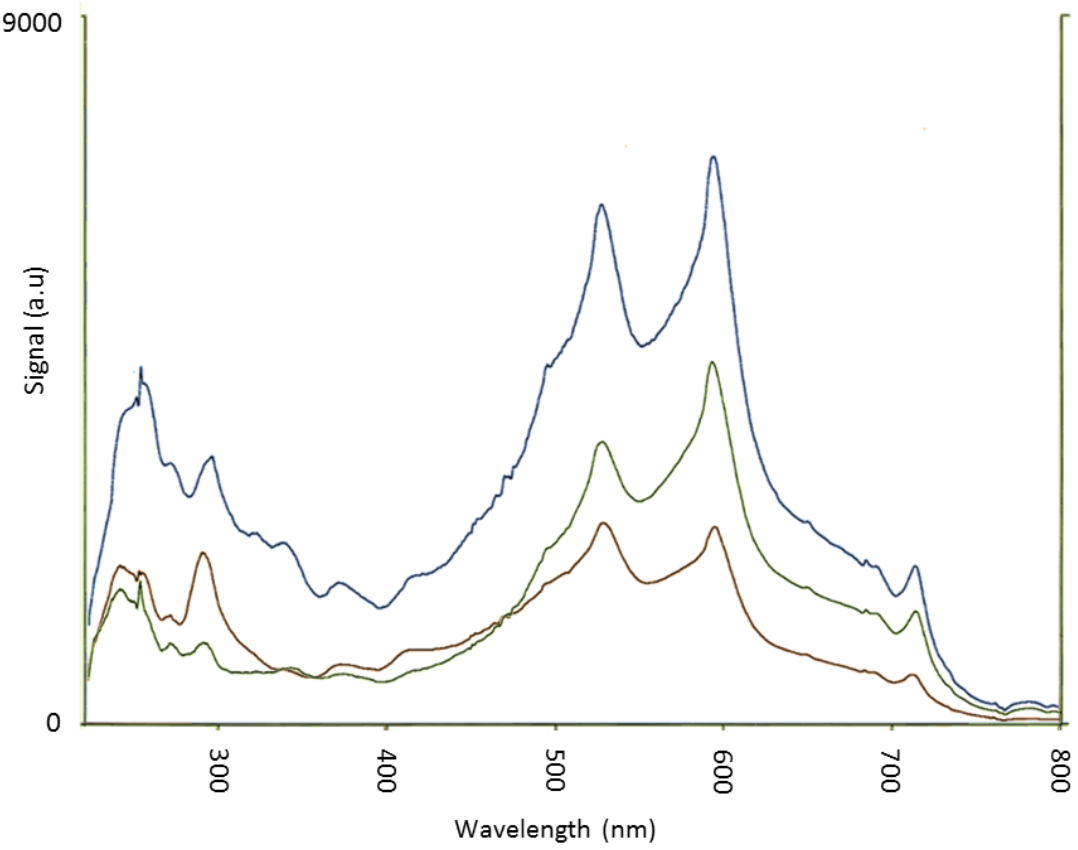


***Figure 3.18**: Excitation spectra of **1** under vacuum (green), 20 bar carbon dioxide (blue) and 14 bar mixed-gas (orange).*

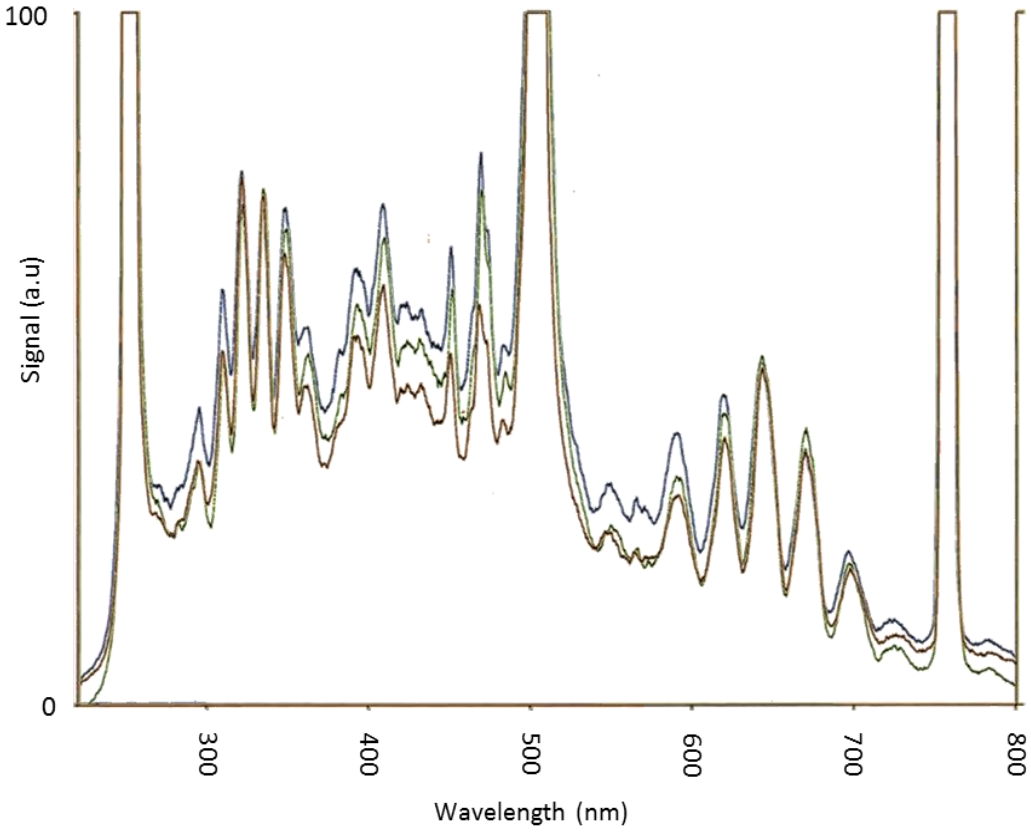


***Figure 3.19**: Emission spectra of **1** under vacuum (green), 20 bar carbon dioxide (blue) and 14 bar mixed-gas (orange).*

It is difficult to say which transitions give rise to the bands in the fluorescence spectra. However, in both the excitation and emission spectra there are no peak shifts upon guest inclusion. A possible explanation might be the longer-range and weaker electrostatic interactions between the guests and ligand of the host as compared to the interaction between the guests and the host's chlorine atom. If there were a strong guest-ligand interaction an exciplex could be formed upon excitation.

Exciplexes are hetero-dimers between two molecules in the excited state that influence the emission of a fluorophore. The result is often a broad featureless emission at wavelengths red-shifted from those of the monomers. In this case the monomer is the apohost. Electronic structure modelling has previously shown that exciplex formation has a strong dependence on separation distance and is generally favourable in cofacial arrangements.[49] The sharp features of the spectrum and no red-shifted peaks confirmed that there is no exciplex formation. The absence of exciplex formation could be due to the long interaction range between the guest and host ligand, the relatively stronger and closer interaction distances between the host's chlorine and guest, and the fact that there are no cofacial arrangements between the gases and the ligand. Figures 3.20 to 3.22 show the closest contacts between the guests and the ligand part of the host, as well as the relative guest-host orientations in each of the systems.

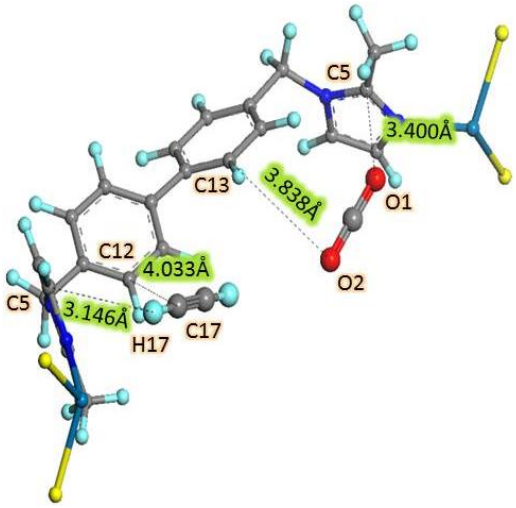


***Figure 3.20**: Closest guest-ligand contacts in the **1**-mixed-gas system. The closest guest-host chlorine interaction is 2.491 Å for acetylene and 3.329 Å for carbon dioxide.*

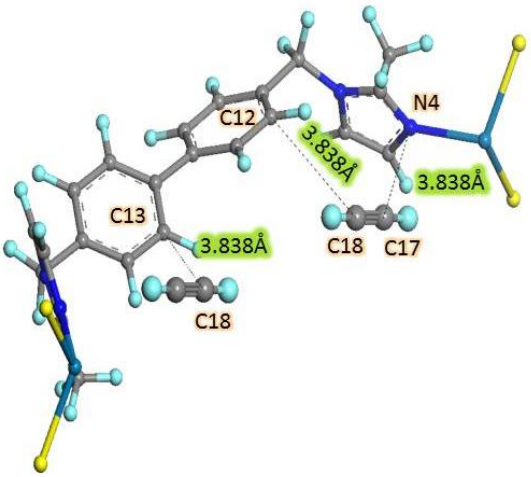


***Figure 3.21**: Closest guest-ligand contacts in the **1**-acetylene system. The closest guest-host chlorine interaction is 2.491 Å.*

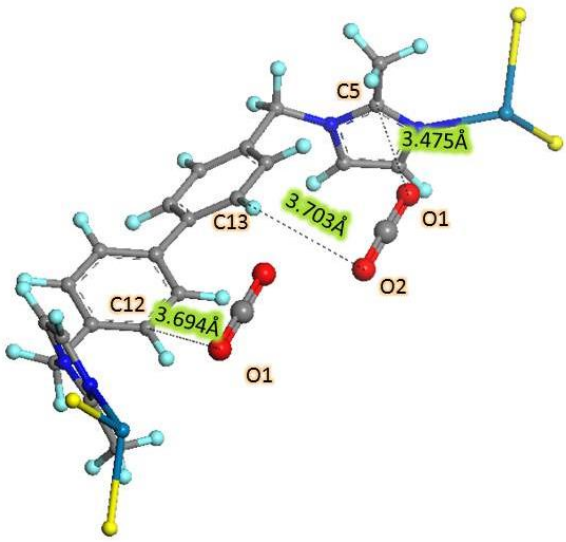


***Figure 3.22**: Closest guest-ligand contacts in the **1**-carbon dioxide system. The closest guest-host chlorine interaction is 3.329 Å.*

## 3.6 Density functional theory studies

### 3.6.1 Interaction energies

Density functional theory studies were employed in order to explain the nature of the host-guest interactions. The atomic coordinates obtained from SCD data were used to build periodic models in the Materials Studio[50] environment. In order to facilitate the dynamic nature of the host, **1**, motion groups were used during the optimisation of the periodic models. In geometry optimisation calculations motion groups are used to constrain all of the atoms to a particular configuration, however the whole entity is allowed to move as a rigid group. Rationally, all aromatic moieties and guests were assigned to individual motion groups. However, in order to keep the unit cell parameters constant, the Cartesian positions of all cadmium atoms and the methylene groups, which bridge the imidazole and benzene moieties, were constrained (Figure 3.23). Before motion groups were assigned to aromatic moieties, all non-hydrogen atomic positions were fixed, and then hydrogen positions were optimised as part of a periodic system. All of the optimisations were carried out using the CASTEP[51] module with PBE-D and a plane wave basis set. The energy cut-off and the SCF convergence thresholds for geometry optimisation were set to 380.0 eV and $5.0 \times 10^{-7}$ eV, respectively.

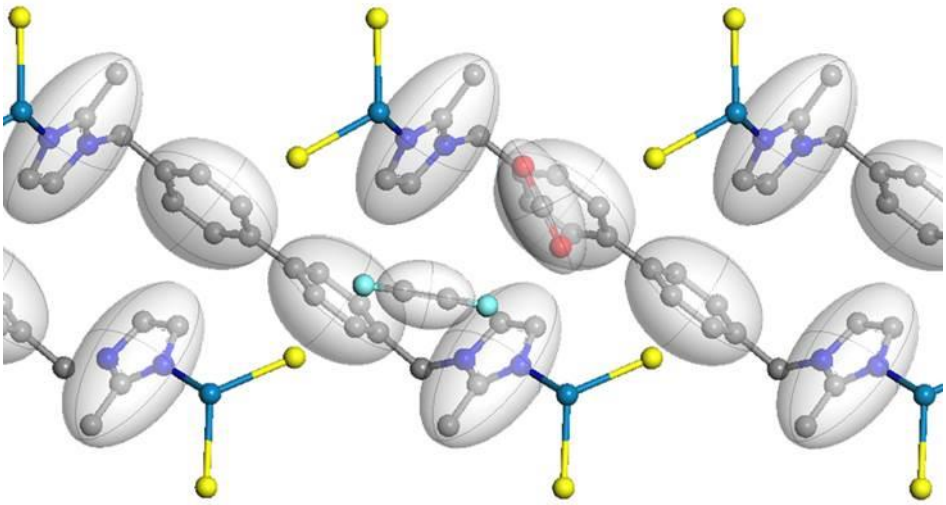

***Figure 3.23**: Motion groups were assigned to all aromatic moieties and guests, whereas the Cartesian coordinates of bridging methylene groups and cadmium atoms were constrained. The host's hydrogens are omitted for clarity.*

The host-guest interaction energies were determined by single-point energy calculations. Subsequently the host atoms were removed from the periodic model and the guest energies were calculated. In addition, both guest molecules were removed from the periodic model and subsequent single-point energies were calculated for the empty hosts. Thereafter, geometries of the empty hosts were optimised and subsequent single point energy calculations were performed in order to determine host relaxation energies. All optimisations and single point energies were performed using

the CASTEP code with PBE-D and a plane wave basis set with the cut-off energy set to 380.0 eV and the SCF threshold set to $5.0 \times 10^{-7}$ eV. The calculated single-point energies are given in Table 3.8.

**Table 3.8**: Single-point energies calculated for the three systems, all in kcal mol$^{-1}$.

| System | Empty host | Optimised Empty host | Occupied host | Two guests alone | Single guest | |
|---|---|---|---|---|---|---|
| | | | | | $CO_2$ | $C_2H_2$ |
| **Acetylene** | -320656.4 | -320657.7 | -336338.3 | -15661.1 | NA | -7829.7 |
| **Carbon dioxide** | -320660.0 | -320659.9 | -368129.2 | -47413.9 | -23706.8 | NA |
| **Mixed system** | -320657.8 | -320658.6 | -352253.8 | -31539.7 | -23706.8 | -7829.7 |

Various interaction energies, such as host-guest and guest-guest interactions, can be calculated from the single-point energies. The interaction energies and the manner in which they were calculated are given in Table 3.9.

**Table 3.9**: Interaction energies (kcal mol$^{-1}$) in the various systems.

| System | Guest-host interaction | Guest-guest interaction | Relaxation energy | Difference in guest energy | |
|---|---|---|---|---|---|
| | | | | $C_2H_2$ | $CO_2$ |
| **Acetylene** | -20.814 | -1.6253 | -1.0248 | 0.0 | N/A |
| **Carbon dioxide** | -55.344 | -0.2800 | -2.675 E-5 | N/A | 0.0 |
| **Mixed gas** | -56.269 | -3.2453 | -0.7705 | -0.00237 | -0.0390 |
| **Method of calculation** | Occupied host's energy - empty host's energy - two guests' energies | Energy of two guests - 2x energy of one guest | Optimised empty host energy - experimental empty host energy | Guest in mixed-gas system - guest in single-gas system | |

The optimised structures are given in Figures 3.24 to 3.26. In cavity (i) of all the Figures, the van der Waals interaction between the guest and host is shown. In Figures 3.20 to 3.22 as well as in Figures 3.24 (iii) to 3.26 (iii) the distances between the guests and the host are given. In addition, Figures 3.24 (ii) to 3.26 (ii) show the Hirshfeld partial charges of the adsorbed guests. The shortest interaction distance is between the various guests and the host chlorine.

In the mixed-gas system the acetylene finds an energy minimum 0.18 Å farther from the host's chlorine atom relative to the single-gas acetylene system. Even though the acetylene in the mixed-gas system is farther from the host's chlorine, its charge distribution is more pronounced. Since the interaction distance and charge distribution in the carbon dioxide and mixed-gas system are similar, the electron density shift in acetylene can be ascribed to the greater electronegative charge on the host chlorine in conjunction with the acetylene-carbon dioxide interaction.

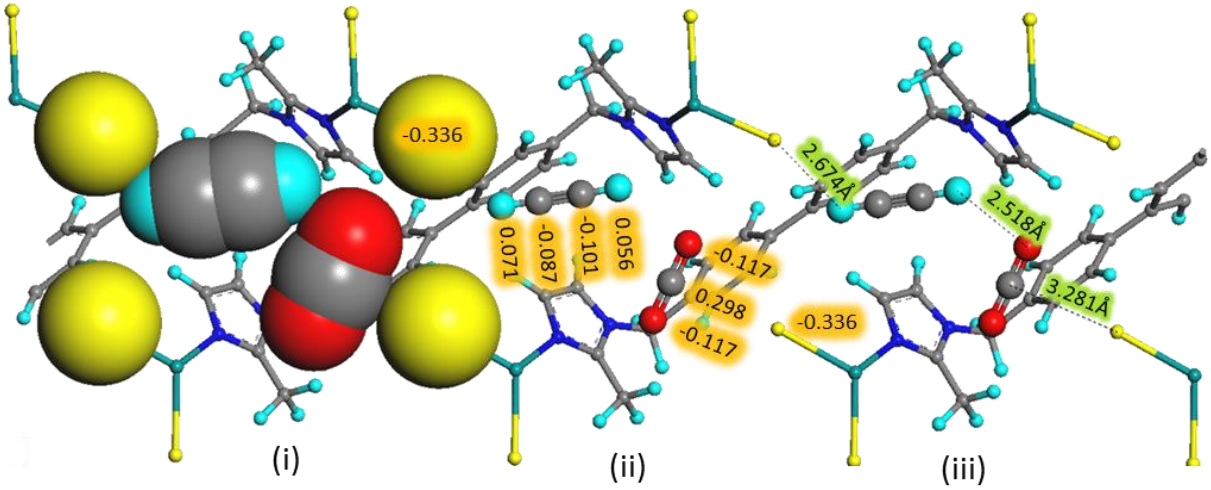


***Figure 3.24**: Optimised structure of the mixed-gas system. Void (i) shows the van der Waals host-guest interaction. Void (ii) shows the partial charges on the guests. Void (iii) shows the closest contacts between host and guest.*

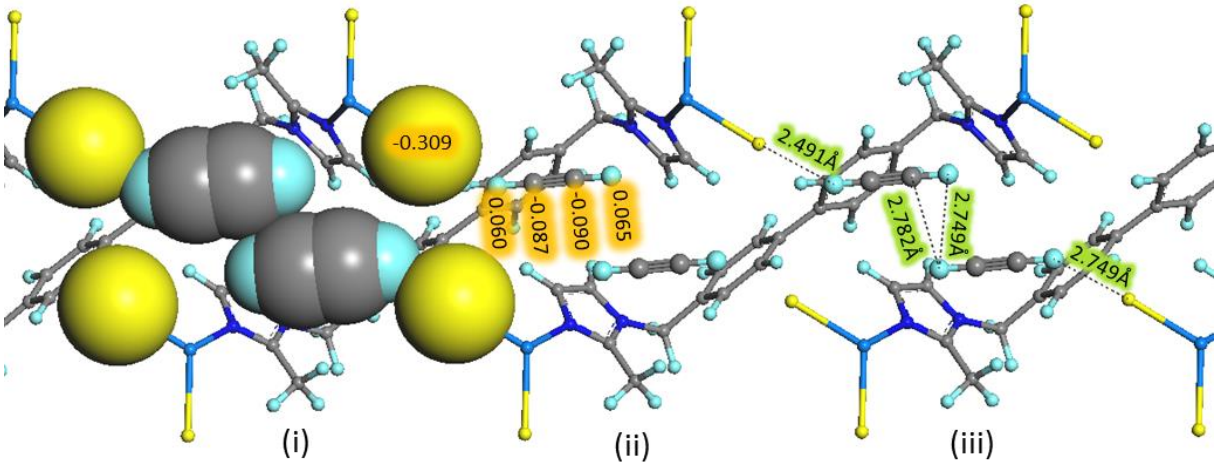


***Figure 3.25**: Optimised structure of the acetylene system. Void (i) shows the van der Waals host-guest interaction. Void (ii) shows the partial charges on the guests. Void (iii) shows the closest contacts between host and guest.*

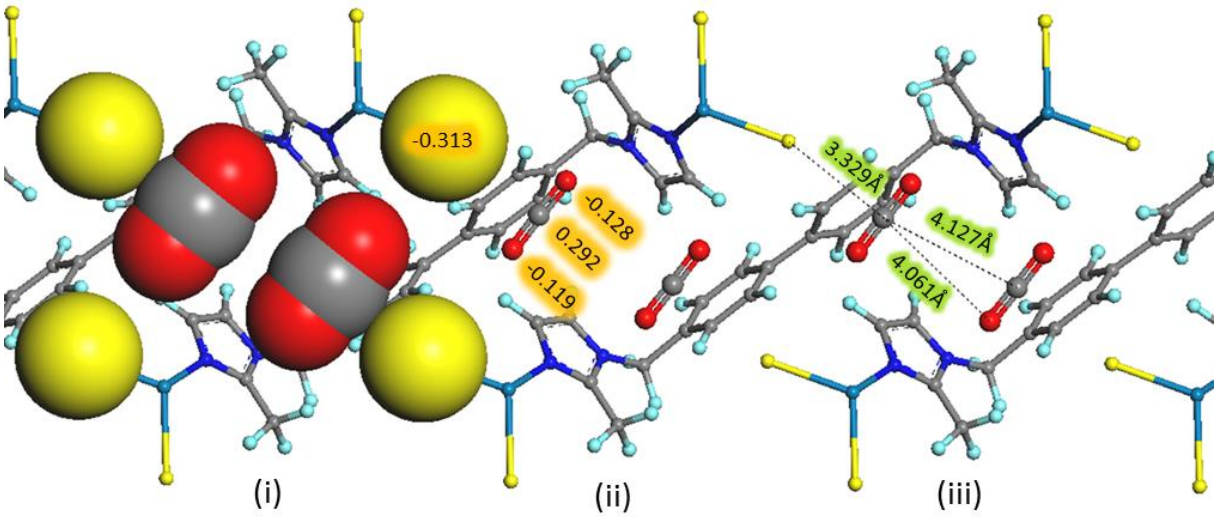


***Figure 3.26**: Optimised structure of the carbon dioxide system. Void (i) shows the van der Waals host-guest interaction. Void (ii) shows the partial charges on the guests. Void (iii) shows the closest contacts between host and guest.*

### 3.6.2 Electrostatic interactions

Electrostatic potential mapping is a convenient tool with which one can visualise electrostatic potential at any given point in three dimensions. With regard to this dissertation potential mapping was used to portray the electrostatic potential in a host's void space onto adsorbed guest molecules.

The combination of electrostatic potential maps and the electrostatic profile of the guest can be used to rationalise the position and orientation of guest molecules in a host's void space. For example, if the void space in a host has a region of negative electrostatic potential, and a guest molecule has a region of positive electrostatic potential, it is highly likely that the guest will orientate itself in such a manner that the negative and positive regions will coincide, and if that is not the case it is most probable that there are either stronger electrostatic or van der Waals interactions elsewhere.

Generally the procedure to generate an electrostatic potential map involves three steps. The first step is to generate an isosurface around the guest molecule that corresponds to the van der Waals volume of the guest molecule. A molecule's electron density is calculated during a single-point energy calculation. The electron density is then used to generate an isosurface around the guest molecule where the guest's electron density corresponds to 0.0067 $e^-/Å^3$, which is similar in volume to the van der Waals volume of the guest.

In the second step the crystallographic data are used to build a model that represents guest-accessible void space and the host lattice surrounding it, and all guest molecules are removed from the model. Consequently the electrostatic potential of the host lattice model is calculated using the VAMP module of the Materials Studio software suite as a single-point energy calculation using the NDDO-PM6[52] Hamiltonian with an SCF convergence threshold of $5 \times 10^{-7}$ kcal $mol^{-1}$. Then, the electrostatic potential is imported into the lattice model with data points spread out on a grid of 0.15 Å spacing.

The third step is to import the guest's isosurface into the lattice model at the original positions of the guest molecules. Thereafter, the electrostatic potential data points that lie on the isosurface of the guest molecule are displayed as an electrostatic potential map. An electrostatic potential map thus displays the host's electrostatic potential that the guest molecule experiences.

In Figures 3.27 to 3.29 the host, **1**, encapsulating two molecules of acetylene, carbon dioxide or the gas mixture are shown respectively. In each figure the top, bottom and side views are given to provide a three-dimensional representation of the host-guest interactions.

The **1**-$CO_2$ system is shown in Figure 3.27. Given the electrostatic profile of carbon dioxide (Figure 3.3) one would expect that there would be a strong electrostatic interaction between the carbon dioxide's $\delta^+$ carbon and the host's $\delta^-$ chlorine, and that is exactly where the strongest host-guest interaction occurs. Here the largest electrostatic potential on the carbon dioxide's oxygen corresponds to -0.0864 Ha. In addition, there are areas of +0.04994 Ha electrostatic potential around carbon dioxide's $\delta^-$ oxygen, which is indicative of additional stabilising host-guest interactions. These smaller interactions originate from the aromatic protons on the host's imidazole groups.

Figure 3.28 shows that, relative to carbon dioxide, there is a more negative electrostatic potential on acetylene's hydrogen due to the host's $\delta^-$ chlorine. Here, the point of maximum negative electrostatic potential is -0.2041 Ha, which is indicative of a much stronger interaction between acetylene and the host relative to the carbon dioxide system. Therefore, one would expect a more favourable interaction energy between acetylene and the host relative to carbon dioxide and the host. However, as shown in Table 3.9, this is not the case; carbon dioxide has the stronger host-guest interaction energy. The phenomenon can be explained by the repelling positive electrostatic potential of +0.0272 Ha on the $\delta^+$ hydrogen of the acetylene molecule, which arises from the host's cadmium ions.

As reported by Jacobs et al.[36] the step in the acetylene sorption isotherm of **1,** is due to an energy barrier that has to be crossed to allow the inclusion of a second molecule of acetylene. It is likely that when the second molecule of acetylene enters the host the repulsive C-H···Cd interaction increases, which creates an energy barrier as the acetylene is pushed toward the cadmium in order to accommodate the second gas molecule in the restricted void space.

The host that encapsulates the acetylene-carbon dioxide mixture is shown in Figure 3.29. In the model the negative electrostatic potential of the host chlorine on acetylene's $\delta^+$ hydrogen remains constant at -0.2041 Ha. However, the repulsive positive electrostatic potential between acetylene and the cadmium increases to +0.0313 Ha. Carbon dioxide also retains the guest-host chlorine interaction, however in the mixed gas system the carbon dioxide is shifted closer to the chlorine and, in effect, the electrostatic potential on carbon dioxide's surface decreases to -0.1091 Ha, indicating a stronger host-guest interaction. The overall gain in stabilisation energy is -0.0778 Ha (-48.825 kcal $mol^{-1}$) relative to the single-gas systems. Thus the difference in orientation and position of the guests in the host void space is one of the biggest driving forces for selectively adsorbing a gas mixture in every void.

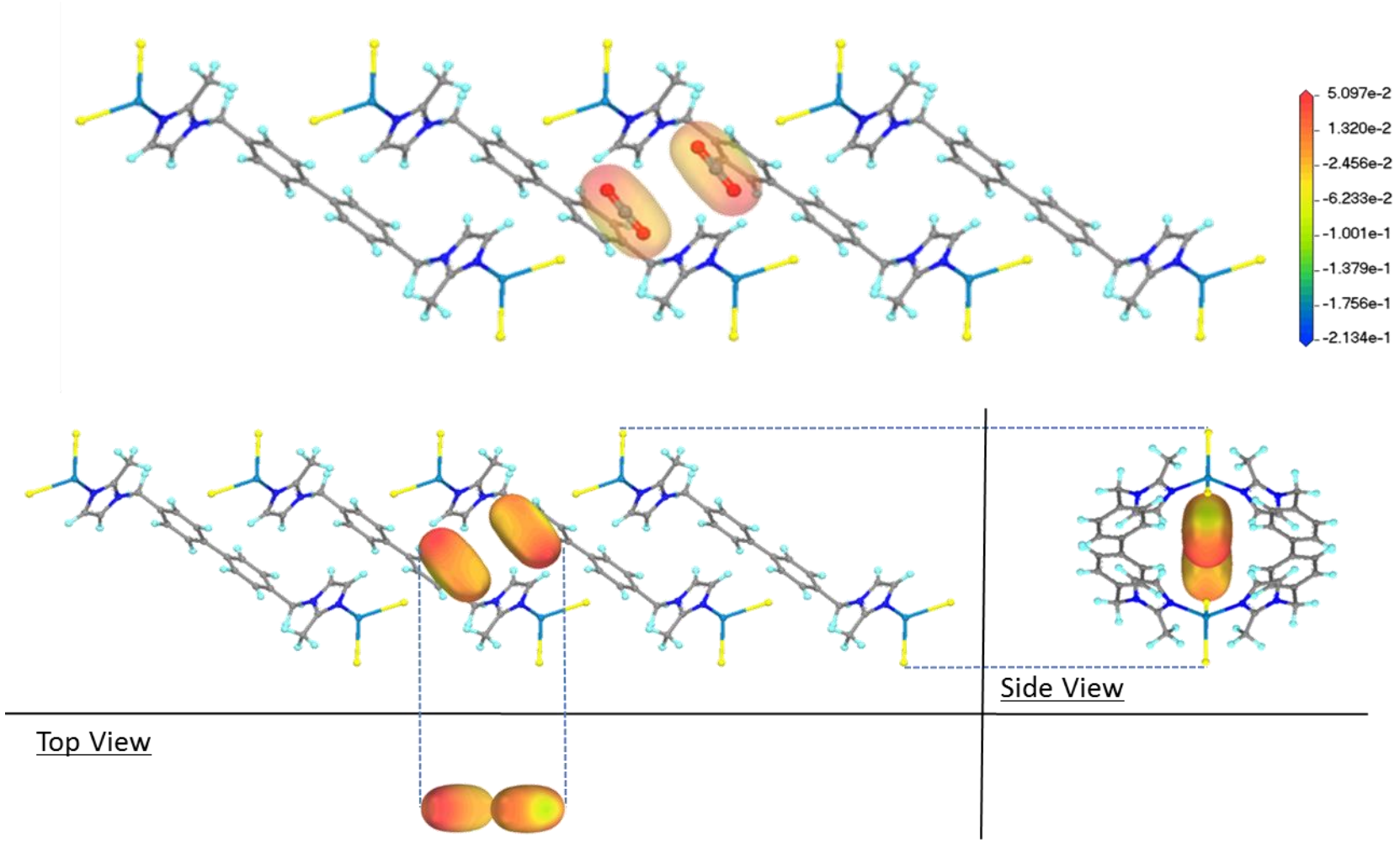


***Figure 3.27**: VAMP electrostatic potential map of the host's electron density mapped onto two carbon dioxide guests encapsulated in the void space. In the map one can see that the host's δ⁻ chlorine to the $CO_2$ guest's δ⁺ carbon is the strongest host-guest electrostatic interaction.*

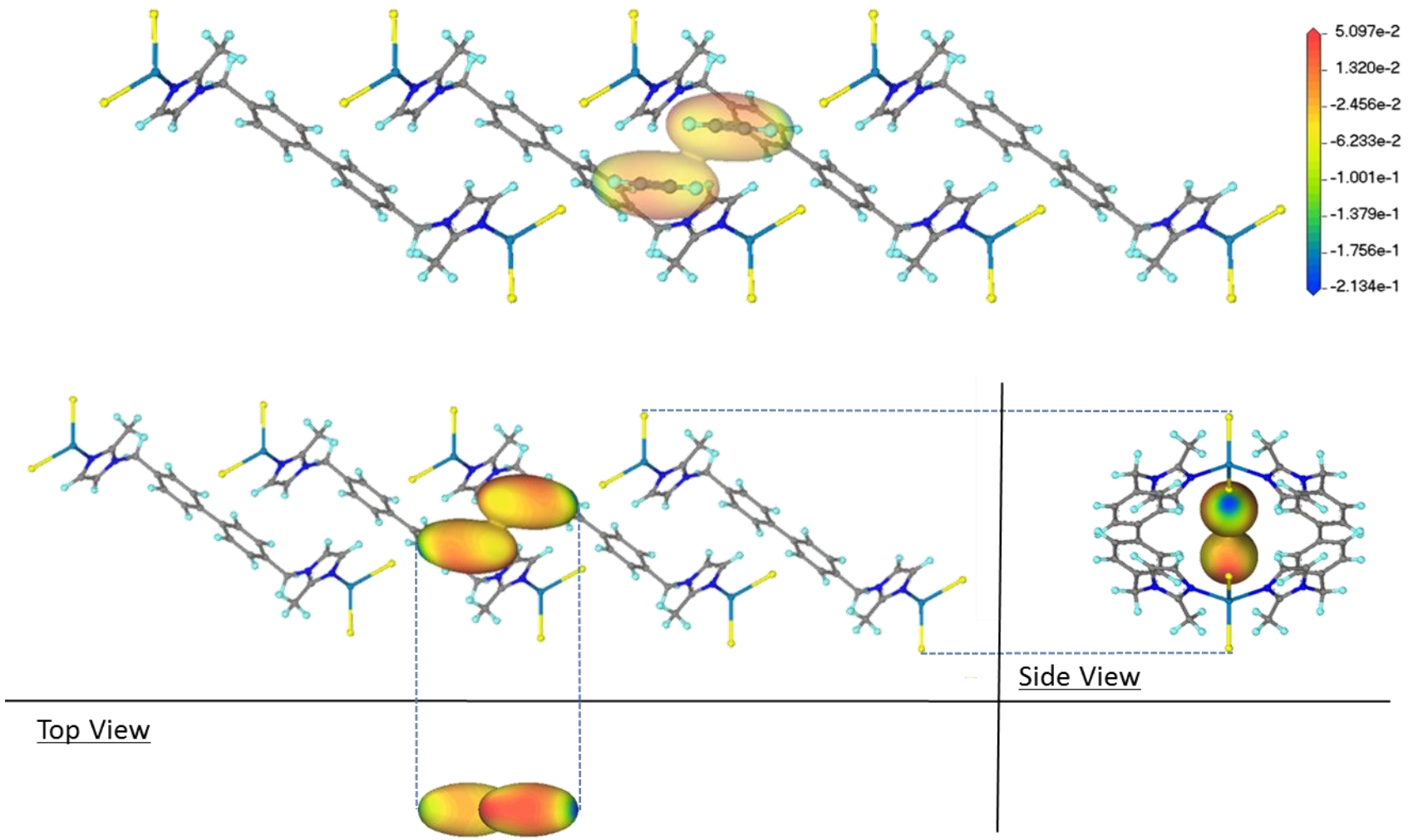


***Figure 3.28**: VAMP electrostatic potential map of the host's electron density mapped onto two carbon dioxide guests encapsulated in the void space. In the map one can see that the $\delta^-$ chlorine of the host to the $\delta^+$ carbon of acetylene is the strongest host-guest electrostatic interaction.*

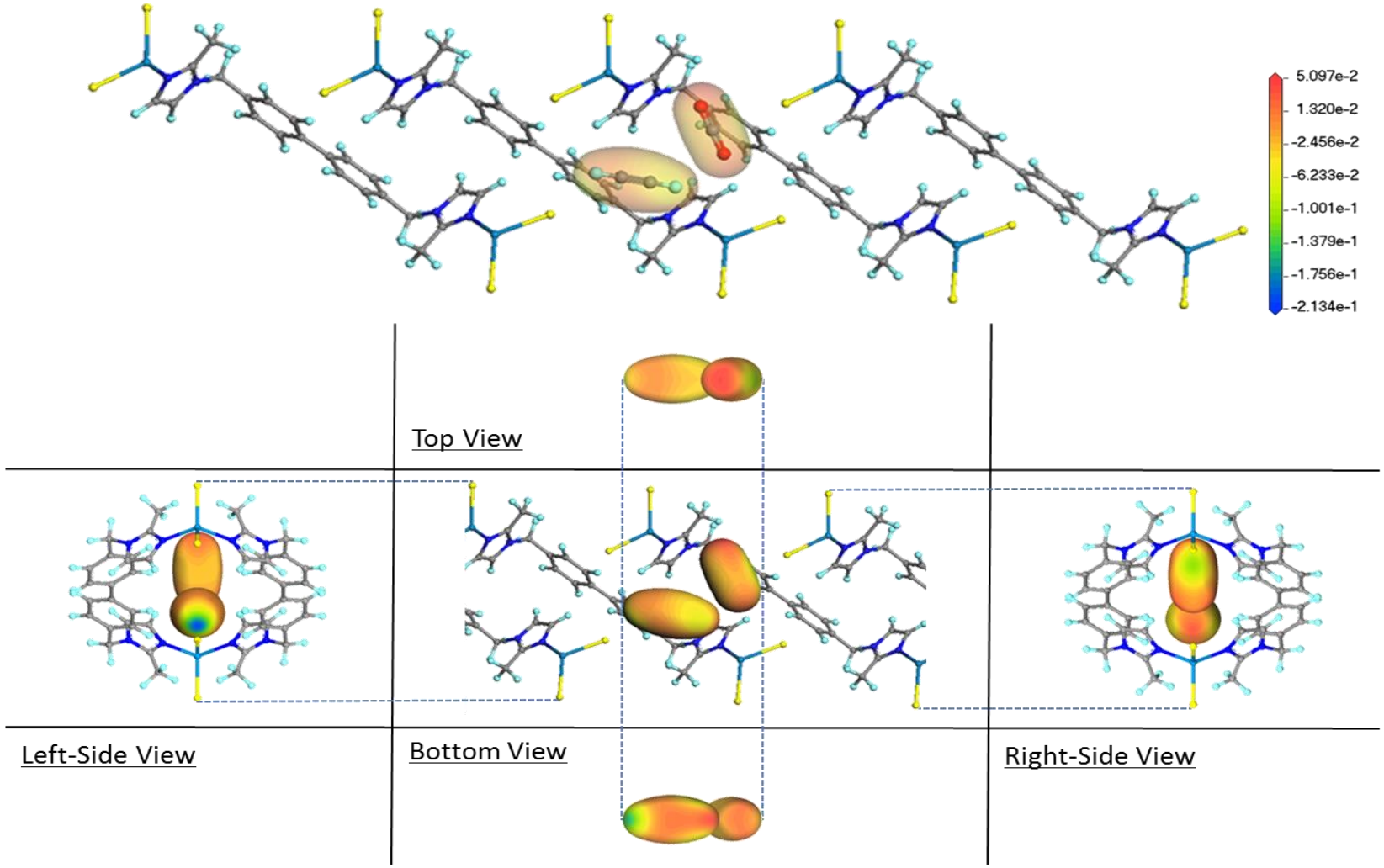


***Figure 3.29**: VAMP electrostatic potential map of the host's electron density mapped onto the mixture of guests that are encapsulated in the void space. In the map one can see that the strongest host-guest interactions remain between the host's $\delta^-$ chlorine and the guest's $\delta^+$ atoms, which are a hydrogen atom in acetylene and carbon atom in carbon dioxide.*

## 3.7 Conclusion

A metallocyclic host known to adsorb two molecules of acetylene or carbon dioxide per host cavity was used to test the assumptions made in the theoretical prediction of selectivity for mixed-gas sorption. The IAST method of calculating selectivity factors were used and, according to the theory, the host was predicted to be selective for acetylene uptake. However, when the mixed-gas sorption isotherm was recorded, it could be seen that less gas than expected was adsorbed. The combination of difference Fourier maps and computational modelling gave convincing results that suggests the host adsorbs both acetylene and carbon dioxide. Infrared and Raman spectroscopy were used to determine that there is a mixture of gases in every host void space. DFT calculations showed that the mixed-gas system has a lower energy structure relative to the single-gas systems. Moreover, the lowest energy guest-guest interaction occurs in the mixed-gas system. Electrostatic potential maps revealed where the strongest guest-host interactions occur. From the potential maps it could be seen that both acetylene and carbon dioxide retained their strong stabilising interaction with the host chlorine when they were included in the mixed-gas system. In addition, the acetylene and carbon dioxide are orientated in such a manner that the two molecules have a favourable electrostatic interaction with each other within the void, as opposed to a destabilising van der Waals repulsion observed in the single-gas acetylene system.

The fact that a 1:1 molar mixture of gas was adsorbed into the host as opposed to predominantly acetylene as predicted, or a random adsorption of gases is quite interesting. It serves as proof of concept that the assumptions made in theories such as the IAST are not valid for all materials. Additional factors such as sorption competition between guests as well as (stronger than the mean) guest-guest interactions may influence a host's selectivity. Therefore, additional experimentation is required to prove selectivity.

This study employed additional methods to determine selectivity, relying on the use of an environmental gas cell for SCD studies and a multi-purpose pressure vessel for fluorescence and Raman spectroscopy. The advantage of the method described here is that it gives information on guest-guest and guest-host interactions that can be used to explain the selectivity of a host.

On a more fundamental level, it is interesting that every cavity in the mixed gas system contains a molecule each of acetylene and carbon dioxide. It may well be that the guests prefer to be adsorbed as a mixture due to the entropic advantage. On the other hand, one can argue that in the gaseous state the guests form a hetero-dimer for a brief period of time. These dimers are short-lived single entities that have their own unique properties. The sorption process might be an equilibrium

exchange between single gas species and the dimers, and as the host is in a lower energy state when it adsorbs a dimer the relaxation in the lattice energy drives the equilibrium to dimer inclusion.

In further studies the selectivity in other model hosts could be investigated with a similar method. In addition, the influence on selectivity during sorption when other gases with similar properties interact could be investigated. With specific knowledge regarding host-guest and guest-guest interactions during sorption, it may be possible to add correction terms to theoretical sorption models to account for guest-guest interactions and competition between guests during a sorption process in order to have a theory with universal application.

## 3.8 References


(1) Liu, J.; Tian, J.; Thallapally, P. K.; McGrail, B. P. *J. Phys. Chem. C* **2012**, *116*, 9575.

(2) Chatti, R.; Bansiwal, A. K.; Thote, J. A.; Kumar, V.; Jadhav, P.; Lokhande, S. K.; Biniwale, R. B.; Labhsetwar, N. K.; Rayalu, S. S. *Microporous Mesoporous Mater.* **2009**, *121*, 84.

(3) Aroua, M. K.; Daud, W. M. A. W.; Yin, C. Y.; Adinata, D. *Sep. Purif. Technol.* **2008**, *62*, 609.

(4) Li, J.-R.; Kuppler, R. J.; Zhou, H.-C. *Chem. Soc. Rev.* **2009**, *38*, 1477.

(5) Li, J.-R.; Sculley, J.; Zhou, H.-C. *Chem. Rev.* **2011**, *112*, 869.

(6) Furukawa, H.; Yaghi, O. M. *J. Am. Chem. Soc.* **2009**, *131*, 8875.

(7) Jones, C. D.; Tan, J. C.; Lloyd, G. O. *Chem. Commun.* **2012**, *48*, 2110.

(8) Jacobs, T.; Gertenbach, J.; Das, D.; Barbour, L. J. *Aust. J. Chem.* **2010**, *63*, 573.

(9) Chen, L.; Reiss, P. S.; Chong, S. Y.; Holden, D.; Jelfs, K. E.; Hasell, T.; Little, M. A.; Kewley, A.; Briggs, M. E.; Stephenson, A.; Thomas, K. M.; Armstrong, J. A.; Bell, J.; Busto, J.; Noel, R.; Liu, J.; Strachan, D. M.; Thallapally, P. K.; Cooper, A. I. *Nat Mater* **2014**, *advance online publication*.

(10) Evans, J. D.; Huang, D. M.; Hill, M. R.; Sumby, C. J.; Thornton, A. W.; Doonan, C. J. *The Journal of Physical Chemistry C.* **2013**, *118*, 1523.

(11) Luo, X.-Z.; Jia, X.-J.; Deng, J.-H.; Zhong, J.-L.; Liu, H.-J.; Wang, K.-J.; Zhong, D.-C. *J. Am. Chem. Soc.* **2013**, *135*, 11684.

(12) He, Y.; Xiang, S.; Chen, B. *J. Am. Chem. Soc.* **2011**, *133*, 14570.

(13) Gary, J. H.; Handwerk, G. E. *Petroleum Refining*; Taylor & Francis, 2001.

(14) Lusi, M.; Barbour, L. J. *Angew. Chem. Int. Ed.* **2012**, *51*, 3928.

(15) Millward, A. R.; Yaghi, O. M. *J. Am. Chem. Soc.* **2005**, *127*, 17998.

(16) Gándara, F.; Furukawa, H.; Lee, S.; Yaghi, O. M. *J. Am. Chem. Soc.* **2014**, *136*, 5271.

(17) Sircar, S.; Golden, T. C.; Rao, M. B. *Carbon* **1996**, *34*, 1.

(18) Couck, S.; Denayer, J. F. M.; Baron, G. V.; Rémy, T.; Gascon, J.; Kapteijn, F. *J. Am. Chem. Soc.* **2009**, *131*, 6326.

(19) Ribeiro, R. P. P. L.; Grande, C. A.; Rodrigues, A. E. *Sep. Sci. Technol.* **2014**, *49*, 1985.

(20) Sircar, S.; Golden, T. C. *Sep. Sci. Technol.* **2000**, *35*, 667.

(21) Yong, Z.; Mata, V.; Rodrigues, A. r. E. *Sep. Purif. Technol.* **2002**, *26*, 195.

(22) Gomes, V. G.; Yee, K. W. K. *Sep. Purif. Technol.* **2002**, *28*, 161.

(23) Liu, J.; Thallapally, P. K.; Strachan, D. *Langmuir* **2012**, *28*, 11584.

(24) Chen, L.; Reiss, P. S.; Chong, S. Y.; Holden, D.; Jelfs, K. E.; Hasell, T.; Little, M. A.; Kewley, A.; Briggs, M. E.; Stephenson, A.; Thomas, K. M.; Armstrong, J. A.; Bell, J.; Busto, J.; Noel, R.; Liu, J.; Strachan, D. M.; Thallapally, P. K.; Cooper, A. I. *Nat Mater* **2014**, *13*, 954.

(25) Atwood, J. L.; Barbour, L. J.; Jerga, A. *Angew. Chem. Int. Ed.* **2004**, *43*, 2948.

(26) Bourne, S. A.; Novoa, J. J.; Braga, D.; Addadi, L. *Engineering of Crystalline Materials Properties: State of the Art in Modeling, Design and Applications*; 1 ed.; Springer: Dordrecht, 2008; Vol. 1, p 111-129.

(27) Grobler, I. PhD, University of Stellenbosch, 2013.

(28) Ruthven, D. M. *Principles of Adsorption and Adsorption Processes*; Wiley: Canada, 1984; Vol. 1.

(29) Myers, A. L.; Prausnitz, J. M. *AIChE J.* **1965**, *11*, 121.

(30) Robinson, L. N. *Water Resources Research Progress*; 1 ed.; Nova Science Publishers: New York, 2008.

(31) Li, J.-R.; Ma, Y.; McCarthy, M. C.; Sculley, J.; Yu, J.; Jeong, H.-K.; Balbuena, P. B.; Zhou, H.-C. *Coord. Chem. Rev.* **2011**, *255*, 1791.

(32) Cessford, N. F.; Seaton, N. A.; Düren, T. *Ind. Eng. Chem. Res.* **2012**, *51*, 4911.

(33) Hand, D. W.; Loper, S.; Ari, M.; Crittenden, J. C. *Environ. Sci. Technol.* **1985**, *19*, 1037.

(34) FitzGerald, S. A.; Pierce, C. J.; Rowsell, J. L. C.; Bloch, E. D.; Mason, J. A. *J. Am. Chem. Soc.* **2013**, *135*, 9458.

(35) Tanaka, H.; Noguchi, D.; Yuzawa, A.; Kodaira, T.; Kanoh, H.; Kaneko, K. *J. Low Temp. Phys.* **2009**, *157*, 352.

(36) Jacobs, T.; Lloyd, G. O.; Gertenbach, J.-A.; Müller-Nedebock, K. K.; Esterhuysen, C.; Barbour, L. J. *Angew. Chem. Int. Ed.* **2012**, *51*, 4913.

(37) Huang, Z. S.; Miller, R. E. *Chem. Phys.* **1989**, *132*, 185.

(38) Lauzin, C.; Oliaee, J. N.; Rezaei, M.; Moazzen-Ahmadi, N. *J. Mol. Spectrosc.* **2011**, *267*, 19.

(39) Prichard, D. G.; Nandi, R. N.; Muenter, J. S.; Howard, B. J. *J. Chem. Phys.* **1988**, *89*, 1245.

(40) De Almeida, W. B. *Chem. Phys.* **1990**, *141*, 297.

(41) Jacobs, T. PhD, University of Stellenbosch, 2009.

(42) Spek, A. *J. Appl. Crystallogr.* **2003**, *36*, 7.

(43) Willock, D. *Molecular Symmetry*; 1 ed.; John Wiley & Sons: West Sussex, 2009.

(44) Shimanouchi, T.; Commerce, D. o., Ed.; Natural Bureau of Standards: Washington D.C., 1972; Vol. 1, p 164.

(45) Perdew, J. P.; Burke, K.; Ernzerhof, M. *Phys. Rev. Lett.* **1996**, *77*, 3865.

(46) Grimme, S. *J. Comput. Chem.* **2004**, *25*, 1463.

(47) Takagi, Y.; Itoh, N.; Nakamura, T. *J. Chem. Soc., Faraday Trans.* **1989**, *85*, 493.

(48) Larkin, P. *Infrared and Raman Spectroscopy; Principles and Spectral Interpretation*; Elsevier Science: Waltham, 2011; Vol. 1.

(49) Allendorf, M. D.; Bauer, C. A.; Bhakta, R. K.; Houk, R. J. T. *Chem. Soc. Rev.* **2009**, *38*, 1330.

(50) 6.0.0 ed.; Accelrys Software Inc.: San Diego, 2011.

(51) Payne, M. C.; Teter, M. P.; Allan, D. C.; Arias, T. A.; Joannopoulos, J. D. *Rev. Mod. Phys.* **1992**, *64*, 1045.

(52) Voityuk, A. A.; Rösch, N. *J. Phys. Chem. A* **2000**, *104*, 4089.

# CHAPTER 4 | A STUDY OF THE HYDROGEN-BONDED ORGANIC FRAMEWORK 8

## 4.1 Introduction

The advantages of porous synthetic materials and, consequently, the reasons why they are studied were discussed in Chapter 3.1. Among these porous materials there are metallocycles (such as **1**), MOFs, and more recently Covalent Organic Frameworks (COFs) and Hydrogen-bonded Organic Frameworks (HOFs).[1] HOFs are interesting to study because they exhibit similar advantageous properties found in other synthetic porous materials such as metallocycles and MOFs. For example, HOF-1 and HOF-3 have shown potential for highly selective $C_2H_2/C_2H_4$ and $CO_2/C_2H_2$ separation, respectively. HOF-2 displays highly enantioselective separation of secondary alcohols, and other organic frameworks are capable of catalysis.[2-5] However, unlike the metal-containing MOFs and metallocycles, pure organic frameworks are entirely composed of light elements; therefore they pose less of a pollution risk. Moreover, they can be easily purified and regenerated by recrystallisation.[5-7]

HOFs consist of organic linkers that are joined by hydrogen bonds, and often also other non-covalent interactions such as π-π stacking interactions. Due to the relatively weak nature of the non-covalent interactions, HOF frameworks often exhibit low stabilities, and they frequently collapse when their guest molecules are removed. Thus, there are few examples of permanently porous and stable HOFs.[1] Consequently, the development of HOFs in terms of framework design as well as topological and functional exploration has lagged significantly behind that of MOFs.[3]

For a HOF to be permanently porous and stable, the host molecules have to form numerous strong hydrogen bonds that are not substantially affected by guest removal.[1] However, the flexibility and relative weakness of hydrogen bonds makes the synthesis of porous HOFs somewhat challenging.[8,9] To realise targeted design and synthesis of porous materials it is of interest to materials scientists to understand the nature of the interactions that can produce stable porous organic frameworks, and even more so when these materials show interesting properties such as selective gas sorption.[5]

HOF-8 is an example of a porous hydrogen-bonded organic framework that has shown interesting sorption properties and high thermal stability.[1] Thus, HOF-8 serves as a suitable model compound for the study of structure-property relationships in organic frameworks. This chapter

reports a study of HOF-8, and involves thermal analysis, gas sorption and structural analysis. In addition, it is shown how useful a coupling between a hot stage and mass spectrometer can be in the field of inclusion chemistry.

## 4.2 Results and discussion

### 4.2.1 Synthesis of 1,3,5-benzene-tri(4-pyridinyl)carboxoamide (BTPC)

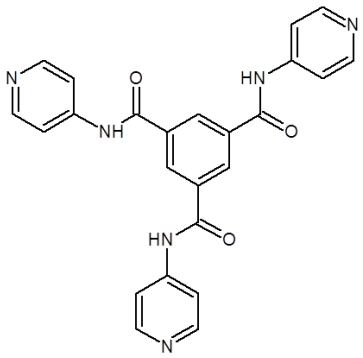

BTPC was synthesised according to a modified literature[1,10] procedure. 20 ml of dry THF containing 12 mmol (3.22 g) 1,3,5-benzenetricarbonyl trichloride was added drop-wise to a 60 ml dry THF solution containing 36 mmol (3.4 g) of 4-aminopyridine and 43.1 mmol (6 ml) of distilled triethylamine at 0°C under a nitrogen atmosphere and continuous stirring. The reaction temperature was allowed to rise to room temperature overnight, resulting in an off-white precipitate. The precipitate was washed three times with THF, followed by water, and dried at 120 °C overnight. The resulting powder was suspended in acetone and stirred at room temperature for three days, filtered and dried at 80 °C overnight, resulting in a white powder of 1,3,5-benzene-tri(4-pyridinyl)carboxoamide. Yield of 49.4%. **$\delta_H$ (DMSO, 400 MHz)**: 11.01 (3H, s), 8.78 (3H, s), 8.54 (6H, d), 7.86 (6H, d). **$\delta_C$ (DMSO, 100MHz)** 114.14, 130.57, 134.94, 145.66, 150.46, 165.22.

### 4.2.2 Synthesis of HOF-8

Single crystals suitable for SCD studies were obtained by the dissolution of 1,3,5-benzene-tri(4-pyridinyl)carboxoamide (0.46 mmol, 0.2 g) in a 40 ml 1:3 (v/v) methanol: chloroform solution, which was then refluxed with continuous stirring for 4 hours. The solution was filtered through a silica column into heated vials and left to evaporate slowly at 50 °C. After 48 hours solvated HOF-8 ($[8{\cdot}C_{24}H_{18}N_6O_3]$ 3.5 $CHCl_3$) was obtained as light-brown block-shaped crystals. The crystal structure will be discussed in Section 4.6.

### 4.2.3 Desolvation (activation) of HOF-8

It was reported[1] that after crystallisation the chloroform solvent in the void space of HOF-8 can be removed by heating the crystals to 260 °C. However, as discussed later, it was found that this activation procedure led to the destruction of the crystals, and therefore an alternative activation procedure was used.

Single crystals of solvated HOF-8 were exposed to supercritical carbon dioxide (sc-$CO_2$) for 48 hours, followed by heating (200 °C) under vacuum (2-3 mmHg) for a further 48 hours. This cycle was repeated twice. Thereafter, the HOF-8 crystals were heated to 260 °C.

In Figure 4.1 (a), the FT IR of HOF-8 shows the fingerprint C=O asymmetric stretch at 2360.43 $cm^{-1}$ that arises from the $CO_2$ that is adsorbed during sc-$CO_2$ exposure. In Figure 4.1 (b) a TGA trace of the solvated HOF-8 (red) is compared to that of HOF-8 that has undergone a single activation cycle (purple). In the purple TGA trace it can be seen that the adsorbed $CO_2$ is released below 100 °C, followed by an additional mass loss that occurs at approximately 250 °C. The mass loss that occurs at approximately 250 °C in the purple trace is roughly half that of the mass loss that occurs in the red trace at the same temperature. This mass loss is most probably remaining solvent. From the TGA traces, one can assume that after the first cycle of sc-$CO_2$ exposure and a heating phase, about half of the solvent molecules in the solvated HOF-8 were released.

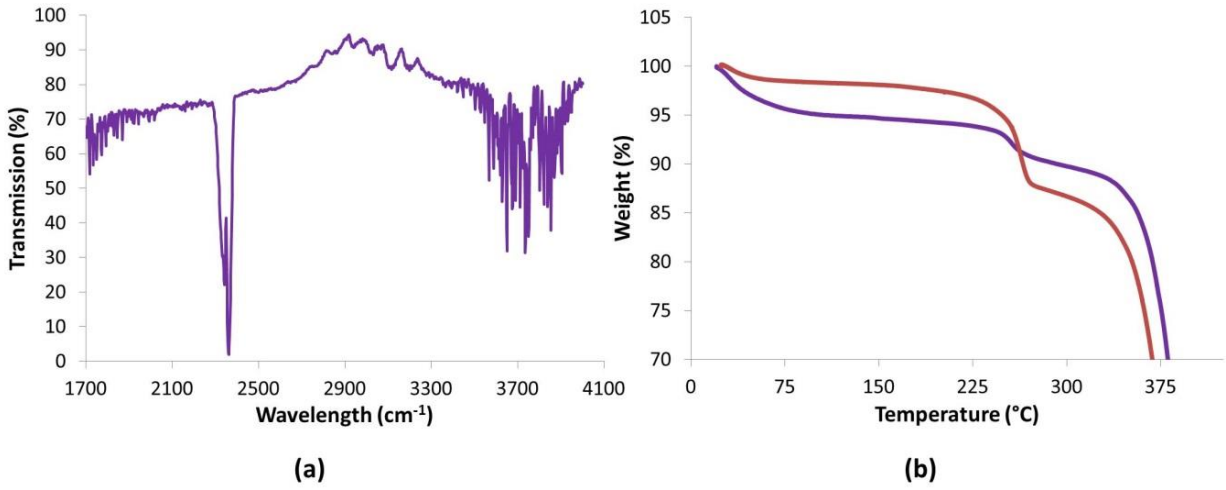


***Figure 4.1**:(a) The asymmetric C=O stretch at approximately 2360.43 $cm^{-1}$ in the IR spectrum of HOF-8 after 48 hour sc-$CO_2$ exposure shows that the framework has taken up $CO_2$. (b) After HOF-8 has taken up $CO_2$ a TGA trace (purple) shows that $CO_2$ can be released from the framework by heating the framework above 100 °C. Comparing the mass loss at 250 °C between the TGA trace of the solvated HOF-8 (red) and the purple trace, it appears that approximately half of the solvent molecules remain in HOF-8 after a single activation cycle.*

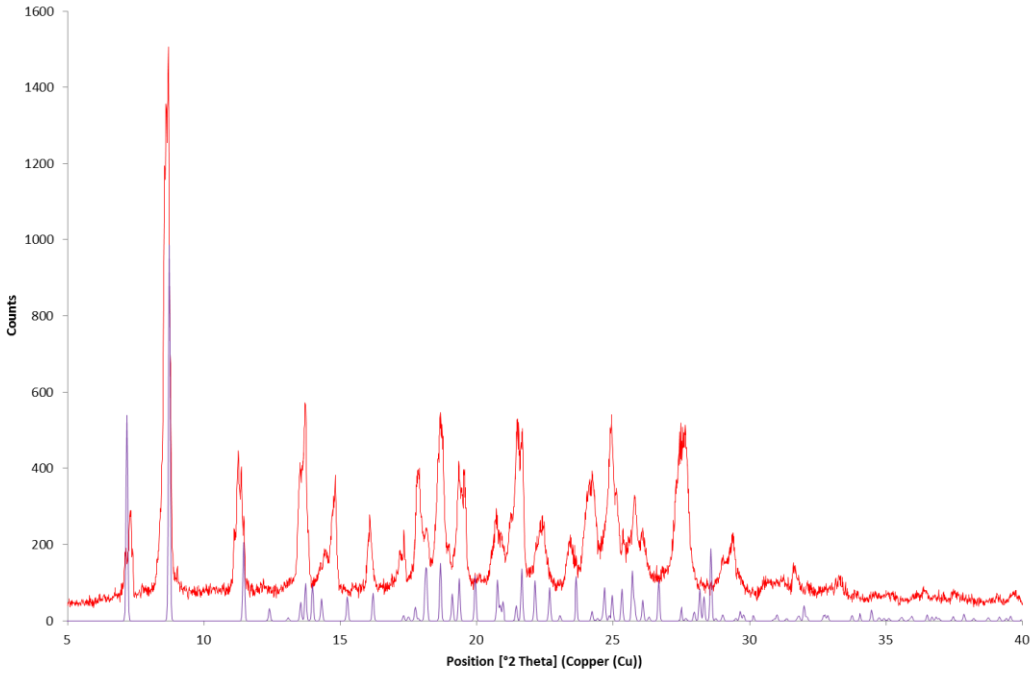


***Figure 4.2**: The simulated powder pattern of solvated HOF-8 (purple) and the experimental pattern of the activated HOF-8 crystals (red). There is good agreement between the patterns, confirming that the activation procedure does not cause HOF-8 crystals to decompose or undergo host rearrangement.*

PXRD analysis showed that the HOF-8 crystals did not decompose or undergo any framework changes during activation. In Figure 4.2 the powder pattern of the activated HOF-8, which was used for adsorption studies, is compared to a simulated powder pattern of the solvated HOF-8. There is a good correlation between the patterns, which indicates that no noteworthy structural changes occur during the activation of HOF-8.

## 4.3 Thermal analysis

### 4.3.1 Thermogravimetric analysis (TGA)

In Figure 4.3 the TGA traces of BTPC, solvated HOF-8 and activated HOF-8 are given in blue, red, and green, respectively. BTPC shows a gradual mass loss of 7.2% between 30 and 125 °C, which is most probably due to the loss of surface solvent, while decomposition commences at 330 °C. The activated HOF-8 gradually undergoes mass loss from 290 °C and at 330 °C decomposition occurs. The as-synthesised HOF-8 also starts to decompose at 330 °C and shows a 12% mass loss between 230 and 275 °C, which corresponds to approximately 3.5 chloroform molecules per unit cell. It was previously reported[1] that the observed mass loss for solvated HOF-8 is due to a ratio of 1:20 chloroform:water molecules, as determined with NMR spectroscopy. Therefore, it is possible that the 12% mass is due to the loss of chloroform and water rather than 3.5 chloroform molecules per formula unit.

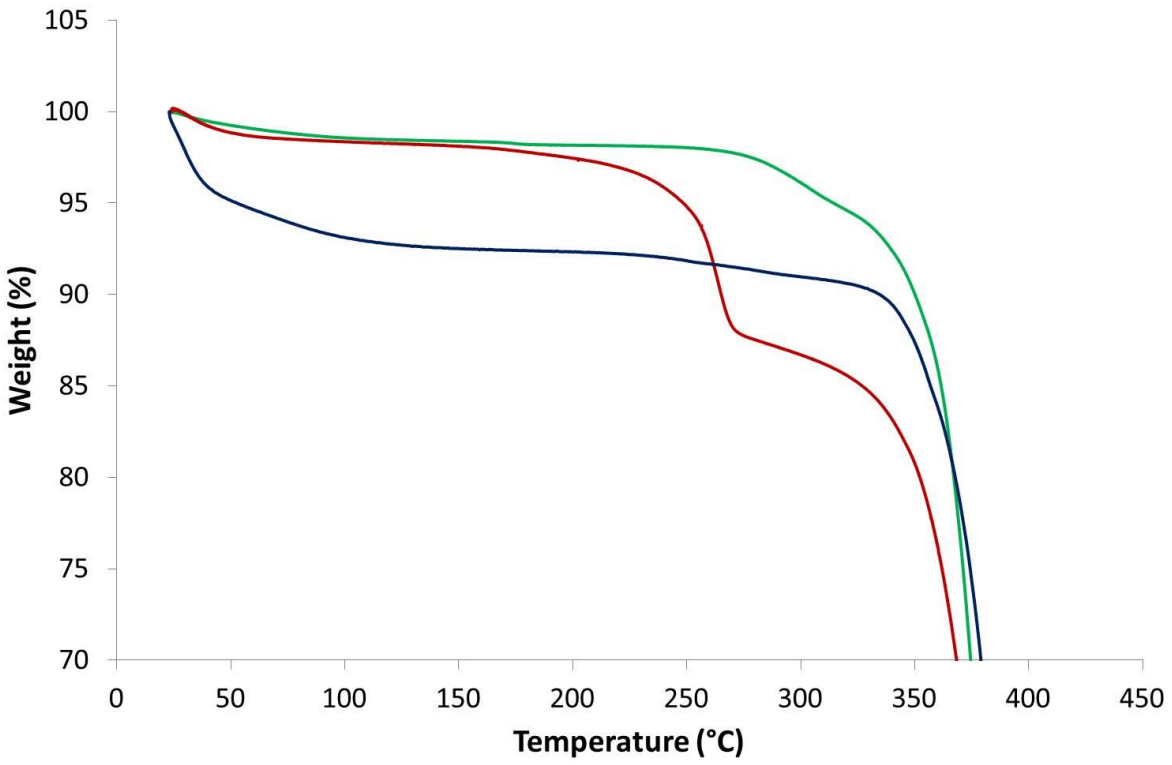


***Figure 4.3**: TGA traces of BTPC (blue), solvated HOF-8 (red) and activated HOF-8 (green). BTPC undergoes a 7.2% mass loss between 30 and 125 °C, and the solvated HOF-8 undergoes a 12% mass loss between 230 and 275 °C.*

### 4.3.2 Hot stage analysis

A hot stage is a useful tool for observing how the morphology of a compound is affected as a function of increasing temperature. For example, one can determine where a single-crystal becomes unusable for SCD, or where a temperature-induced phase change occurs. In the field of inclusion chemistry, the correlation of a TGA trace and hot stage photos is useful, because one can determine the temperature at which guest loss occurs, the amount of guest loss, the onset temperature of host decomposition, and how the morphology changes during guest loss and decomposition.

For example, the TGA trace of solvated HOF-8 (Figure 4.4) shows that the 12% solvent molecules by mass are released from HOF-8 just above 250 °C, and the hot stage photographs show that the rapid solvent loss causes the single crystals to dissolve* during the guest loss. This is an useful and important observation, because TGA alone might lead one to think that an intact apohost can be obtained by simply heating HOF-8 crystals to 260 °C (as reported[1]), however as one can see it leads to the destruction of single-crystals. It is for this reason that an alternative activation procedure was used, and in Figure 4.5 one can see that, HOF-8 crystals can be activated with the

*It seems as if the crystal dissolves in the solvent that it releases. This process is similar to deliquescence, but it is not well defined, and therefore dissolved is used for simplicity.

alternative activation procedure and will then probably be suitable for SCD up to 300 °C. Thereafter cracks appear in the crystals, followed by substantial deterioration after 320 °C.

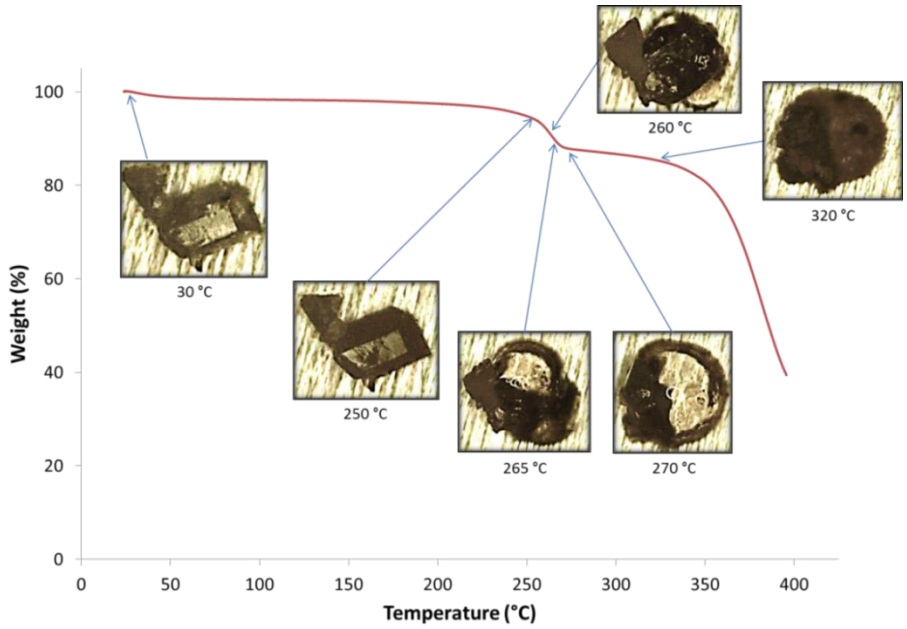


***Figure 4.4**: Hot stage photographs correlated to a TGA trace show that the solvated HOF-8 crystals start to dissolve at 260 °C as solvent is released.*

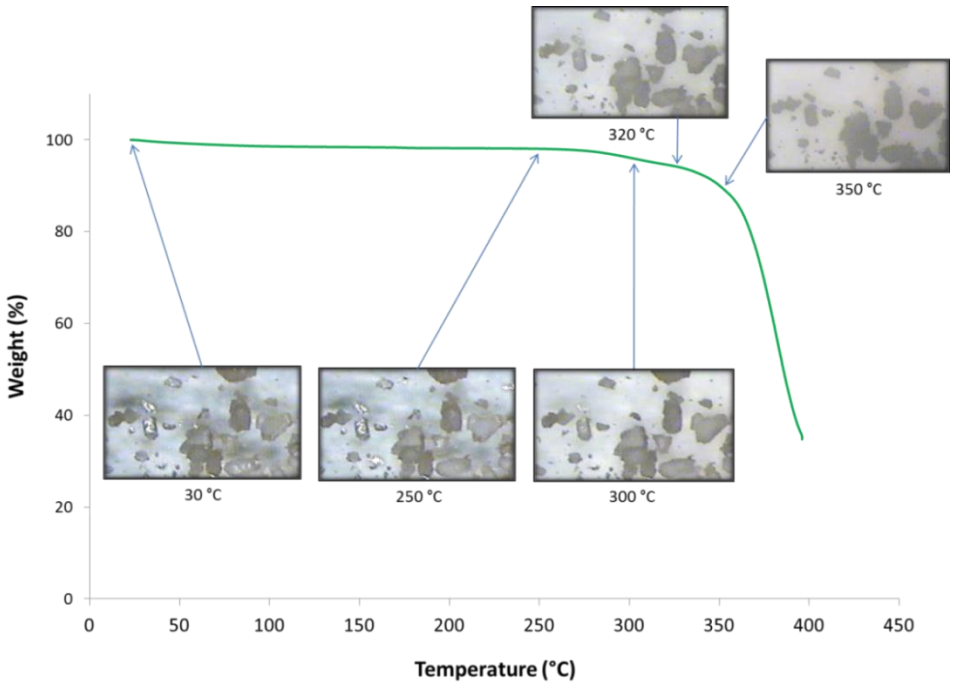


***Figure 4.5**: Hot stage photographs correlated to a TGA trace show that activated HOF-8 crystals are stable up to 300 °C.*

Variable temperature PXRD reported in the literature[1] showed that HOF-8 is crystalline up to 350 °C. However, there is a notable loss of intensity in the powder patterns after 240 °C which, in

light of this work, is most probably due to the disruption of the crystal lattice during solvent loss and consequent temperature-related degradation of the compound. Nevertheless, HOF-8 has remarkable thermal-stability, and as discussed in Section 4.5, it can be ascribed to the multiple non-covalent interactions in the packing arrangement of HOF-8. Other examples in the literature can put the thermal stability of HOF-8 into perspective. For example, HOF-1 starts to decompose at 400 °C,[5] and a pyrazole-based compound reported by Teng-Hau *et al.*[4] is stable up to 250 °C.

### 4.3.3 Differential scanning calorimetry

Previously it was reported that 1,3,5-benzene-tri(4-pyridinyl)carboxamide crystallises as a hydrate in the space group *Pbca* (Figure 4.7),[10] whereas in this study, and elsewhere[1], it was found that HOF-8 crystallises in the space group *C2/c*. To determine if HOF-8 can undergo a thermally-induced phase change, DSC analysis was performed on solvated HOF-8 between -173 and 300 °C. The DSC trace of HOF-8 is given in Figure 4.6. Initially (red trace) there are two endotherms due to solvent loss at approximately 70 and 250 °C. Consequently, the blue trace indicates that except for the peaks at -140 °C, which are caused by contraction and expansion of the DSC's flange, there are no other observable thermal events (peaks) that occur during the heating and cooling cycle. Thus HOF-8 does not appear to undergo a temperature-induced phase change in the specified temperature range.

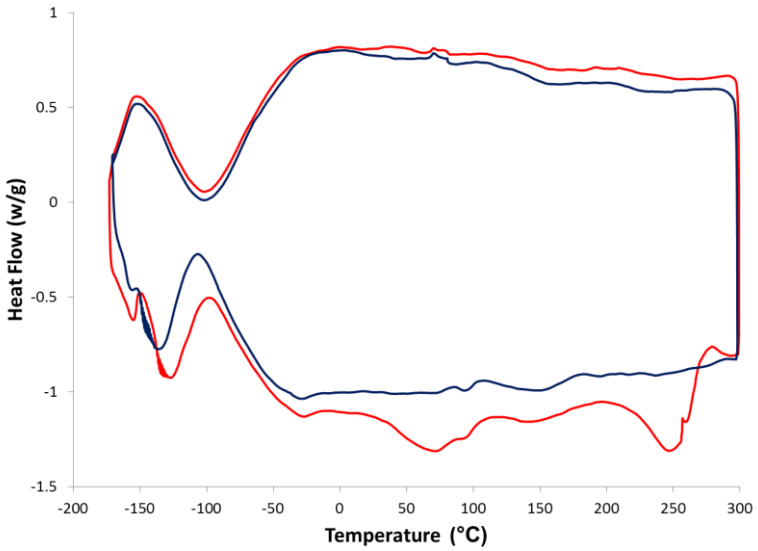


***Figure 4.6**: DSC trace of solvated HOF-8. The red trace is the first DSC cycle. At approximately 70 and 250 °C there are two endotherms due to solvent loss. During the second (blue trace) DSC cycle, one can see that there are no indications of phase transitions between -173 and 300 °C.*

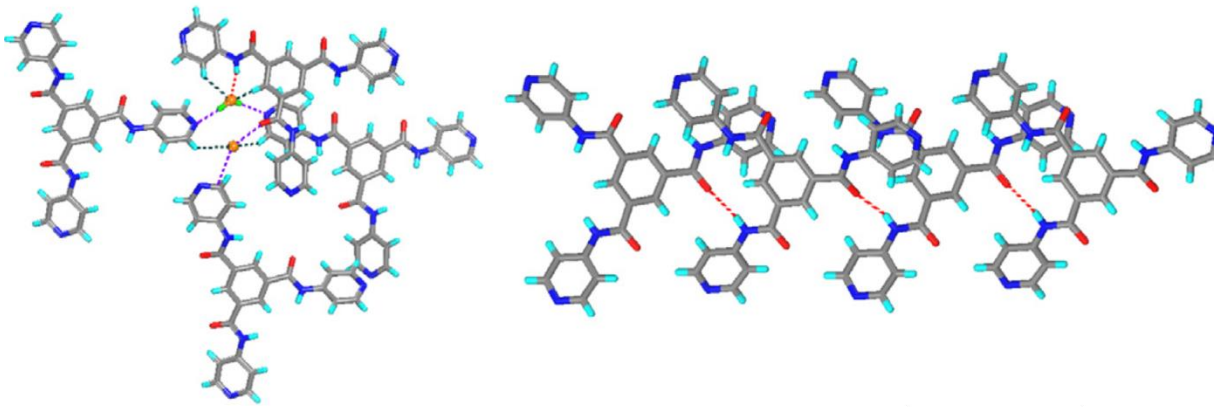

***Figure 4.7**: The reported[10] crystal structure of BPTC, which crystallises in the space group Pbca. Water molecules disrupt the N···H-N bonds found in HOF-8, which leads to alternative C=O···H-N hydrogen bonds to form between neighbouring molecules.*

## 4.4 Powder X-ray diffraction.

As described in Section 4.1.3, generation of the activated form of HOF-8 involved two heating cycles up to 200 °C. Moreover, it was shown in Section 4.2.2 that solvated HOF-8 is not as thermally stable as the desolvated form. Therefore, in order to confirm that solvated HOF-8 remains crystalline during the heating cycles beyond 200 °C it was subjected to variable temperature PXRD. The powder patterns, which were recorded from -173 °C to 217 °C at 30 °C intervals, are given in Figure 4.8. The powder patterns confirm that solvated HOF-8 remains crystalline up to 217 °C. In addition, one can see that some peaks merge and change in intensity as the temperature increases. For example, at 2Θ = 7°, 12°, 18.5° and 28° there are temperature-related changes in the intensity or position of peaks. Such shifts arise from changes in the unit-cell parameters, and are often due to thermal expansion or solvent loss.

Thermal expansion is a common phenomenon; in fact most materials expand or contract when they are heated at constant pressure. However, if a material shows substantial positive or negative thermal expansion it can be useful for applications such as thermomechanical actuation.[11] On the other hand, changes in unit-cell parameters due to solvent loss are frequently observed but rarely significant.

To determine the cause of the peak shifts, the changes in unit cell parameters as well as the number of void electrons were examined with a variable-temperature SCD study of the solvated HOF-8 between -173 to 7 °C. Unit-cell parameters are given in Table 4.1, and it can be seen that there are marginal changes accompanied by a decreasing number of void electrons. At -83 °C there

is a sudden increase in the number of void electrons, which might be caused by nitrogen adsorption from the cryostream. Nevertheless, the trend of changing unit cell parameters is not affected. Therefore, it can be concluded that HOF-8 undergoes minor temperature-related changes in unit-cell parameters; however these changes are most likely due to solvent loss.

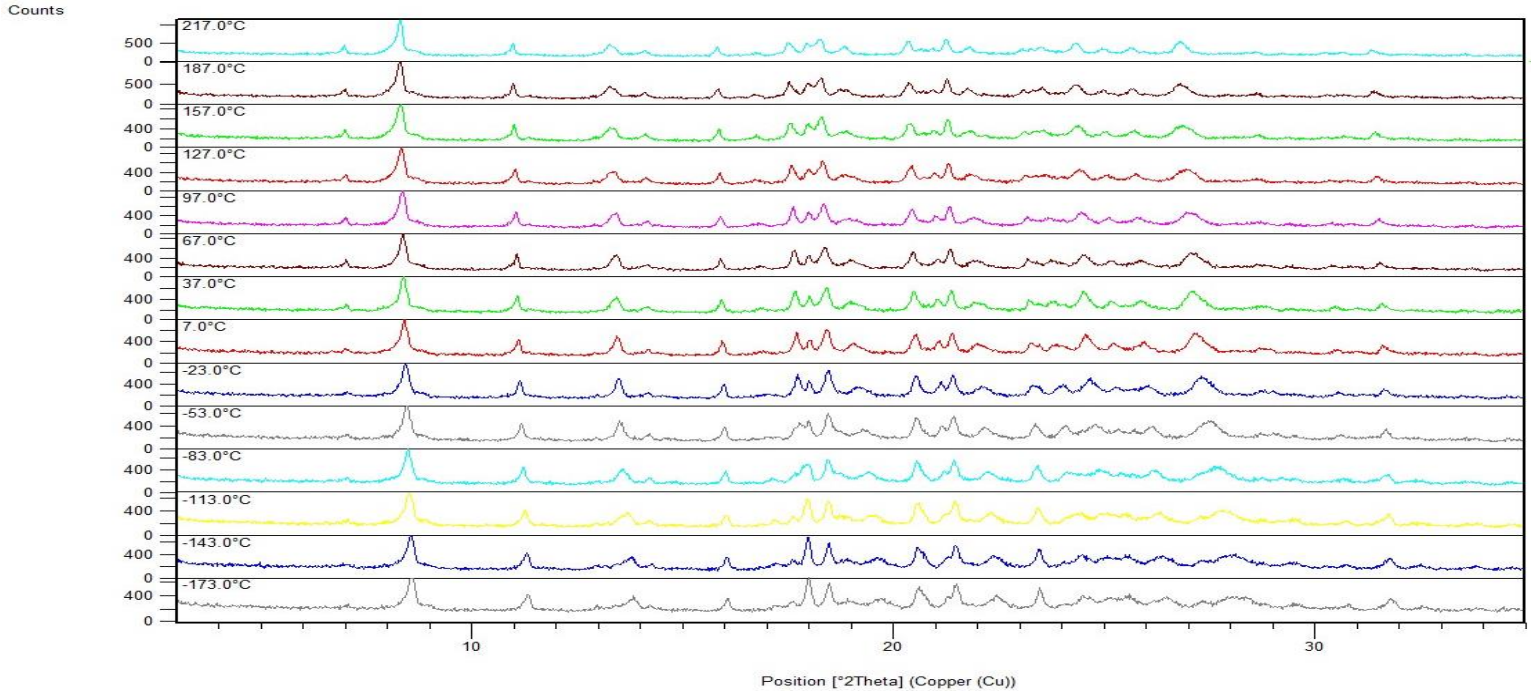


**Figure 4.8**: Variable temperature PXRD patterns for the solvated HOF-8 show gradual changes that may be due to either thermal expansion or solvent loss.

**Table 4.1**: Variable temperature unit cell parameters of the solvated HOF-8.

| **Experimental Temperature** | -173 °C | -143 °C | -113 °C | -83 °C | -53 °C | -23 °C | 7 °C |
|---|---|---|---|---|---|---|---|
| **Cell length a (Å)** | 23.540(4) | 23.678(7) | 23.872(4) | 24.067(5) | 24.252(9) | 24.383(9) | 24.548(1) |
| **Cell length b (Å)** | 15.587(3) | 15.616(4) | 15.559(3) | 15.545(3) | 15.536(6) | 15.536(6) | 15.493(9) |
| **Cell length c (Å)** | 15.537(3) | 15.572(5) | 15.617(3) | 15.662(3) | 15.712(6) | 15.751(6) | 15.792(7) |
| **Cell angle β (°)** | 121.4(1) | 121.7(6) | 122.2(1) | 122.7(1) | 123.0(6) | 123.2 (6) | 123.5(6) |
| **Void electrons** | 121 | 120 | 119 | 78 | 110 | 105 | 106 |
| **Void volume*/unit cell (Å$^3$)** | 997 | 1018 | 1031 | 1050 | 1070 | 1082 | 1197 |

*Volumes were calculated in Materials Studio with 1.5 Å probe radius.

## 4.5 Gas sorption

Porous materials that can capture flue gases are appealing if they selectively adsorb carbon dioxide under high pressure and low temperature, and then release the adsorbed gas under reduced pressure and high temperature. Prerequisites of such materials are that they possess thermal stability above 300 °C, have a low manufacturing cost, and are not sensitive to, or do not adsorb, moisture from the flue gas feed.[12,13] Luo *et al*. reported that HOF-8 is selective for carbon dioxide uptake over nitrogen between 0 and 1 bar, and shows high thermal stability,[1] which makes it an appealing material to separate carbon dioxide from nitrogen in flue gas feeds. However, as will be shown in Section 4.6, HOF-8 also adsorbs water. Nevertheless, on a fundamental level, it is of interest to study and rationalise the sorption behaviour of a porous organic framework such as HOF-8, since this contributes to our knowledge of structure-property relationships.

The following section discusses an extended study of the adsorption properties of HOF-8, with the aim of determining whether the theoretical selectivity of carbon dioxide over nitrogen prevails up to 20 bar. The section also describes an investigation of the sorption of methane, ethylene, ethane, propane and butane by HOF-8. The sorption isotherms for carbon dioxide and nitrogen between 0 and 20 bar are compared in Figure 4.9, followed by a comparison of methane, ethylene and ethane sorption between 0 and 20 bar in Figure 4.10. Finally, the propane sorption isotherm between 0 and 8 bar, as well as that for butane sorption between 0 and 2 bar, are given in Figure 4.11.

Although it was reported[1] that HOF-8 adsorbs no nitrogen between 0 and 1 bar at 298K, this study shows that it adsorbs nitrogen between 0 and 20 bar at 298K (Figure 4.9). At 20 bar HOF-8 shows a threefold preference for carbon dioxide over nitrogen. This preference is most likely due to an electrostatic interaction that can occur between the guest and host's carboxamide oxygen atoms that line its solvent-accessible cavity, as will be discussed in Section 4.6.

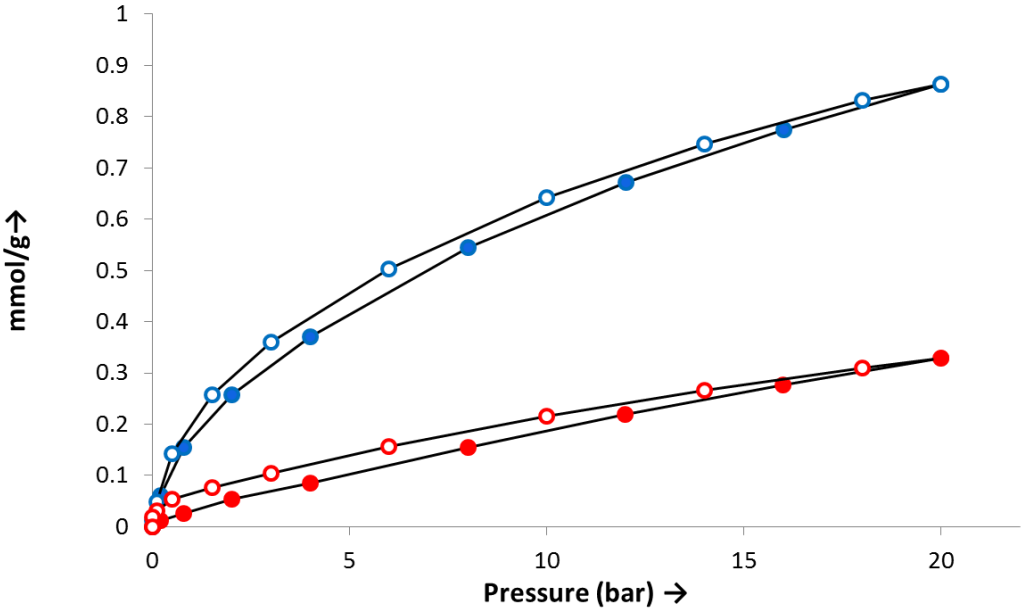


***Figure 4.9**: HOF-8 sorption and desorption isotherms for carbon dioxide are given in the upper and lower blue symbols respectively. Similarly the nitrogen sorption and desorption isotherms are given in maroon. At 20 bar HOF-8 adsorbs approximately three times more carbon dioxide than nitrogen, and HOF-8 displays a relatively small amount of hysteresis for both carbon dioxide and nitrogen during desorption.*

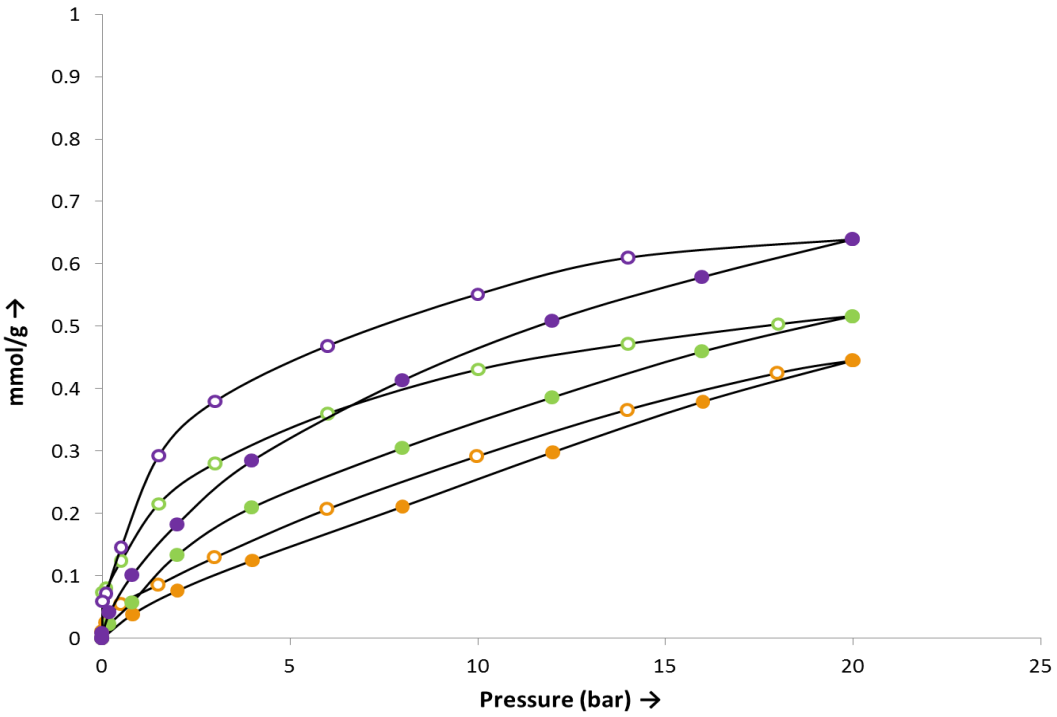


***Figure 4.10**: HOF-8 sorption (lower curve) and desorption (upper curve) isotherms for ethylene (purple), ethane (green) and methane (orange). HOF-8 shows the highest uptake and the most hysteresis for ethylene.*

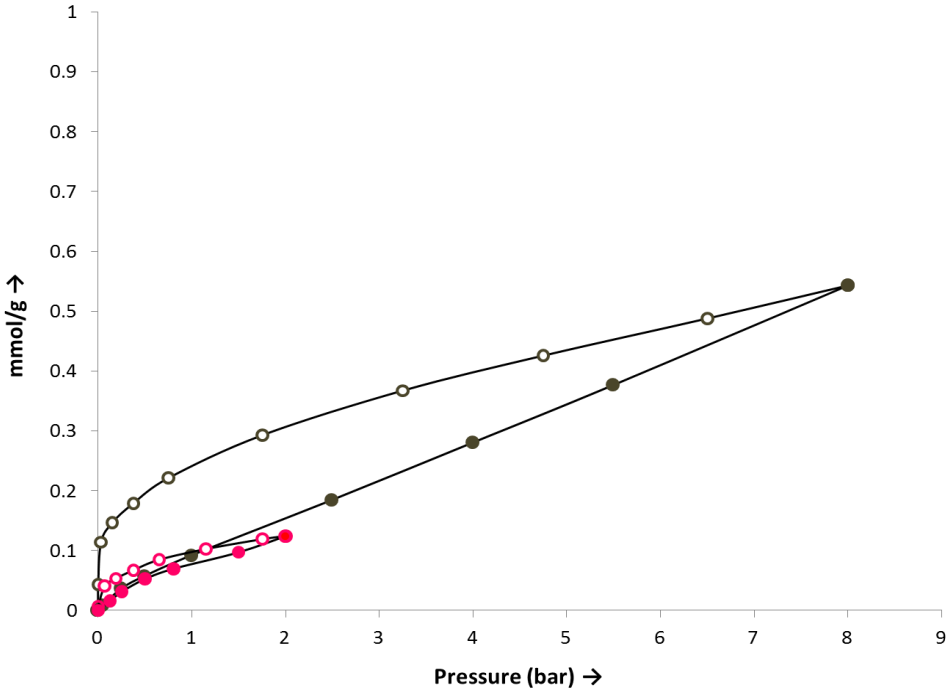


***Figure 4.11**: HOF-8 sorption (upper curve) and desorption (lower curve) isotherms for propane (olive green) and butane (red). HOF-8 shows favourable adsorption and substantial hysteresis relative to all the studied alkanes at 8 bar, whereas butane adsorption does not display significant adsorption.*

It is clear that HOF-8 is able to adsorb all of the alkanes in the series studied. Furthermore, between methane, ethane and ethylene HOF-8 shows the highest affinity for ethylene adsorption, and during desorption of ethylene HOF-8 displays the most hysteresis. This sorption preference is most probably also due to an electrostatic interaction between the host's carboxamide oxygen atoms and the π-system in ethylene.

At 8 bar HOF-8 has the highest uptake of propane relative to methane, ethylene and ethane. In fact, at 8 bar HOF-8 adsorbs comparable amounts of carbon dioxide and propane. Furthermore, during propane desorption there is a relatively large amount of hysteresis. There are two plausible explanations for this sorption behaviour, the first of which is adsorbate-surface interactions and the second being size/shape exclusion.

It has been shown that molecules with higher quadrupole moments usually display stronger adsorbate-adsorbent interactions, especially if relatively polar functional groups such as $NH_2$ are present along the host's cavity. This observation has been used in a number of cases to improve selective adsorption capacity for systems such as $CO_2/N_2$, $CO_2/H_2$ and $CO_2/CH_4$.[14] HOF-8 has an array of polar carboxamide oxygen atoms that line the surface of its solvent-accessible channels. Therefore, one might expect HOF-8 to have a higher sorption affinity for molecules with higher quadrupole moments.

In Table 4.2 the reported[15] computed quadrupole moments of the series of studied gases are given at different levels of theory utilising the cc-pV(T+d)Z basis set. The reader is referred to the publication by Höfinger and Wendland[16] regarding the selection of a level of theory and basis set in the calculations of quadrupole moments.

**Table 4.2**: Quadrupole moments of various gases calculated with different levels of theory utilising the cc-pV(T+d)Z basis set. All values are given in Debye Angstrom (D Å) units.

| Level of theory | Carbon dioxide | Nitrogen | Methane | Ethylene | Ethane | Propane | Butane |
|---|---|---|---|---|---|---|---|
| **B3PW91** | -4.317 | -1.578 | Not available | -3.217 | -0.661 | 0.638 | -1.065 |
| **MP2** | -5.111 | -1.711 | Not available | -3.231 | -0.753 | 0.729 | Not available |
| **BLB95** | -4.434 | -1.561 | 0.021 | -3.178 | -0.666 | 0.635 | -1.002 |

The adsorption affinity of HOF-8 for carbon dioxide over nitrogen can be correlated to the quadrupole moments of these gases. Carbon dioxide has a much higher quadrupole moment than nitrogen, and therefore one would expect a higher affinity for carbon dioxide uptake, which is what is observed in Figure 4.9. A similar trend is seen in the sorption of methane, ethylene and ethane. Of the three alkanes, methane, with the smallest quadrupole moment, is adsorbed the least, whereas HOF-8 adsorbs a relatively higher concentration of ethylene, which has the larger quadrupole moment.

Sorption selectivity based on the quadrupole moment theory describes most of the observed trends very well, but there are two anomalies. The first is the low amount of butane adsorbed. At 2.0 bar similar amounts of butane and methane are adsorbed, however butane has a much higher quadrupole moment. It is possible that the sorption capacity of HOF-8 for butane is limited by steric factors. In other words, the size/shape of butane prohibits favourable adsorption.

The second anomaly is that propane is adsorbed in similar quantities to carbon dioxide at 8 bar, even though it is bulkier and has a smaller positive quadrupole moment. The fact that propane is the only gas to have a positive quadrupole moment suggests a possible explanation for this observation.

Molecules that have negative quadrupole moments normally have their nuclear charge distribution in an oblate spheroid around the molecular *z*-axis, whereas molecules with a positive quadrupole moment have their nuclear charge distributed as a prolate spheroid around the *z*-axis. It has been observed that if a high Péclet number (the ratio of rate of advection over rate of diffusion) is observed during sorption, prolate-type molecules will be adsorbed in a higher concentration relative to oblate-type molecules.[17] Thus, it is possible that propane has a high mass transfer rate

during sorption, and because propane has a positive quadrupole moment the sorption into HOF-8 is favoured above that of the other alkanes, despite its larger size.

In brief, HOF-8's sorption behaviour can largely be explained by quadrupole electrostatic interactions, and the sorption is affected by the type of quadrupole moment of the adsorbate; however as soon as steric hindrance comes into play, weak electrostatic forces play a less prominent role in adsorption affinity.

## 4.6 Single crystal X-ray diffraction

Structural data of the solvated HOF-8 at -173 °C were used to study the supramolecular interactions that give rise to the topology and physical properties of the organic framework.

Structure elucidation showed that HOF-8 crystallises in the space group *C*2/*c*. Figure 4.12 shows how each BTPC subunit connects to three other BTPC molecules through six N···H-N hydrogen bonds, and this bonding causes each BTPC unit to be snugly surrounded and stabilised by the neighbouring units. Moreover, on a slightly larger scale, one can see that the hydrogen bonding drives the BTPC molecules to assemble in a circular fashion around the crystallographic *a*-axis, forming layers of ring-like structures (see Figure 4.13). These layers are further stabilised when they stack through π···π interactions between two adjacent layers along the crystallographic *c*-axis, forming continuous three-dimensional channels. Each unit cell contains two channels, each with an approximate void volume of 500 $Å^3$ per unit cell.

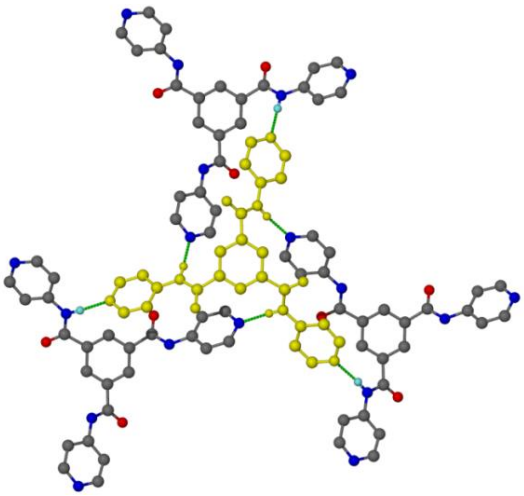

***Figure 4.12**: The ball-and-stick representation shows a single BTPC molecule (yellow) hydrogen-bonded (green bonds) to three other BTPC molecules. Irrelevant hydrogen atoms have been omitted for clarity.*

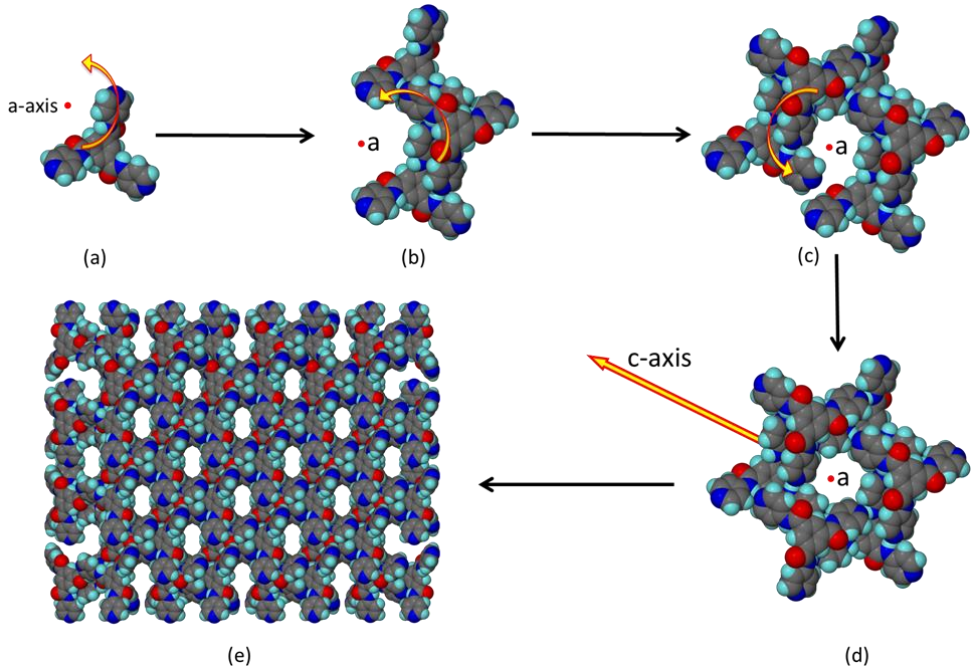


***Figure 4.13**: (a-c) BTPC molecules hydrogen bond in a circular fashion around the crystallographic a-axis, and the circular motif stacks along the crystallographic c-axis (d) to form continuous 3D open channels (e).*

HOF-8 is crystallised from a 1:3 methanol:chloroform mixture. However, during the modelling of SCD data no methanol could be identified. The apparent selectively is interesting because methanol has a smaller molecular volume than chloroform as is shown in Figure 4.14. Therefore, it is highly unlikely that the selectivity is based on size exclusion. The alternative would be that selectivity is based on host-guest electrostatic interactions.

Figure 4.14 shows the electrostatic profiles of methanol and chloroform mapped onto their solvent excluded volumes. Blue and red indicate positive and negative electrostatic profiles, respectively. The electrostatic profiles show that chloroform is polarised, with distinct $\delta^+$ and $\delta^-$ regions. On the other hand, methanol has a $\delta^-$ region and two regions with $\delta^+$ electrostatic potential. The differences between the electrostatic profiles of the guest molecules make it quite feasible that HOF-8 mainly includes chloroform during crystallisation because of compatible host-guest electrostatic interactions.

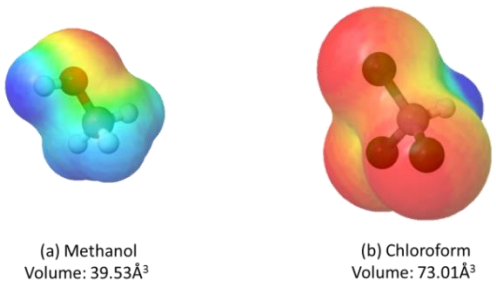


***Figure 4.14**: Electrostatic profiles are mapped onto the solvent excluded volume isosurfaces of (a) methanol and (b) chloroform.[18] The volumes were calculated in Materials Studio using a 1.5 Å probe.*

The crystallographic model of the solvent accessible channel along the crystallographic *c*-axis of solvated HOF-8 is shown in Figure 4.15. The solvate has a solvent-accessible channel of 499 Å$^3$ per unit cell, and is shown as a transparent blue isosurface. The channels are filled with chloroform molecules that are disordered over four positions, and which are shown as space-filled models.

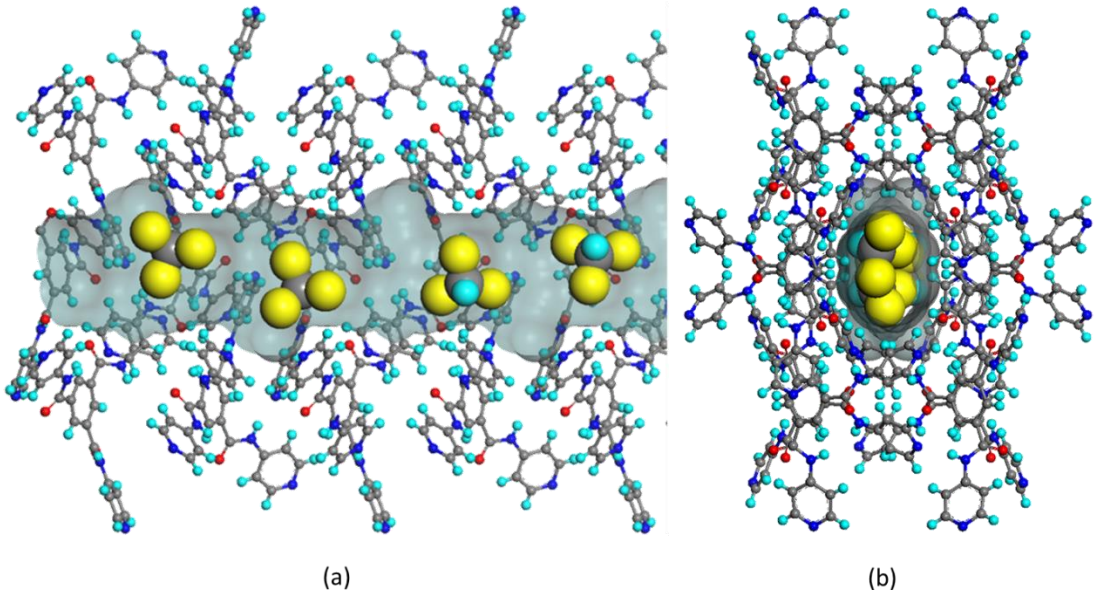


***Figure 4.15**: Chloroform molecules disordered over four positions are shown in the solvent-accessible void space (a) perpendicular to and (b) down the crystallographic c-axis.*

At first glance the four disordered positions of the chloroform molecules seem arbitrary. However, upon closer inspection one can see that electrostatics play a key role in the orientation of the chloroform molecules. For example, one electrostatic host-guest interaction is a 2.23 Å C=O···H-C hydrogen-bond between the host's carboxamide oxygen atom and the $\delta^+$ proton on chloroform (Figure 4.16). In addition, the $\delta^-$ chlorinated side of the chloroform molecule faces an array of marginally $\delta^+$ protons on the surface of the solvent-accessible channel.

It is possible that HOF-8 does not include methanol during crystallisation because in the confined space where methanol would have to form a hydrogen bond with the carboxamide oxygen

there would be electrostatic repulsion between the carboxamide and methanol oxygen atoms, reducing the ability of methanol to hydrogen bond to the host. If so, chloroform will be more likely to hydrogen-bond to the host, especially when there is three times more chloroform than methanol. Furthermore, if methanol were to hydrogen bond to the same carboxamide oxygen as chloroform does, the $\delta^+$ hydrogens on the methanol carbon atom will be repelled by the protons on the opposite side of the channel.

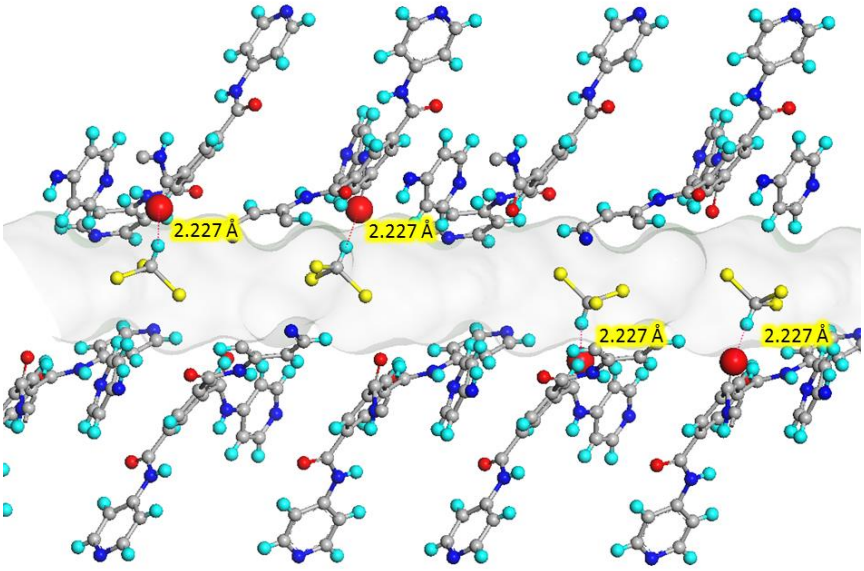


***Figure 4.16**: The positions of the chloroform molecules in HOF-8 are due to a hydrogen bond between chloroform's $\delta^+$ proton and the carboxamide oxygen of HOF-8.*

Structural data for desolvated HOF-8 as well as HOF-8 with included $CO_2$ were collected. However, the desolvated HOF-8 has diffuse electron density in its void space that could not be accounted for, or modelled. In addition, the guest molecules in the $CO_2$-containing structure are also disordered and could not be modelled.

## 4.7 Hot stage-Mass spectrometry

In SCD studies the modelling of unknown residual electron density in a host's void space can be troublesome, especially if crystals were obtained from a mixture of solvents, or after a competitive adsorption experiment. Moreover, desolvated porous materials often adsorb gases such as nitrogen, carbon dioxide and water vapour from the atmosphere and it is not always a simple task to determine which molecules were adsorbed. Analytical techniques such as TGA can be used to determine at which temperature these guest molecules are released from a host, and a hot stage can be used to observe how a host's morphology is changed as guest molecules are released, but neither of the instruments can actually identify the released guests.

Currently, methods such as Nuclear Magnetic Resonance spectroscopy (NMR), mass spectrometry (MS) or IR spectroscopy are used to determine the identity of the guest molecules. These methods are robust, reliable and remarkably useful. However, in the field of supramolecular chemistry it would be useful to have an analytical technique that can show how a host's macro-scale structure is affected at the temperature where guest molecules are expelled, while simultaneously identifying the released guest molecules.

To obtain this combination of information a hot stage microscope was coupled to a mass spectrometer (HS-MS). The coupling allows one to determine the identity of the guest molecules that are released due to increasing temperature, while simultaneously observing the change in the host's morphology. Moreover, as described in section 4.3.2, TGA data can easily be correlated to hot stage data, and in such a way it can be incorporated with HS-MS data. This allows one to detect which guest molecules are released where a mass loss occurs on a TGA trace, while simultaneously determining how the guest's morphology is affected by the mass loss.

In Section 4.1.3 it is shown that after HOF-8 was exposed to sc-$CO_2$, carbon dioxide was adsorbed into the structure, forcing out some of the crystallisation solvent. However, there were some guest molecules left in the solvent-accessible channels. After SCD data were collected for one of these crystals it was not possible to model the guest molecules, because these could be disordered chloroform, methanol, carbon dioxide, water or a combination of these. In addition, the subsequent activation step was to heat the crystals, and as was seen in Figure 4.4 the solvated HOF-8 crystals were destroyed at 260 °C due to rapid solvent loss. In this case, the HS-MS analysis is useful to determine which guest molecules are still present in the solvent accessible-channels, and when the crystals start to deteriorate after one cycle of activation.

The mass spectrometer's pressure vs time spectrum (P vs t) is given in Figure 4.17, along with hot stage photographs annotated with the time and temperature at which they were taken. The pressure scale on the *P* vs *t* plot is logarithmic so that the identities of all of the guests that might be in the host's void space can be monitored. Nitrogen (red) is used as a baseline to determine if there are any leaks in the system during the analysis. If the pressure of nitrogen decreases during analysis, one can assume that there is no leak in the system. This is particularly important when determining if water or carbon dioxide are released from the host molecules, because gases from the atmosphere might cause misleading data. For example, if one is detecting for the release of carbon dioxide from the crystal, a leak would cause an increase in carbon dioxide concentration in the system, giving the false impression that the crystal contains and is releasing carbon dioxide. It should be noted that the mass spectrometer was not calibrated for quantitative analysis, therefore the relative pressure of each species is not important, but the change in the pressure (signal) of the gas is.

A number of observations can be made from Figure 4.17. Firstly, after HOF-8 crystals were exposed to sc-$CO_2$, there is no rapid solvent loss that destroys the crystals at 260 °C. The first cracks in the crystals start to appear at 270 °C. In addition, one can see that at 1h 12 min, when the crystals were at 270 °C, the pressure signal of carbon dioxide and water starts to rise, which indicates that HOF-8 is releasing water and carbon dioxide at 270 °C. Up to 320 °C, when the crystals start to decompose, no other guest molecules are released. Therefore, it can be concluded that, during activation of HOF-8 after the crystals had been exposed to sc-$CO_2$, all the chloroform and methanol molecules in the host's void-space had been replaced by water and carbon dioxide, and that the crystals do not dissolve as was seen in Figure 4.4 for solvated HOF-8.

After HOF-8 was activated it was found that if the crystals were exposed to the atmosphere they start to take up unknown guest molecules; the presence of these guest(s) is the origin of the unidentified diffuse electron density in the SCD data. In Figure 4.18 the TGA data of the activated HOF-8 crystals that had been exposed to the atmosphere for 2 days are correlated with the HS-MS data. TGA shows that after 250 °C a 2% mass loss occurs for activated HOF-8. HS-MS shows that at the temperature where the mass loss occurs on the TGA trace there is an increase in water vapour pressure, which implies that HOF-8 adsorbs water from the atmosphere after activation. In addition, the hot stage photographs show that single crystals still crack at 270 °C, which is probably due to the release of water.

In brief these two examples show how useful the combination of a HS-MS analysis can be. It was determined that solvent molecules can be removed from HOF-8 by submerging the crystals in sc-$CO_2$. Furthermore, the analysis was used to determine that in the structural modelling of the desolvated HOF-8, water was the unknown guest that made up the diffuse electron density. Therefore, the desolvated HOF-8 is hygroscopic, and when water is rapidly released from HOF-8 the crystals start to deteriorate.

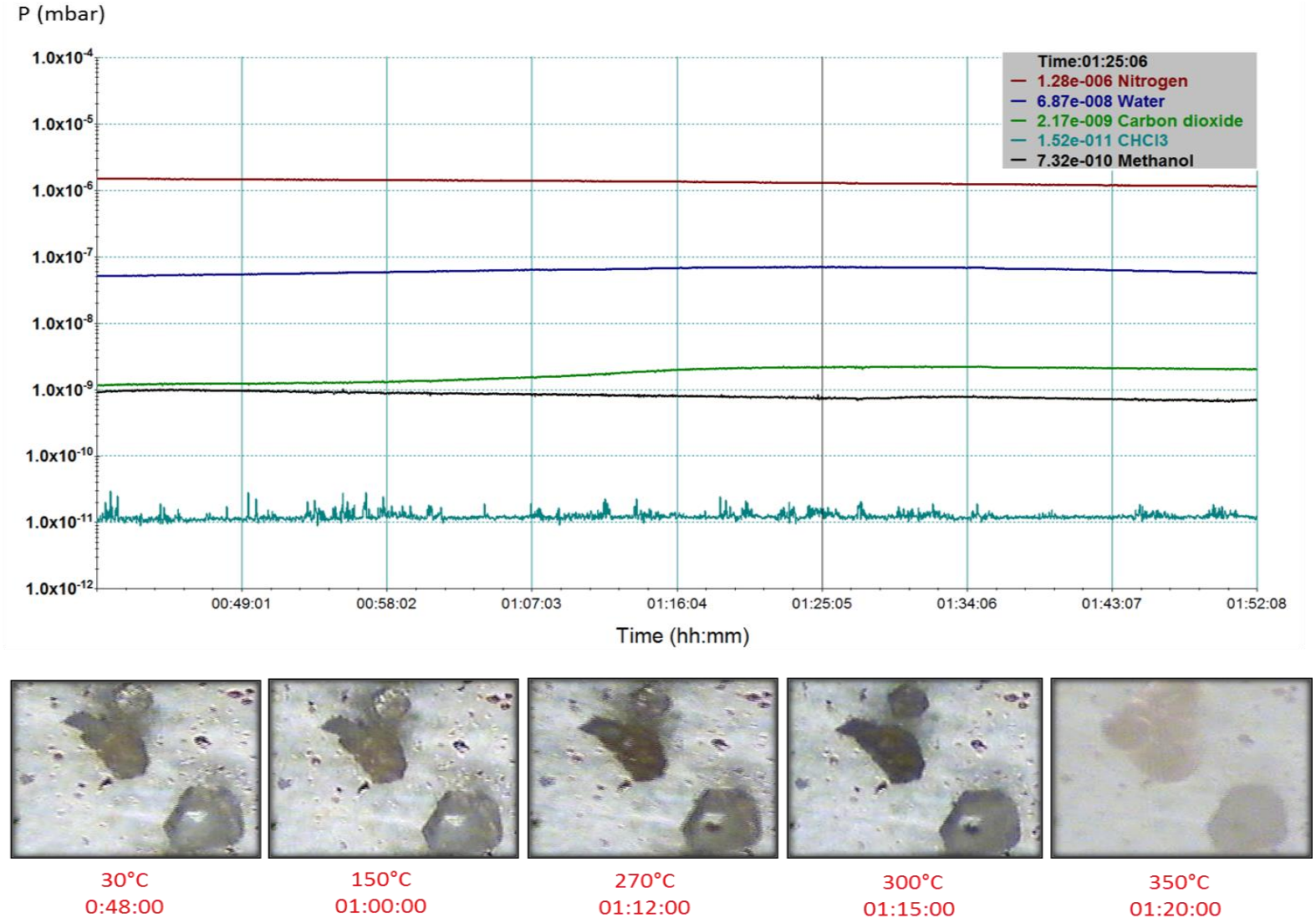


***Figure 4.17**: A HS-MS analysis shows that after solvated HOF-8 crystals were exposed to sc-$CO_2$ all the chloroform molecules had been replaced by water and carbon dioxide, which prevents HOF-8 crystals from breaking down at 260 °C due to rapid solvent loss.*

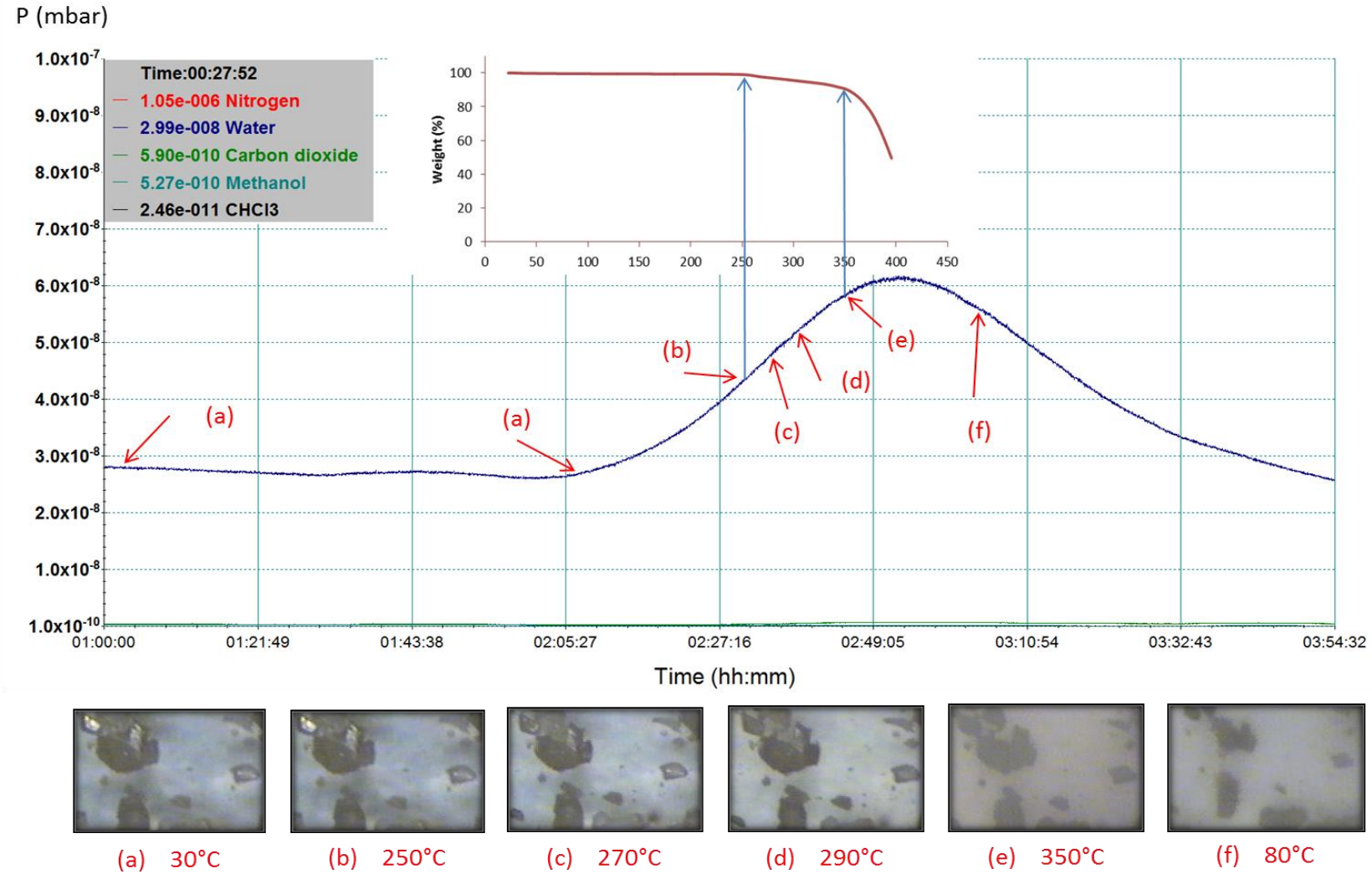


***Figure 4.18**: Hot stage-mass spectrum data are correlated to TGA data for activated HOF-8 which had adsorbed unknown molecules from the atmosphere. The figure shows how one can determine that at 250 °C, where a mass loss occurs on the TGA trace, water and traces of carbon dioxide are released, and that the released guests do not affect the integrity of the crystals, as they only start to deteriorate after 270 °C.*

## 4.8 Conclusion

Porous hydrogen-bonded organic frameworks are an example of a class of synthetic porous materials that have recently attracted much attention because many possess some desired chemical, optical, electronic or magnetic properties.[19] On a fundamental level these properties arise from supramolecular interactions between subunits of the host, and interactions between the host and guest. Ideally, with enough knowledge regarding host-host and host-guest interactions scientists will be able to predict and design a material with desired properties based on the form and functional groups of its subunits. To realise this it is essential to investigate and understand how supramolecular interactions give rise to a material's properties. Additionally, it is important that new analytical techniques be developed that are specifically designed to aid in the investigation of a material's properties so that a more informed and in-depth understanding might be the basic starting point of analysis. Various properties of the hydrogen-bonded organic framework, HOF-8, were investigated. Some of the properties that have been reported are elaborated with more in-depth studies, and in some cases different results were obtained. In addition, the advantage of using a combination of analytical techniques was discussed.

The chapter begins by discussing the synthesis of HOF-8. This is followed by a description of an alternative activation procedure to that reported, because using hot stage analysis it was found that the reported method of activation would lead to the destruction of HOF-8 crystals. The combination of the TGA-hot stage analytical techniques serves as the first example of how a combination of analytical techniques provide better insight into experimental results.

The next section briefly touches on HOF-8's ability to undergo a phase change or thermal expansion. DSC shows that no thermal events occurred between -173 and 300 °C, which imply that HOF-8 does not undergo a temperature-induced phase change. In addition, SCD shows that the temperature-related changes observed in the PXRD patterns of HOF-8 are not due to substantial thermal expansion, but rather to solvent loss.

Subsequently, the sorption properties of HOF-8 with respect to carbon dioxide, nitrogen, and a series of alkanes are described. It was found that, in general, HOF-8 shows a preference for the adsorption of molecules with higher quadrupole moments. Moreover, butane is adsorbed in low quantities, implying that HOF-8 can exhibit size/shape selectivity during sorption. It is postulated that the preference of HOF-8 for propane is based on the latter's positive quadrupole moment and a high rate of advection during sorption.

The next section concerns SCD studies of the solvated HOF-8. This study postulates that the stability of HOF-8 is due to six N···H-N hydrogen bonds that connect one BTPC to three others in a

snug fit. In addition, it is described how electrostatics may be the reason why HOF-8 includes chloroform and not methanol from a solvent mixture during crystallisation.

Finally, the usefulness of a combined analytical technique is described; coupling a hot stage microscope to a mass spectrometer allows one to observe how the morphology of the host is affected by the release of guest molecules, while simultaneously identifying the released molecules. The HS-MS method is particularly useful for SCD as one can identify which guest molecules are responsible for residual electron density in a host's void space, and one can see if single crystals start to deteriorate upon solvent loss.

In a broad sense, a study such as this is but a twig on the tree of knowledge; however it aids in the quest to understand structure-property relationships. For example, it has been shown that HOF-8 is vulnerable during desorption, and thereafter it readily adsorbs moisture. Moreover, if the moisture is released by simply heating the crystals, the single crystals start to crack at 270 °C before decomposition. Finally, HOF-8 can adsorb a variety of gases and is seems that the carboxamide oxygen atoms that line the solvent-accessible channels have a significant tremendous influence on the uptake of guest molecules, in that HOF-8 displays a preference for gases with higher quadrupole moments.

## 4.9 References


(1) Luo, X.-Z.; Jia, X.-J.; Deng, J.-H.; Zhong, J.-L.; Liu, H.-J.; Wang, K.-J.; Zhong, D.-C. *J. Am. Chem. Soc.* **2013**, *135*, 11684.

(2) Li, P.; He, Y.; Zhao, Y.; Weng, L.; Wang, H.; Krishna, R.; Wu, H.; Zhou, W.; O'Keeffe, M.; Han, Y.; Chen, B. *Angew. Chem. Int. Ed.* **2015**, *54*, 574.

(3) Li, P.; He, Y.; Guang, J.; Weng, L.; Zhao, J. C.-G.; Xiang, S.; Chen, B. *J. Am. Chem. Soc.* **2014**, *136*, 547.

(4) Li, P.; He, Y.; Arman, H. D.; Krishna, R.; Wang, H.; Weng, L.; Chen, B. *Chem. Commun.* **2014**, *50*, 13081.

(5) Liu, B.; Ben, T.; Xu, J.; Deng, F.; Qiu, S. *New J. Chem.* **2014**, *38*, 2292.

(6) Mastalerz, M.; Oppel, I. M. *Angew. Chem. Int. Ed.* **2012**, *51*, 5252.

(7) Plaut, D. J.; Lund, K. M.; Ward, M. D. *Chem. Commun.* **2000**, 769.

(8) Couderc, G.; Hulliger, J. *Chem. Soc. Rev.* **2010**, *39*, 1545.

(9) Hou, X.; Wang, Z.; Overby, M.; Ugrinov, A.; Oian, C.; Singh, R.; Chu, Q. R. *Chem. Commun.* **2014**, *50*, 5209.

(10) Rajput, L.; Biradha, K. *J. Mol. Struct.* **2011**, *991*, 97.

(11) Das, D.; Jacobs, T.; Barbour, L. J. *Nat Mater* **2010**, *9*, 36.

(12) Yu, C.-H.; Huang, C.-H.; Tan, C.-S. *AAOR* **2012**, *12*, 745.

(13) Dantas, T. L. P.; Luna, F. M. T.; Silva Jr, I. J.; Torres, A. E. B.; de Azevedo, D. C. S.; Rodrigues, A. E.; Moreira, R. F. P. M. *Chem. Eng. J.* **2011**, *172*, 698.

(14) Li, J.-R.; Sculley, J.; Zhou, H.-C. *Chem. Rev.* **2011**, *112*, 869.

(15) Russel, D.; Johnson, I. I. I. In *16a*; August 2013 ed.; NIST Computational Chemistry Comparison and Benchmark Database: Bethesda, 2013.

(16) Höfinger, S.; Wendland, M. *Int. J. Quantum Chem* **2002**, *86*, 199.

(17) Rodríguez-Reinoso, F.; McEnaney, B.; Rouquerol, J.; Unger, K. *Characterization of Porous Solids VI: Proceedings of the 6th International Symposium on the Characterization of Porous Solids (COPS-VI), Allicante, Spain, May 8 - 11 2002*; 6 ed.; Elsevier Science: Allicante, 2002; Vol. 144.

(18) Sewell, J.; Molfield project: 2014; Vol. 2014.

(19) Desiraju, G. R. *J. Chem. Sci.* **2010**, *122*, 667.

# CHAPTER 5 | CONCLUDING REMARKS AND FUTURE WORK

This dissertation begins with a general introduction to the field of supramolecular chemistry, followed by a materials and methods section that, among others, describes a volumetric sorption device, multi-purpose high-pressure vessel, gas blending device and a hot stage-mass spectrometer, which were specially constructed to perform specialised experiments during this study. The materials and methods chapter is followed by two chapters of results and discussions. Both of these chapters are concerned with the study of structure-property relationships in porous materials. Specific attention is given in Chapter 3 to the adsorption selectivity properties of a transiently porous metallocycle, whereas Chapter 4 involves a broader study of the structure-property relationships of a Hydrogen-bonded Organic Framework (HOF).

Chapter 3 describes the adsorption selectivity of a porous material with a view to proving the principle that theoretical models such as the IAST, which is used to predict if a compound will have a preference for the adsorption of one compound over another in a gas mixture, is not always appropriate. In many of these models two single-gas adsorption isotherms are compared, and if a compound adsorbs more of gas A relative to gas B the compound is said to be selective for gas A. However, as shown and discussed in Chapter 3, this assumption is not necessarily valid because the adsorption process of gas mixtures might involve additional guest-guest and/or host-guest interactions that influence how the gases are accommodated, and in effect change the selectivity. In this study a transiently porous metallocycle was used as a model compound due to its confined void-space, which enables structural data with relatively little disorder in the position of the guest molecules and a good description of host-guest interactions can therefore be obtained. With the aid of high-pressure SCD, IR and DFT calculations it was found that even though single-gas isotherms predict that **1** has theoretical adsorption selectivity for acetylene over carbon dioxide, it will adsorb both gases equally during mixed-gas sorption. The change in adsorption preference could be ascribed to more energetically favoured host-guest and guest-guest interactions in the mixed-gas system. It is postulated that the additional guest-guest interaction between carbon dioxide and acetylene in the mixed-gas system causes the two gases to act as a single entity rather than two single entities during sorption. Moreover, since the inclusion of both molecules in each host cavity is energetically favoured, the lattice energy gained during the equilibrium exchange of single molecules for a mixture of molecules drives the host to preferentially include a 50:50 mixture of carbon dioxide and acetylene.

This shows that it cannot be assumed that the adsorption of a gas mixture will yield the average of two independent single-gas adsorptions, and consideration has to be given to possible interactions between the guests and/or the host and guests, which can change the overall sorption behaviour. Therefore, even though theoretical models that predict sorption selectivity may be applicable in some cases, this will not always be the case. Consequently, it is important that a compound should not be reported as selective if the selectivity is theoretical and based on single-gas sorption isotherms. Moreover, when a compound exhibits true selectivity it will benefit the field of crystal engineering to explain the supramolecular interactions that give rise to the selectivity, so that such explanations can be used in the development of porous materials that can separate and store gases.

Chapter 4 involves a broader, fundamental study of the structure-property relationships in a porous Hydrogen-bonded Organic Framework (HOF). There has been relatively little research devoted to these frameworks, however their potential is well recognised in various fields such as chemical capture and storage, catalysis or gas separation. The advantage of HOFs is that they do not contain expensive and toxic metals; however the absence of covalent bonds between subunits reduces their stability. Therefore, one can rationalise why it is beneficial to understand which interactions can yield a stable organic framework that has the same properties (and possibly additional properties) as other porous metal-organic frameworks.

Chapter 4 includes the description of an adapted method to prepare and activate HOF-8, followed by DSC and variable temperature PXRD analysis which showed that the organic framework does not undergo a temperature-related phase change or any significant thermal expansion. The subsequent section of the chapter involved a comprehensive study of the sorption behaviour of HOF-8, which shows a greater preference for the adsorption of gases with relative higher quadrupole moments, and the adsorption affinity is reduced with gases larger than propane. Crystallographic studies have revealed how the packing arrangement of HOF-8 gives rise to its stability. Furthermore, the crystallographic data give an indication of how HOF-8 is seemingly selective for the inclusion of chloroform over methanol when it is crystallised from a methanol-chloroform mixture. The final section of Chapter 4 introduces a useful hot stage-mass spectrometry analytical technique, which is helpful for observing how single crystals are affected by the release of guest molecules, while simultaneously identifying the guest(s).

Both of the studies confirm why the literature reiterates that an understanding of host-guest and guest-guest interactions can lead to the development of materials that possess desired properties. For example, it has been reported that porous hosts with smaller apertures are better for

gas separations.[1,2] However, Chapter 3 shows that the small apertures need to have a complementary and specific electrostatic environment within the void space that will exclude all but one gas in a gas mixture, especially if the gases have similar physical properties. Theoretical models are useful to predict selectivity and are often used when a researcher does not have the resources to conduct competitive adsorption experiments. However, it would be beneficial to develop empirical correction terms in these models that can account for interactions that will influence adsorption behaviour during mixed-gas sorption. Consequently, there is an opening for future studies derived from this work. In such a study various other gas combinations that have similar physical properties, such as carbon dioxide and nitrous oxide, can be used to determine the threshold of guest-guest interaction energy that will have a significant influence on adsorption selectivity. In addition, the electrostatic environment in a host's void space can be changed (e.g. by changing the transition metal from cadmium to zinc, or by exchanging chloride for iodide functionalities) in order to alter the host-guest interaction site and interaction energy such that it can be determined which host-guest interactions can overcome stronger guest-guest interactions. Both of these studies can be used to derive empirical correction terms for guest-guest and host-guest interactions in theoretical models that predict selectivity.

Another future extension of this study would be to determine how selective adsorption can be engineered into a compound by considering quadrupole moments. For example, if one could determine which host-void topology and functional groups would provide materials with the capability to selectively adsorb guests with positive quadrupole moments, then one might be able to develop a material that can selectively adsorb propane from all the lower alkane gases. In addition, if one knows which functional groups have the strongest interaction with a guest with a quadrupole moment in a certain range, one might be able to control the interaction site between a host and guest, which will be useful in fields such as catalysis.

In essence, there are many fundamental studies that will keep on shedding light on more structure-property relationships in porous materials. However, there are many reported porous synthetic compounds, and as the number increases, it is important that basic analyses should yield a wide range of in-depth results so that more information can be gained in a shorter time span. Therefore, it is important for researchers to invest time in the development of new analytical techniques and instruments with the equipment available to them. One such instrument that can be developed in our research group, which will be useful in selective adsorption experiments, would be a coupling between a volumetric sorption analyser and a mass spectrometer. This coupling would allow the continuous analysis of the gas composition in the headspace of a sample during mixed-gas

sorption and desorption, so that one can determine which gas(es) are adsorbed, in what quantities it/they are adsorbed and at which stage during sorption a gas in the mixture is adsorbed or desorbed.

Over the past few decades many studies have contributed small steps towards what we currently understand in crystal engineering. However, there are still many more avenues to explore in this field, each with new challenges and breakthroughs and it is important that, in order to progress, these new challenges are faced with a sound knowledge and understanding. It is studies such as this that incrementally deepen our knowledge of supramolecular systems, and as such, are necessary for advancing of supramolecular chemistry.

## 5.1 References

(1) Li, J.-R.; Kuppler, R. J.; Zhou, H.-C. *Chem. Soc. Rev.* **2009**, *38*, 1477.

(2) Li, J.-R.; Sculley, J.; Zhou, H.-C. *Chem. Rev.* **2011**, *112*, 869.

*"Nature is the source of all true knowledge. She has her own logic, her own laws, she has neither effect without cause nor invention without necessity."*

**-Leonardo da Vinci**